Real-time Measurement of Glial Progenitor Chemotactic Migration

by

Richard A. Able Jr.

A dissertation submitted to the Graduate Faculty in Biochemistry in partial fulfillment of the requirements for the degree of Doctor of Philosophy, the City University of New York

2011

This manuscript has been read and accepted for the

Graduate Faculty in Biochemistry in satisfaction of the

dissertation requirement for the degree of Doctor of Philosophy

Dr. Maribel Vazquez

Date

Chair of Examining Committee

Dr. Edward Kennelly

Date

Executive Officer

Dr. Karen Hubbard

Dr. Mark Steinberg

Dr. David Foster

Dr. Peter Canoll

Dr. Eric Holland

Supervisory Committee

THE CITY UNIVERSITY OF NEW YORK

Abstract

Real-time Measurement of Glial Progenitor Chemotactic Migration

by

Richard A. Able Jr.

Advisor: Dr. Maribel Vazquez

Gliomas are the most commonly diagnosed form of central nervous system tumors, occurring primarily in adults. Like many malignant cancers, gliomas pathologically exhibit very aggressive spreading and lead to an average diagnosed survival expectancy of twelve months. This prognosis is due in large part to the uncontrolled division and migration of malignant tumor cells within healthy brain, which makes complete surgical resection impossible. Gliomas are known to contain numerous genotypic and phenotypic alterations that affect cell proliferation and survival. Previous research has indicated that both gliomas and their precursor cells exhibit distinct migration patterns in brain tissue, which may be induced by specific cytokines and their concentration gradients. Here, we investigated the migration of four brain tumor cell (BTCs) lines (U-87 MG; U-251 MG; Daoy; and XFM^{PDGF}) and three RCAS-infected glial progenitor cell (GPCs) populations (GPC^{LacZ}, GPC^{PDGF}, and GPC^{kRas}) toward various growth factors, including but not limited to: EGF, HGF/SF, PDGF-BB, and TGF-α.

Mouse neural cultures of nestin expressing glial progenitor cells that have been engineered to display the Avian Leukosis Virus (ALV) target receptor, tv-a, were infected with

the RCAS viral vectors RCAS-LacZ, RCAS-PDGF-B, and RCAS-kRas, and are referred to as Ntv-a glial progenitor cells (Ntv-a-GPCs). Upon successful infection, the Ntv-a-GPCs were capable of constitutively producing β-galactosidase, PDGF-B, and kRas, respectively. Additionally, when these viral vectors were injected into the brains of transgenic Ntv-a mouse pups, only the RCAS-PDGF-B viral titer induced gliomas (Dai et al, 2001; Holland et al, 2000). For the purpose of this work it is relevant to note that the Ntv-a cell lines used, with the exception of the XFM^{PDGF} cells, were never injected into the mouse brain. Conversely, the XFM^{PDGF} cell population represents an excised tumor from the brain of a ≤ 12-week-old Ntv-a transgenic mouse having the Ink4a-Arf -/- genetic background. After cranial injection with a RCAS-PDGF-B viral titer, tumors of the oligodendroglioma classification developed within 1-12 weeks in 100% of the injected mice (Tchougounova et al, 2007). We use these oligodendrogliomas as our mouse tumor model. Additionally, Daoy medulloblastomas were used to model the migration of the most common childhood human brain tumor, while the U-87 MG and U-251 MG were used to model glioblastomas, the most common adult brain tumor.

The design and characterization of our stand-alone bridged μLane system demonstrated sustained steady-state concentration gradients over 2-3 days while enabling the diffusivity measurement of $0.82 \pm 0.01 \times 10^{-6}$ cm^2 / s for Dextran molecules having a molecular weight similar to growth factors examined here. A modified version of this device was then used to examine the migratory response of human MB-derived Daoy, glioblastomas, and neonatal mouse glial progenitors, which has led to the characterization of differential invasion patterns that each cell line utilizes when exposed to various growth factor concentration gradients.

This data is fundamental for understanding how BTCs and GPCs use cytokines to communicate with each other and alter cellular functions, specifically migration. Additionally,

we demonstrate EGF-induced Akt activation in the migration of MB-derived Daoy cells, and the induced recruitment GPCs towards picomolar concentrations of both HGF and TGF-α. We suggest based on our results that glial progenitors consisting of varying genetic background can migrate in very distinct patterns and may contribute to the selectivity of glioma recruitment/or progenitor sorting.

SPECIFIC AIMS

The global hypothesis of this research asserts that tumor-associated growth factors induce glial progenitor cells (GPCs) to migrate along specific pathways in the brain in order to contribute to brain tumor growth and dissemination. This thesis work had three specific aims that enabled us to utilize microfluidic devices to evaluate the extent of chemotactic migration of both glial progenitor and brain tumor-derived cells. The specific aims of this thesis are as follows:

AIM 1: Evaluate the chemotactic migration of glial progenitor cells (GPCs) and brain tumor cells (BTCs) in response to tumor-conditioned media and cytokines in vitro.

Modified Boyden transwell assays were used to measure the number of motile cells of different populations of RCAS-infected glial progenitor cells toward the conditioned media of established glioma cell lines (U-87 MG and U-251 MG) and primary brain tumors (XFM^{PDGF}). The data gathered from the use of this in vitro system evaluated the ability of U-87 MG, U-251 MG, and XFM^{PDGF} conditioned media to induce the directional motility of GPCs and BTCs. Additionally, transwell assays were used to measure cellular invasion through extracellular matrix coated filters as a response to various concentrations of the tumor-associated cytokines, PDGF-BB, HGF/SF, and TGF-α.

AIM 2: Assess the expression of cognate receptors in treated GPCs and BTCs.

Detection of the phosphorylated forms of the cognate receptors of PDGF-BB, HGF/SF, EGF and TGF-α (p-PDGFR-β, p-c-Met and p-EGF-R, respectively) was performed in growth factor stimulated GPCs and BTCs via immunoblotting and/or immunocytochemistry.

AIM 3: Utilize a microfluidic system to enable the visualization of cell migration into a three-dimensional matrix.

Experiments were designed in order to visualize directional cell migration in response to specific cytokine concentration gradients for the purpose of quantifying change in cell morphology, velocity, displaced population and distance of infiltration. A microfluidic system was developed and utilized to model specific cytokine gradients that mimic the gradients present in vivo, and to analyze the effects of these gradients on GPC and BTC migration. These studies focused on analyzing cell invasion in response to similar experimental conditions as those in the transwell assays.

ACKNOWLEDGMENTS

This process has been very challenging throughout and I will not attempt to say that I would have been able to complete the work represented in this dissertation without the assistance and support of many individuals, of whom all are not mentioned here. I share this accomplishment with many.

First, to my advisor Dr. Maribel Vazquez, thank you for accepting me into your laboratory and since the very beginning entrusting me with an immense level of responsibility. Thank you for spending so much time on molding me to become a professional, for allowing me enough space to figure things out on my own while encouraging me to continue forward, expecting no less than my best and most importantly for reminding me when this was not the case. Thank you for your patience when things were not working and for your incredible enthusiasm when things were. Your optimism was my beacon.

To Dr. Claude Brathwaite, thank you for your mentorship and providing both moral and professional support throughout my graduate school experience. Without your perspective on many issues completion of this dissertation would have been impossible. Based entirely on your creativity and confidence in my abilities, I have been able to present at dozens of national conferences, multiple international conferences, serve on scientific panels, develop and direct integrative workshops, and even serve on the Alliance for Minority Participation governing board. I look forward to many years of continued discussion.

Thank you to my laboratory peers over the years, especially post-doctoral researcher Dr. Veronica Dudu. There is no other person in this world that I have discussed my research strategy with more than you. Thank you for keeping me intellectually challenged and for ensuring that I

learned every technical skill set possible while you were in the laboratory. Thank you for your detective style questioning and insistence for fact checking during every conversation. Your presence made the graduate program manageable.

To Judy Li, thank you for ensuring that I had all the information needed to meet the requirements of the program. Without your timely email reminders many of the deadlines would have never been met. You are an asset to the department and students. Also to my classmates, thank you for the long study sessions in the beginning and for choosing me to represent you for several years on both the Doctoral Student Council and the Biochemistry Executive Committee. Your confidence meant a lot to me.

Thank you also to S. Rosenthal, J. Kunin, J. Sebastian, C. Badeau, J. Perry, B. Smith, E. Nixon, C. LaRosa, Dr. W. Mackey, Dr. S. Eva, Dr. Y. Williams-Bey, A. Todd, R. Willis, M. Langley, S. Wilson, J. Blaize, A. Wise, N. Hosannah, R. Furgeson, C. Fernandez, P. Hawthorne, and H. Qazi for your advice, creativity, support, and friendship.

Lastly, to my wife, Mia Able, and family members who have supported my decisions without protest, I owe you the most. Thank you for having confidence in my ability to lead and for supporting a process that was very foreign to you. I am not sure that you believed me after the fiftieth time that I said “I will finish in two-months”, but here we are. Thank you for the continued reminder of why I continue to work harder today than I did yesterday.

TABLE OF CONTENTS

LIST OF ABBREVIATIONS

3D	3-Dimensional
ALV	Avian Leukosis Virus
BTC	Brain Tumor Cell
CM	Conditioned Medium
c-Met	Cellular-mesenchymal-epithelial transition factor
EGF	Epidermal Growth Factor
EGFR	Epidermal Growth Factor Receptor
ECM	Extracellular Matrix
GEMM	Genetically Engineered Mouse Models
GPC	Glial Progenitor Cell
GFP	Green Fluorescent Protein
HGF/SF	Hepatocyte Growth Factor/Scatter Factor
PDGF-BB	Platelet-Derived Growth Factor-BB
PDGFR-(α/β)	Platelet-Derived Growth Factor Receptor- α or -β
Ntva	Nestin-Avian Luekosis Virus gene for Receptor A
QD	Quantum dot
	RCAS Replication-competent avian sarcoma-leukosis virus long terminal repeat (LTR) with a splice acceptor
RCF	Relative Chemoattractant Factor
RTK	Receptor Tyrosine Kinase
Shh	Sonic Hedgehog
TGF-α	Transforming Growth Factor-α

LIST OF FIGURES

CHAPTER 1. Introduction: Migration and Invasion of Brain Tumors

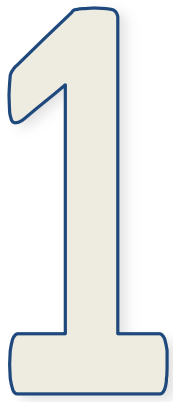

CHAPTER 1. Introduction: Migration and Invasion of Brain Tumors

Richard A. Able, Jr. [1,2,*], Veronica Dudu[1,*], and Maribel Vazquez[1,+]

[1]Department of Biomedical Engineering, The City College of The City University of New York (CCNY), 160 Convent Avenue, Steinman Hall Room 403D, New York, NY 10031

[2]Department of Biochemistry, The City Graduate Center of The City University of New York (CCNY), 365 Fifth Avenue, New York, NY 10016

Glioma – Exploring Its Biology and Practical Relevance, Edited by Anirban Ghosh p. cm.

ISBN 978-953-307-379-8: September 2011

Vazquez@ccny.cuny.edu

Phone: 212.650.5209 Fax: 212.650.6727

+Corresponding Author

* These authors contributed equally to this work

Keywords: Glioblastoma, Medulloblastoma, Invasion, Migration

1.1.0. Overview

Recent advances in molecular biology have led to new insights in the development, growth and infiltrative behaviors of primary brain tumors (Demuth & Berens, 2004; Huse & Holland, 2010; Johnson et al, 2009; Kanu et al, 2009). These tumors are derived from various brain cell lineages and have been historically classified on the basis of morphological and, more recently, immunohistochemical features with less emphasis on their underlying molecular pathogenesis (Huse & Holland, 2010). The detailed molecular characterization of brain tumors has laid the groundwork for augmentation of standard treatment with patient-specific designed targeted therapies (Johnson et al, 2009; Kanu et al, 2009). Nevertheless, these tumors are extremely aggressive in their infiltration of brain tissue (Altman et al, 2007; Hensel et al, 1998; Yamahara et al, 2010). Further, it now appears that the physiological conditions of the normal brain itself constitute a biological environment conducive to the uncontrolled dissemination of primary tumors (Bellail et al, 2004; Sontheimer, 2004). In this introduction chapter, the invasive behavior of two major types of brain tumors are discussed: gliomas and medulloblastomas – the most common tumors diagnosed in adult and pediatric brain, respectively (Rickert & Paulus, 2001). The material has been divided into five categories: i) Characteristics of malignant brain tumors; ii) Mechanisms of tumor cell migration; iii) Models for the study of brain tumor invasion in vivo and ex vivo; iv) In vitro assays for tumor cell migration; and v) Future prospects of anti-invasive brain tumor therapy.

1.1.1. Characteristics of malignant brain tumors

There are two major classes of cells in the brain, namely neurons and glia. Glial cells are said to account for greater than 80% of all the cells in the human brain and are the precursors of gliomas (Lindberg et al, 2009; Masui et al, 2010; Verkhratsky, 2007). Morphologically, the glial cells consist of astrocytes, oligodendrocytes, N2-expressing glia, Schwann cells and the microglia, each providing a distinct function (Verkhratsky, 2007). There are two modern views on the phylogeny of glia and the evolutionary specificity of neural cell development (Figure 1). The classical theory postulates the very early separation of neuronal and glial lineages, whereby neuronal and glial precursors are completely committed to the development of the respective mature cells. More recently, in vivo and in vitro based studies of gliomagenesis suggested the dedifferentiation of mature astrocytes to a glial progenitor-like state (Dai et al, 2001; Dufour et al, 2009; Robel et al, 2011). Such findings have engendered a new way of thinking about neural development that proposes 'stem-like' properties for glial progenitors. This second theory suggests that radial glial cells are the central element in subsequent neurogenesis, because they act as neural progenitors during development giving rise to neurons, astrocytes and oligodendrocytes (Figure 1).

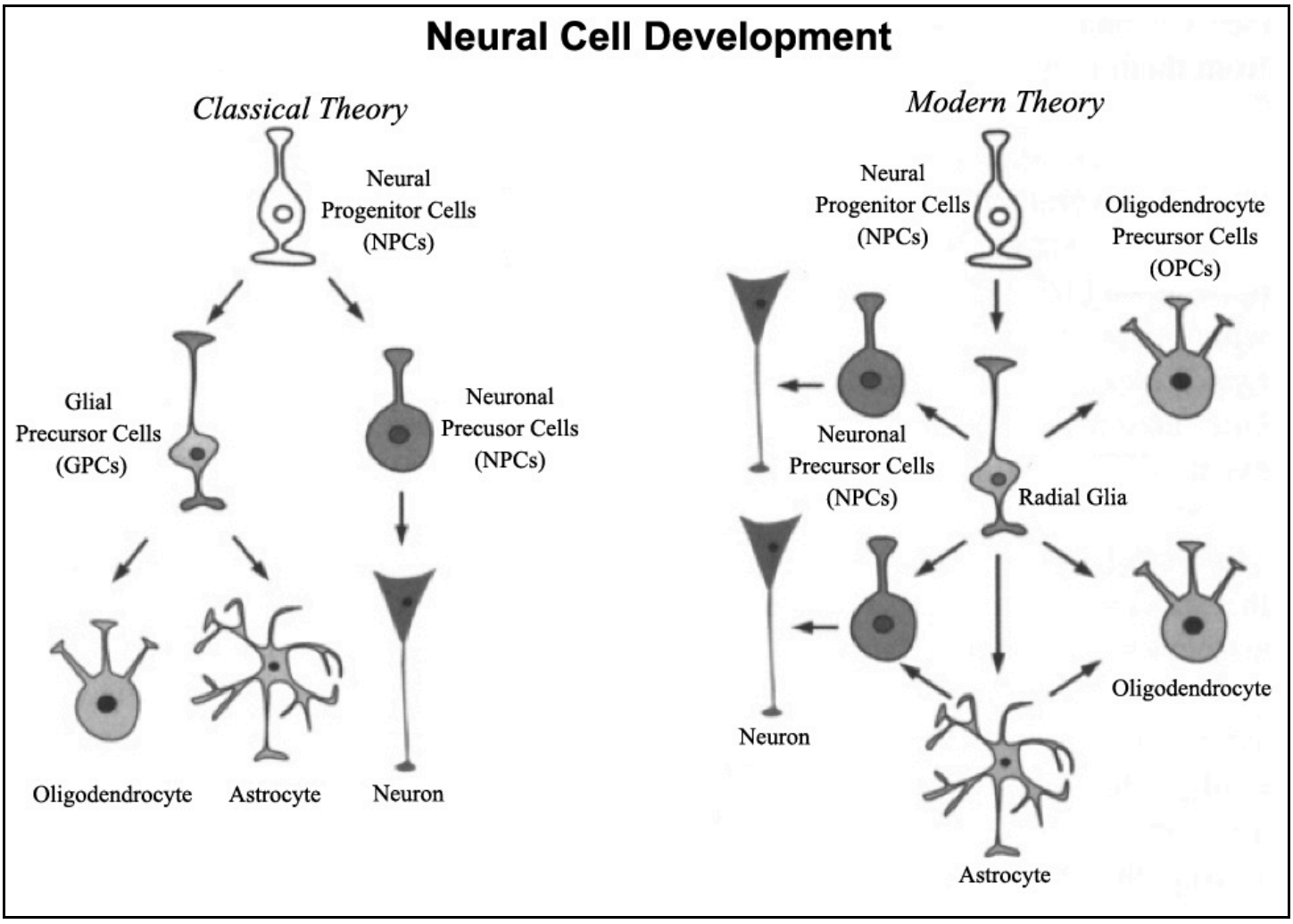

Figure 1: Schematic representation of modern views on pathways of neural cell development. The Classical and Modern theories of neural cell development (Verkhratsky, 2007).

Gliomas are commonly found in the anterior cerebral hemisphere of the brain (Larjavaara et al, 2007; Lim et al, 2007; Louis et al, 2007) and are classified based on well-characterized histological features (Louis, 2006; Scheithauer, 2009; Trembath et al, 2008). The World Health Organization (WHO) defines gliomas by cell type, location and grade, and categorizes them into four classes (Lassman, 2004): i) Grade I tumors, or pilocytic astrocytomas, ii) Grade II tumors, also called low-grade astrocytomas; iii) Grade III tumors, or anaplastic astrocytomas; and iv) Grade IV tumors, also known as glioblastoma multiforme (GBM). Grade I tumors typically do not invade surrounding brain and are often curable with surgery, while tumors of grades II to IV are diffuse and invade normal brain, with grade III and IV tumors being most aggressive. Note, Grade III and IV tumors are called "high-grade" or "malignant" tumors although they almost never metastasize to other tissues of the body (Lassman, 2004).

The etiological events causing glioma formation have not been clearly defined, but are thought to involve genetic alterations that disrupt cell cycle arrest pathways (Zhou et al, 2005; Zhou et al, 2010), and cause aberrant receptor tyrosine kinase activity (Figure 2A) (Dai et al, 2001). For instance, activation of receptors such as the Hepatocyte Growth Factor Receptor, c-Met (Gentile et al, 2008), Platelet-Derived Growth Factor Receptor (PDGFR) (Cattaneo et al, 2006; Natarajan et al, 2006), and Epidermal Growth Factor Receptor (EGFR) (Chicoine & Silbergeld, 1997) are now well-known to stimulate glioma motility. Additionally, marker specific glial progenitor cell (GPC), neural stem cell (NSC) and cancer stem cell (CSC) populations are being investigated for their roles as possible initiators of gliomagenesis (Briancon-Marjollet et al, 2010).

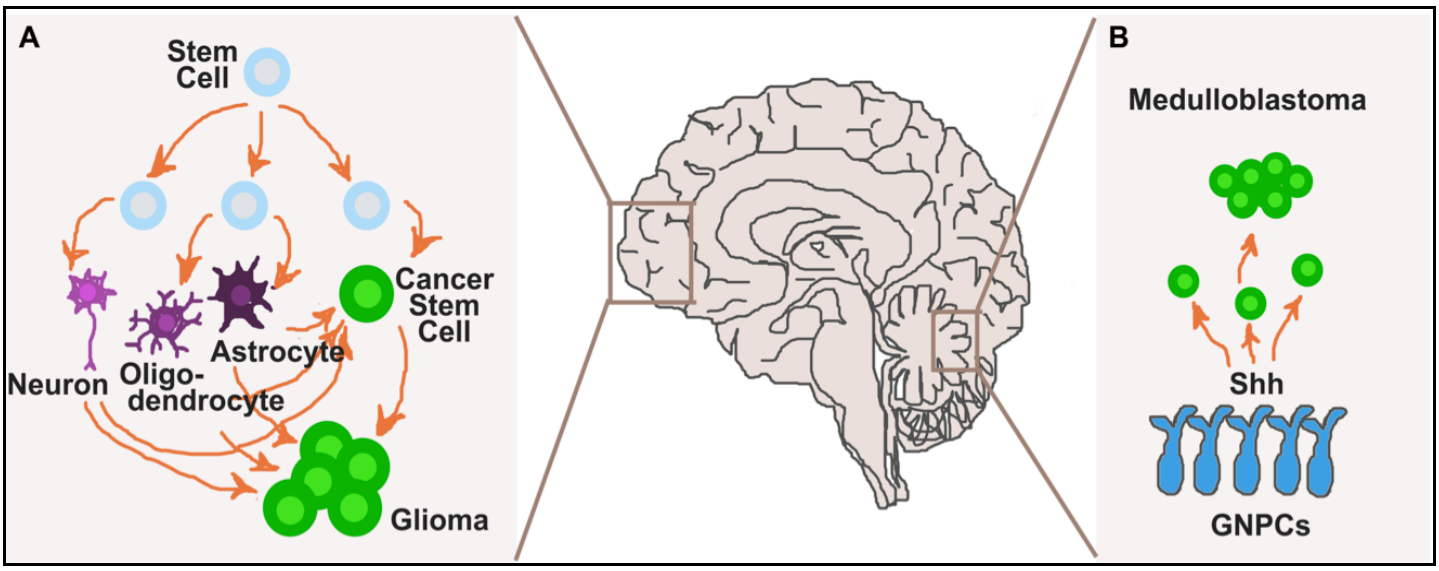

Figure 2: Origin of brain tumors: development gone wrong. (A) During normal brain development, neural stem cells give rise to three main adult cell types: neurons, oligodendrocytes and astrocytes. Genetic alterations occur within these differentiated cells that can lead to the rise of malignant tumors. Alternatively, immature stem cells may serve as cancer stem cells that confer both radio- and chemoresistance phenotypes to gliomas. (B) Medulloblastomas originate in the cerebellum, from granule neuron precursor cells (GNPCs), upon un-controlled activation of Sonic Hedgehog (Shh) signaling pathway.

The current standard of care for gliomas is surgical removal of the tumor followed by post-operative radio- and chemotherapy (Stupp & Weber, 2005). However, due to their diffusely invasive properties, gliomas are one of the most difficult tumors to isolate or treat (Burger et al, 1985). Furthermore, while cell migration is fundamental to normal brain development and homeostasis, unconstrained migration of pathological and diseased cells makes the complete resection of tumor lesions, often performed for other types of tumors, an ineffective clinical treatment in the brain. Prior to the advance of high-throughput genetic screening techniques clinicians depended primarily on GBM recurrence for prognosis of patient survival. Later, the generation of models that combined gene expression and molecular markers made it possible to subcategorize gliomas, enabling the increase in grade-specific predictability (Zhou et al, 2010). Recent findings suggest the possibility that the recurrent growth of GBMs is derived from chemo- and radio-resistant cancer stem cell renewal and/or growth of diffusively invasive cells (Hadjipanayis & Van Meir, 2009). Evidence emerging over the past decade has suggested the existence of stem-like cells within brain tumors, which are currently examined as potential sources of tumor resistance and recurrence (Galli et al, 2004; Lenkiewicz et al, 2009; Singh & Dirks, 2007). The inability to remove high-grade gliomas in their entirety, or to prohibit their migration to other parts of the brain has led to low survival rates among brain cancer patients (Demuth & Berens, 2004). Patients with GBM have a median survival of about 1 year, while patients with anaplastic gliomas can survive 2-3 years, and those with grade II gliomas often survive 10-15 years (Louis et al, 2007).

Medulloblastomas (MBs) encompass a collection of clinically and molecularly diverse tumor subtypes, and are characterized by high tumor invasiveness to extraneural tissues and reoccurrence in the cerebellum after total resection (Dhall, 2009). Four different MB subtypes

have been included in the current WHO classification (Louis et al, 2007): i) Classic MB; ii) Desmoplastic/nodular MB, iii) MB with extensive nodularity, and iv) Anaplastic or large cell MB. Two other variants, medullomyoblastoma and melanotic MB, are much more rare. MBs are overwhelmingly found in pediatric patients, but can rarely occur within adult brain, where the tumor characteristics become very atypical. Adult MB is arguably a biologically distinct challenge in that it exhibits a higher proportion of desmoplastic histological characteristics, shows more proclivity toward cerebellar hemispheric origin, possesses different proliferative and apoptotic indices, and demonstrates a notorious tendency for late relapse with respect to the pediatric variants (Chan et al, 2000; Sarkar et al, 2002).

MBs are thought to arise within the cerebellum, with approximately 25% originating from granule neuron precursor cells (GNPCs) (Gibson et al, 2010) after aberrant activation of the Sonic Hedgehog (Shh) pathway (Figure 2B). A number of genetic alterations have been associated with MB (Biegel et al, 1997; Bigner et al, 1997; Herms et al, 2000; Yin et al, 2002). Studies of the receptors and intracellular signaling pathways that support proliferation and survival of GNPCs have shown a dysregulation of the Shh pathway, the canonical Wnt pathway, or the ERB-B pathway in both familiar and sporadic MBs (Gilbertson, 2004). A recent study showed that Wnt-subtype tumors infiltrate the dorsal brainstem, whereas Shh-subtype tumors are located within the cerebellar hemispheres (Gibson et al, 2010). These results have profound implications for future research and treatment of this childhood cancer, because to date, few data link such genetic alterations to metastasis in MB.

The treatment of patients with standard risk tumors, i.e. those who had tumors completely resected and with no evidence of dissemination to any other part of the body (Nishikawa, 2010), has been somewhat successful with survival rates of up to 40% for gliomas over the last five

years (Van Meir et al, 2010). In contrast, the cure of metastatic disease has until recently been limited to single cases (Fruhwald & Plass, 2002). Although promising, the current treatment options for high-risk brain tumors are associated with neural and neuroendocrine side effects, with a tremendous decline in quality of life among survivors (Edelstein et al, 2011; Palmer et al, 2001), as well as growth reoccurrence and aggressive brain infiltration (Farin et al, 2006).

In the case of gliomas, the migration of cells from primary tumors to other locations within the brain has been one of the most clinically challenging and poorly understood processes that contribute to the poor prognosis of patients. The following sections will discuss the fundamental mechanisms of cellular migration, the common in vivo models used to examine tumor cell migration within the brain, and current in vitro technologies utilized to characterize and better understand the migration of cells derived from gliomas and MBs.

1.1.2. The Role of Growth Factors in Tumor Growth and Migration

There is strong evidence that glioma growth is accelerated through autocrine signaling mechanisms (Hanahan & Weinberg, 2000). In addition to extensive proliferative growth via autocrine signaling, glioblastoma-induced attraction of endogenous neural precursor cells has also been identified as a method of extending tumor survival and increasing growth (Glass et al, 2005). Due to the secretion of various cytokines during autocrine signaling, the concentration of growth factors in the local extracellular environment surrounding developing tumors is elevated to abnormally high levels. Over time, the growth factors diffuse and generate concentration gradients that are sensed by the neighboring cells, thus inducing responsive cells like progenitors to migrate toward the developing tumor during tumor growth (Figure 3). Conversely, diffusely invasive glioma cells are induced to do so by soluble cytokines and growth factors that stimulate directional and random tumor cell motility (Brockmann et al, 2003).

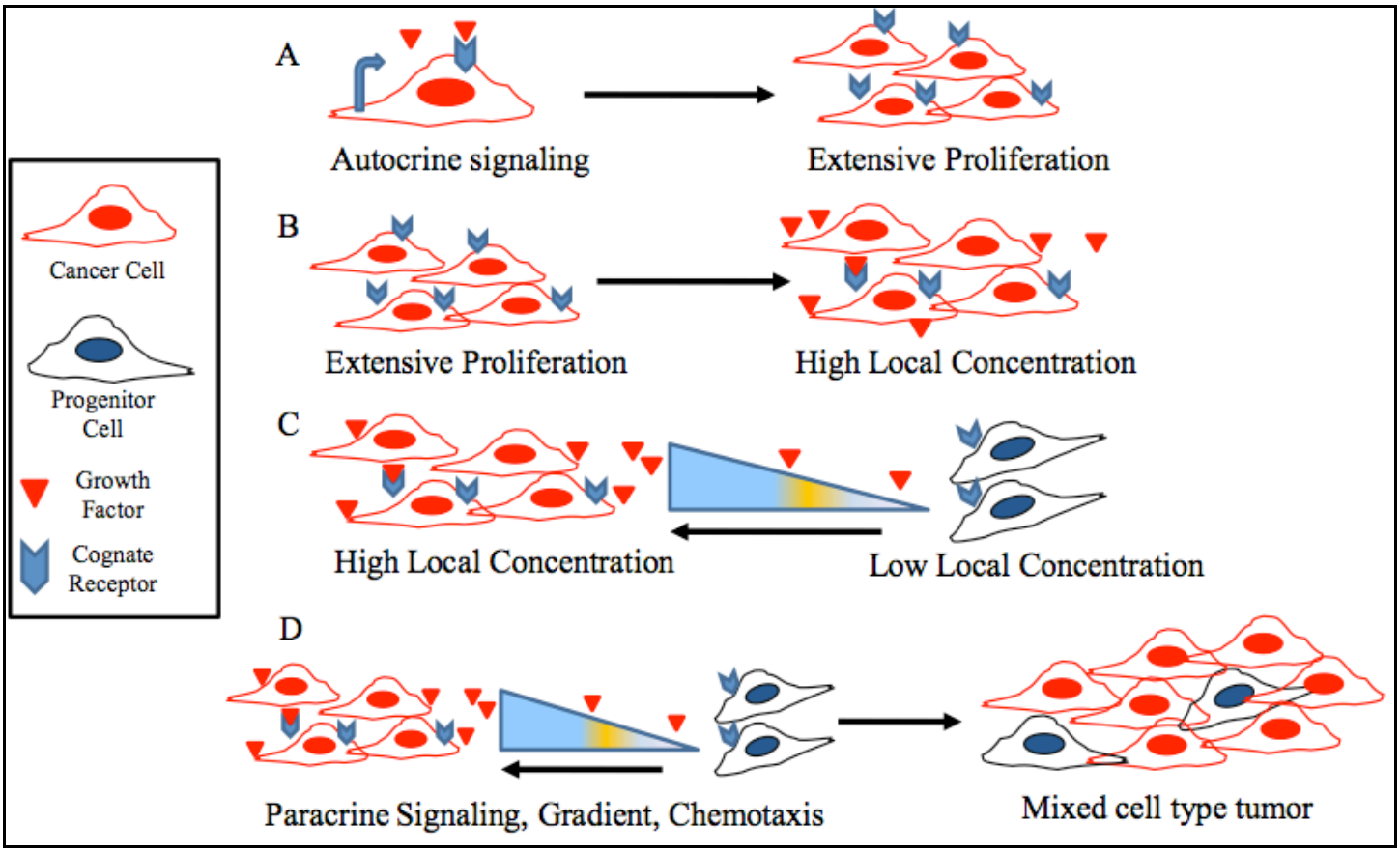

Figure 3: Proposed mechanism for tumor growth via aggressive recruitment of glial progenitor cells. (A) A single cancer cell via autocrine signaling undergoes extensive proliferation that leads to the development of a tumor. (B) Each cancer cell in the tumor secretes growth factors resulting in a high local concentration. (C) Neighboring progenitors respond to the growth factor concentration gradient by migrating toward the tumor. (D) The result is a rapid growth of tumors comprising mixed cell types.

Glial cells express various combinations of cytokine and chemokine receptors, under physiological conditions and generally maintain homeostasis through the control of their proliferation, growth and metabolism. These receptors are involved in numerous physiological processes of glial cells and are commonly found altered in tumor cells. For example, co-expression of PDGF and PDGFR has been shown at all brain tumor stages including low-grade astrocytomas, anaplastic astrocytomas, and glioblastoma multiforme (Maher et al, 2001). These results suggest the possible existence in the gliomas of an autocrine loop comprising of PDGF and its receptors (Dai et al, 2001). PDGF is a powerful mitogen for cells of mesenchymal and glial origin, and has been implicated in the regulation of cell proliferation during normal as well as pathological conditions (Ostman et al, 1992). Since the mid-1970s it has been know that the PDGF family consists of cationic homo- and heterodimers of disulfide-bonded A- and B polypeptide chains, each 100 amino acid residues long, that bind to and cause the dimerization of α and β receptors (Westermark & Heldin, 1989). More recently, novel family members PDGF-C and PDGF-D have been discovered, which has triggered a search for novel activities and complementary fine-tuning between the members of this family of growth factors (Reigstad et al, 2005). PDGF also appears to be ubiquitous in neurons throughout the CNS, where it is suggested to play an important role in neuron survival and regeneration, and in mediation of glial cell proliferation and differentiation. Moreover, aberrant synthesis of PDGF and concomitant autocrine growth stimulation may be an important step in the neoplastic conversion of PDGF receptor-positive cells (Westermark & Heldin, 1989).

Growth factors originally were linked to tumorigenesis, as a number of retroviral oncogenes were found to derive from peptide growth factors and their receptors. In 1983, there were two pioneering articles published that suggested the possibility that PDGF autocrine signaling was involved in tumor formation (Doolittle et al, 1983; Waterfield et al, 1983). Evidence for the involvement of autocrine stimulation came later with the finding that the oncogene v-sis of the simian sarcoma virus is derived from the mammalian gene encoding the B chain of PDGF (Nister et al, 1988; Westermark & Heldin, 1991). To date, there are over twenty known retroviral oncogenes that have associated cellular proto-oncogenes that are mostly involved in cell survival pathways.

1.1.3. Mechanism of Migration

The migration of brain cancer cells is highly complex, involving interactions with extracellular matrix, and chemoattractants that either diffuse from blood vessels and/or are produced by neighboring cells (Condeelis & Segall, 2003; Sahai, 2005). As a consequence of such complexity, the molecular mechanisms of primary brain tumor migration and metastasis are poorly understood. Over the last several years, a critical group of suspected growth factors has been the topic of research for their role as regulators of tumor biology and chemotaxis (Hamel & Westphal, 2000). It is believed that over time secreted cytokines diffuse and generate concentration gradients that are sensed by glioma and MB-derived cells, leading to the detachment and migration of these cells away from the primary tumor (Chicoine & Silbergeld, 1997; Piperi et al, 2005). Therefore, brain tumor invasion is believed to be induced by soluble cytokines that stimulate directional and/or random tumor cell motility (Brockmann et al, 2003). Alternatively, cancer cells may communicate with specific distant targets through secreted microvesicles that contain growth factors and receptors, functional mRNAs, and miRNAs (Cocucci et al, 2009; Skog et al, 2008; Valadi et al, 2007). Such microvesicles are shed by most cell types, including cancer cells, and have been found in sera from numerous cancer patients (Cocucci et al, 2009; Skog et al, 2008).

While the effects of mitogens on the in vitro motility and invasion of glioma cells have been well-documented using conventional assays, such as transwell chambers and spheroid models (discussed in this chapter), the ability of soluble cytokines to drive various cellular functions (i.e. migration and/or proliferative growth) has been shown to depend upon several determinant factors. Some of these factors have been addressed in the literature, such as dosage-dependence (Gonzalez-Perez & Quinones-Hinojosa, 2010; Shih et al, 2004), contact inhibition

(Weidner et al, 1990), as well as autocrine and paracrine signaling-driven tumor growth via extensive proliferation and aggressive recruitment of surrounding cells to the tumor (Betsholtz et al, 1984; Fomchenko & Holland, 2005; Hermansson et al, 1988; Rood et al, 2004). The diligent study of Central Nervous System tumor cell (CNSTC) invasion has identified four commonly overexpressed receptor tyrosine kinases as targets for anti-invasive therapies (EGFR, c-MET, PDGFR, and Vascular Epidermal Growth Factor Receptor (VEGFR)) (Abounader, 2009; Arora & Scholar, 2005; Huang et al, 2009; Zwick et al, 2001).

Cancer cell locomotion is highly sensitive to stimuli from the ECM as well as from the surrounding media. Receptors on the plasma membrane can activate cellular signaling pathways that alter the mechano-transduction of a cell via reorganization of motility-related organelles and cellular compartments. As an example, tumor-derived cells are known to increase cell motility in response to protease inhibitors and adhesion inhibitors (Sahai, 2005). The modes of cancer cell migration vary according to whether the cells undergo single cell, chain, or collective migration, as described below. Tumor-derived cells disseminate from the bulk tumor mass individually via mesenchymal or amoeboid movement. However, in many tumors both single cell and collective cell migration may be present depending on the molecular cues dictating migration (Friedl & Wolf, 2003).

During the mesenchymal-type migration often observed in gliomas, cells exhibit a highly polarized and fibroblastic morphology (Zhong et al, 2010). Cells undergo the classical, overlapping processes generally exhibited during mammalian cell migration: cell polarization, protrusion of leading edge, traction at the trailing edge, and detachment (Figure 4) (Friedl & Wolf, 2003; Lauffenburger & Horwitz, 1996). First, cells become highly fibroblast-like, with bipolar opposites. Second, a growing number of actin filaments begin to push the cell membrane

outwards on the leading edge via the formation of lamellipodia or filopodia. Actin polymerization then initiates signal transduction pathways along the leading edge. Next, cell integrins come into contact with ECM ligands and cluster to recruit intracellular signaling proteins that induce phosphorylation signaling, or so-called "outside in" signaling (Hynes, 2002; Miyamoto et al, 1995) via focal adhesion kinases. Afterwards, surface proteases act to cleave ECM molecules via production of soluble MMPs in order to degrade surrounding ECM. Finally, cell contraction occurs via myosin that leads to focal contact disassembly at the trailing edge and actin cleavage and filament turnover (Wear et al, 2000).

Contrarily, during amoeboid movement, cells utilize a "fast gliding" mechanism driven by weak interactions with the substrate (Figure 4). As such, cells like neutrophils and lymphocytes exhibit a shape-driven migration with appreciable lack of focal adhesions that allows them to circumnavigate rather than degrade surrounding ECM during migration (Friedl et al, 2001). The result is an increased cell motility, as well as cell ability to undergo early detachment and metastatic spread from primary tumors. Cancer cells may undergo conversion from mesenchymal to amoeboid type migration in order to alter integrin distribution and actin cytoskeleton organization for increased dissemination (Wolf et al, 2003).

Collective migration is a well-studied phenomenon that is characteristic of embryological development, such as during the migration of cell clusters or sheets in the ectoderm following closure of the neural tube (Davidson & Keller, 1999). In vitro studies (Friedl et al, 1995; Nabeshima et al, 1995) showed that cells can migrate as a functional unit, and that in contrast to single motile cells, cell-cell adhesion can lead to a particular form of cortical actin filament present along cell junctions. This enables formation of a larger, multicellular contractile body. Here, a select set of highly motile cells are designated as so-called "path-generating" cells that

create migratory traction via pseudopod activity (Friedl et al, 1995; Hegerfeldt et al, 2002; Nabeshima et al, 1995). It is then believed that cells located in the inner and trailing regions are passively dragged behind during dissemination. In tumors, collective migration has been observed as protruding sheets that maintain contact with the primary site, or as cell clusters that detach from their origin and extend along paths of least resistance (Byers et al, 1995; Hashizume et al, 1996; Madhavan et al, 2001). Collective migration offers the advantage of protection from immunological response. Further, heterogeneous sets of cells that move as one functional unit can work together to promote the invasion of less motile, but potentially apoptosis-resistant, sub-populations that increase tumor survival. To complicate matters, cells may transition between collective and individual cell migration with dedifferentiated cells to increase dissemination and metastatic spread (Friedl & Wolf, 2003).

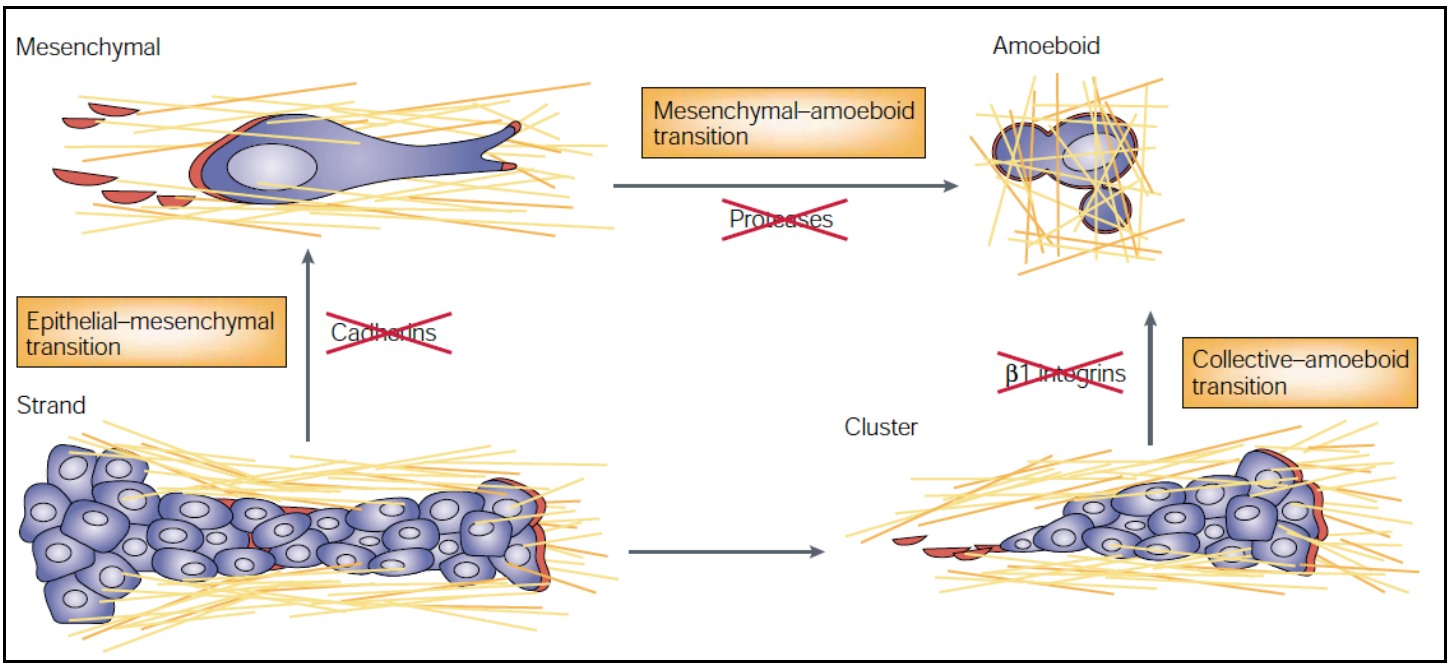

Figure 4: Plasticity of tumor invasion mechanisms. Disseminating cancer cells can undergo a variety of adaptation reactions in response to changes in their molecular migration program. In cancer-cell collectives, such as epithelial sheets or strands, individual cells that have lost cell–cell interactions (such as by inhibition of cadherin function) can detach, and use integrins and proteases to develop a mesenchymal-type migration (epithelial–mesenchymal transition). When proteases such as matrix metalloproteinases (MMPs), serine proteases and cathepsins are blocked in cells that are undergoing mesenchymal migration, these cells can adapt by using protease-independent amoeboid crawling (mesenchymal–amoeboid transition). Amoeboid single-cell migration can also result from cell collectives and clusters after treatment with adhesion-disrupting anti-β1 integrin antibodies. By directly and indirectly interfering with cell–cell junctions, as well as adhesion to collagen fibers, single cells detach and migrate by β1-integrin-independent amoeboid mechanisms. All these transitions can be induced by drugs that are designed to inhibit cancer-cell migration, such as integrin or cadherin antagonists and protease inhibitors. Similar transitions might also occur spontaneously during tumor progression. (Courtesy of Friedl and Wolf, 2003)

1.1.4. Models for the study of brain tumor invasion in vivo and ex vivo

Glioma and MB models have been largely developed by studying altered oncogene expression through retroviral transfection of murine neural tissue of genetically engineered mouse models (GEMMs) (Fisher et al, 1999; Hatton et al, 2008; Heyer et al, 2010; Huse & Holland, 2010; Pazzaglia et al, 2002; Pazzaglia et al, 2006; Romer & Curran, 2004). Via this powerful methodology, diverse tumor types with distinct histological features have been generated dependent upon the specific genetic background of the cell of tumor origin and the disease location of interest (Furnari et al, 2007). In particular, the histological features of GEMM and implanted xenograph derived tumors have been shown to be similar to human brain tumors presented in identical CNS locations, and have shed light on the diverse nature of human gliomas found clinically (Candolfi et al, 2007).

Historically, it has been suggested that glioma cell infiltration throughout the brain primarily utilizes mechanisms of migration innately patterned by neural progenitors during normal brain development (Cayre et al, 2009; Kakita & Goldman, 1999; Scherer, 1940). Confirmation of this similarity has been accomplished in vivo via implanted xenographs that result in spontaneous intracranial glioblastomas in six different animal model variations that show reproducible invasion of tumor cells into non-neoplastic brain regions (Candolfi et al, 2007) (Figure 5). More recently, several labs began utilizing GEMMs to specifically examine glial progenitor recruitment in vivo (Assanah et al, 2006; Masui et al, 2010). For instance, Assanah and colleagues have demonstrated via the histological analysis of cortical sections from GEMMs that overexpression of tumor inducing proteins like PDGF can induce malignant glioma cells to invade across the corpus callosum into the contralateral hemisphere and overlying cortex (Assanah et al, 2006; Assanah et al, 2009).

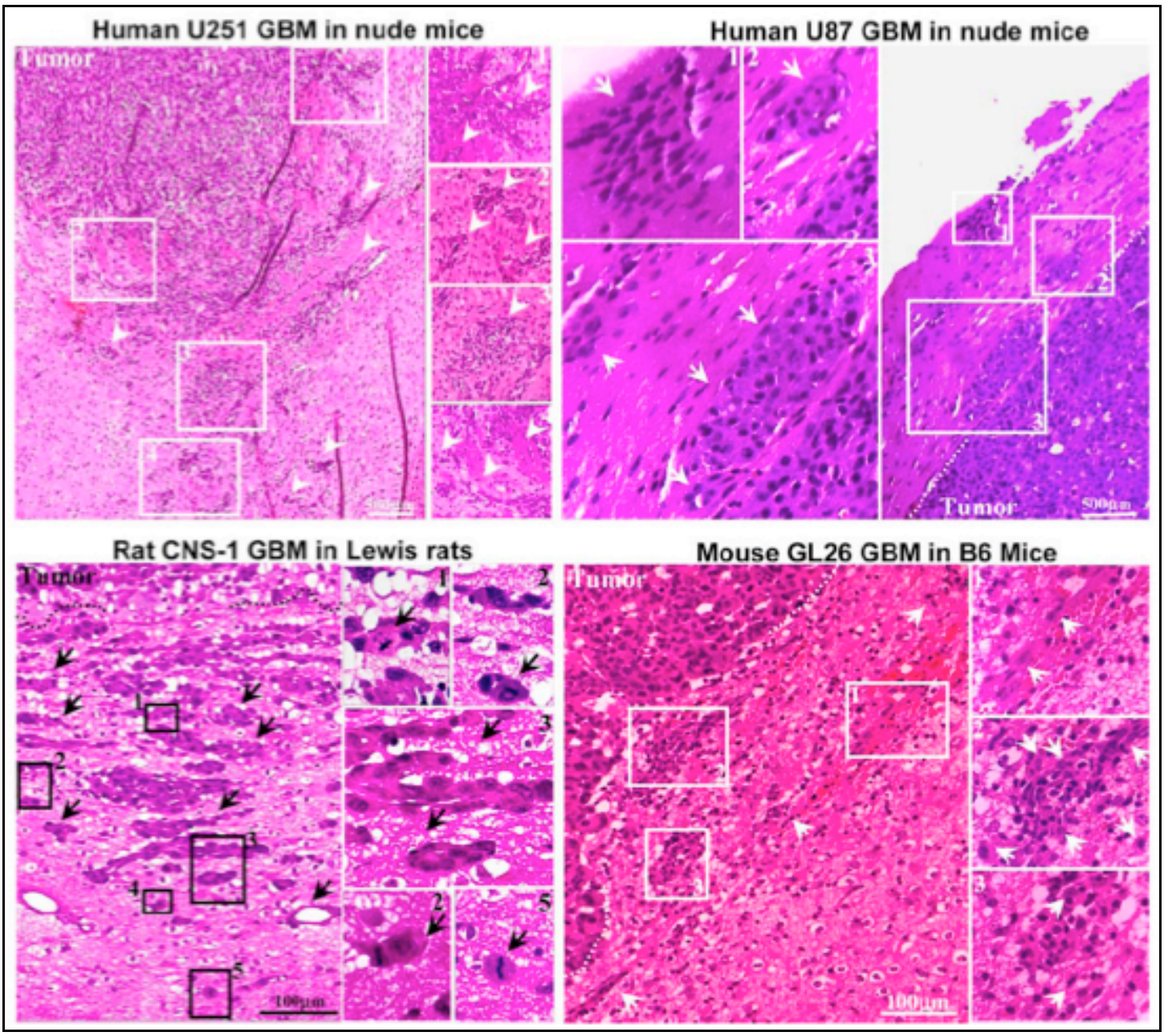

Figure 5: Neoplastic cellular infiltration into surrounding non-neoplastic brain tissue in syngeneic rat (CNS-1) and mouse (GL26) GBM models and human glioma xenografts in nude mice (U251 and U87). Paraffin sections (5 μm) from GBM were stained with hematoxylin and eosin for evaluating neoplastic invasion. The numbers in low-magnification microphotographs depict areas magnified in the microphotographs on the right. Arrows indicate malignant cells, clusters of GBM cells, and tumoral blood vessels infiltrating surrounding brain parenchyma. The indistinct tumor borders and the malignant cells clearly entering the non-neoplastic brain tissue suggest an invasive phenotype. (From Candolfi et al., 2007)

The diffusive invasion and increased recurrence of gliomas post-operatively have been attributed to the same therapies used to treat the disease. Narayana and colleagues reported clinical results of 61 high-grade glioblastoma patients treated with bevacizumab, the humanized anti-angiogenesis drug that antagonizes VEGF-A. Their results showed that 82% of the patients treated with bevacizumab suffer from tumor regrowth and 70% died from the disease within 19 months (Narayana et al, 2009). Pàez-Ribes and colleagues reported similar results showing that although the use of angiogenesis inhibitors, such as Sunitinib and SU10944, extend that survival time of treated mice to an additional 7 weeks versus non-treated mice, the kinase inhibitors tend to also evoke an increase in glioma cell invasion as well as to promote tumor progression (Paez-Ribes et al, 2009). A closer examination using xenographs of human tumor spheroids implanted into rat brains, and further treated with the bevacizumab, led to a reduction in contrast enhancement in magnetic resonance imaging (MRI) analysis while enhancing glioma cell diffusion by 68% versus non-treated rats (Figure 6) (Keunen et al, 2011).

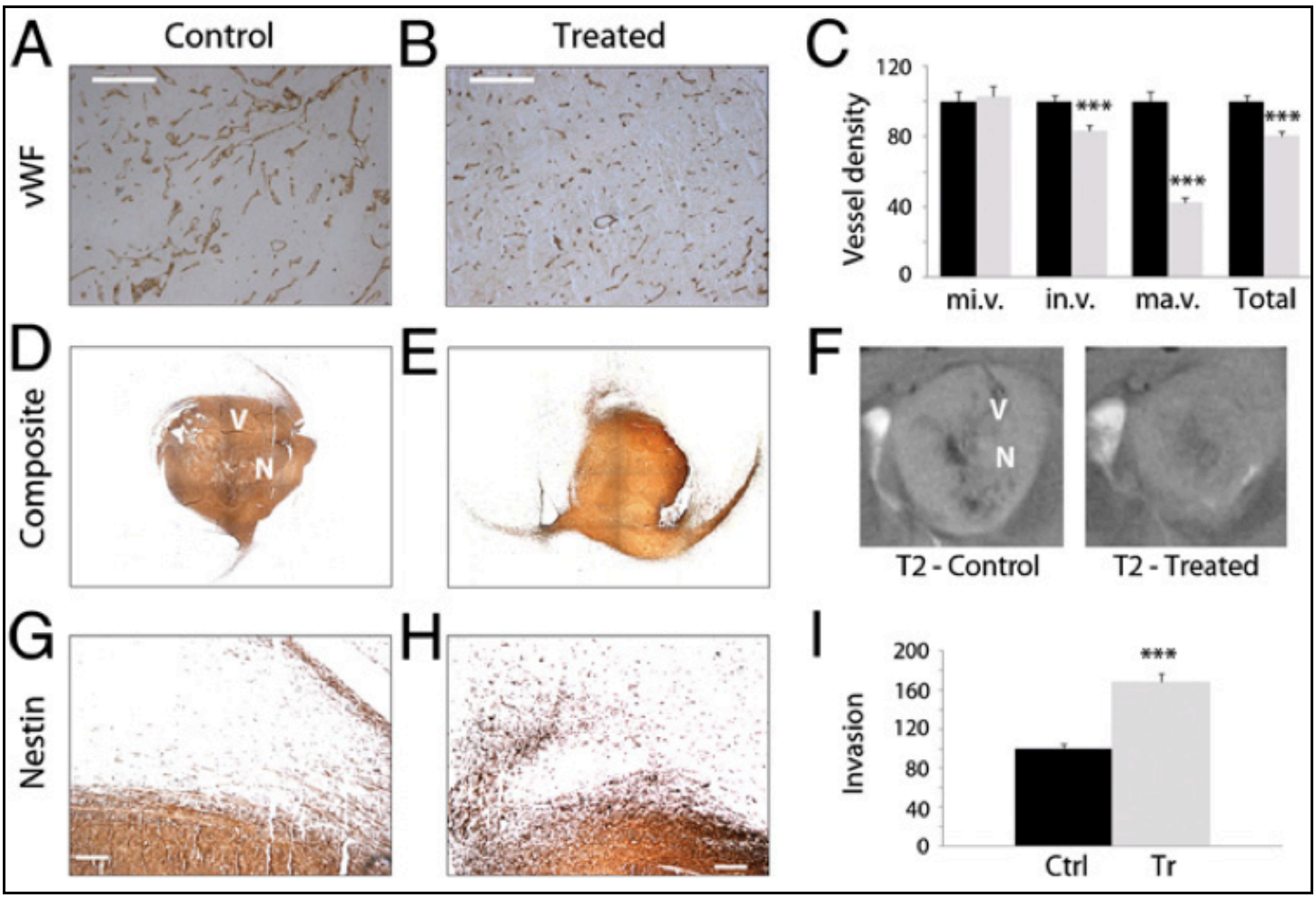

Figure 6: Changes in blood vessel morphology and tumor cell invasion after bev treatment. Immunostaining for von Willebrand factor (vWF) (A and B) and quantification thereof (C), indicating a significant reduction in the density of medium and large blood vessels and in total vessel number after bev treatment. (Scale bar: 200 μm.) Nestin-stained composite images (D and E) reveal a more homogeneous appearance of the treated compared with untreated tumors, also reflected in corresponding T2-weighted MRI images (F). Large vessels ("V") appear as dark tortuous lines in nestin and T2- weighted images and necrotic areas ("N") as brighter spots. Quantification of the nestin-positive cells outside the tumor core (G and H) shows a 68% increase in cell invasion after treatment (I). mi.v: microvessels; in.v: intermediate-sized vessels; ma.v: macrovessels; Ctrl: controls; Tr: treated. (Scale bars: ± SE.) ***P < 0.001. (From Keunen et al., 2011)

Characterization of MB migration in vivo has yet to be analyzed at large, as most of the reports to-date focused on tumor growth and not its dissemination. Nevertheless, a select number of in vivo studies examined tumor cell migration and invasion. Hatton and colleagues illustrated in a GEMM for MB that 94% of the mice developed MB by 2 months of age, and that these tumors frequently exhibited leptomeningeal spread, a common feature of the human disease (Hatton et al, 2008). Keunen and colleagues implanted human MB cells in the brain of nude mice, and thereafter followed them in vivo at single-cell level via fluorescence microscopy (MacDonald et al, 1998). These MB cells were shown to invade the brain and to form distant micro-metastases. In another study, MB cells were engineered to overexpress HGF and were implanted subcutaneously and intra-cranially (Li et al, 2005). The study reported activated c-Met that strongly increased MB xenograft growth and invasive characteristics with finger-like protrusions, metastatic growth, and leptomeningeal spread. Such findings illustrate that the HGF/c-Met pathway is one of the mediators of MB malignancy.

The ability to visualize brain tumor invasion in direct response to specific genetic aberrations and alterations made to the immediate environment has been critical in understanding the characteristics of this process. An advance made in this direction was accomplished via the detection of specific biomarkers involved in the progression or migration of CNSTCs, e.g. Receptor Tyrosine Kinases (RTKs), using conjugated antibodies that enabled in vivo monitoring via MRI (Towner et al, 2008). Alternatively to in vivo imaging procedures, ex vivo brain tumor invasion assays that enable the study of tissue outside of the living system have had a tremendous impact in the field. Brain slices from mice and rats have been used to quantify the invasion of human gliomas (Nakada et al, 2004), and have demonstrated suppressed invasion of on 2D surfaces, suggesting that the brain environment alone is capable of regulating protein

function and, consequentially, the pattern and directionality of glioma migration (Beadle et al, 2008). Additionally, not only have ex vivo cell cultures been used to study the invasive properties of CNS tumors, but also to characterize the expression of molecular markers (Riffkin et al, 2001) and to evaluate the therapeutic potential of co-cultured T-cells for anti-tumor activity (Ahmed et al, 2007).

By reducing the incidence of recurrent growth, clinicians envision the possibility of detecting and directly tracking migratory tumor cells in vivo, and therefore enabling operative procedures limited to a single total resection surgery. In order to accomplish this goal, there is a stringent need for development of enhanced imaging tools to allow visualization of migrating tumor cells. Meanwhile, the most successful quantitative assessment of CNSTCs migration has been accomplished outside of the brain itself, in engineered systems redesigned to mimic specific in vivo conditions. We will discuss these in vitro assays further, which have been utilized to evaluate a variety of cellular functions, from growth patterns and rates, to invasive motility of cells derived from highly malignant brain tumors.

1.1.5. Models for the study of brain tumor invasion in vitro

Tumor cells of the brain have been characterized as having a highly infiltrative phenotype for spreading into the healthy surrounding parenchyma. This malignant property is arguably the principle reason for tumor recurrence and high mortality rates (Lim et al, 2007). The interaction of integrins, membrane anchored heterodimeric proteins, with various extracellular matrix (ECM) proteins has been explored extensively, as it is one of the key events that occurs during the invasion of tumor cells within their local microenvironments (Teodorczyk & Martin-Villalba, 2010). Another key process of tumor invasion is the cellular secretion/production of proteases

that degrade ECM proteins in order to create pores through which the cells may migrate; such proteases include serine proteases, various matrix metalloproteases (MMPs), and Cathepsins (Rao, 2003). In addition to stimulating tumor invasion via degradation of ECM protein components, it is assumed that MMPs are capable of enhancing tumor growth by indirectly triggering the release of growth factors trapped within the basement membrane itself (Mott & Werb, 2004). Lastly, another key aspect of tumor dissemination is played by the activation of RTK signaling pathways. During the destruction of the basement membrane by MMPs, soluble growth factors are un-sequestered from the ECM and bind to their cognate cellular receptors to trigger a cascade of events that enhance cellular migration (Zucker et al, 2000).

In vitro invasion assays are important tools for investigating the tumor-matrix interactions and the effects of extracellular macromolecules on these interactions. While not identical to in vivo behavior, the study of tumor cell migration in vitro is advantageous due to the tightly-controlled experimental conditions, higher experimental throughput, and lower costs. The following section discusses the most commonly used in vitro assays, in the order of increased complexity.

1.1.5.1. Culture Dish Assays

Culture dish assays have the advantage of design simplicity and execution, while providing insightful information pertaining to cell-to-cell and cell-to-environment interactions. Coated culture dishes have been widely used to examine the roles played by specific ECM proteins, integrins, MMPs, and RTKs in stimulating the migration of brain tumor-derived cells, as detailed here.

Integrins are membrane heterodimeric proteins that mediate cell-environment attachment (Hynes, 1987; Tucker, 2006). In addition to anchoring cells to their environment, integrins have been shown to serve as signal mediators for ECM proteins that were found to stimulate tumor migration in vitro (Ohnishi et al, 1997; Tysnes et al, 1996). The most abundant ECM proteins found to interact with integrins in the brain are fibronectin, laminin, fibrinogen, tenascin-C, thrombodpondin, neuron-glia cell adhesion molecules (Ng-CAMs), and collagens IV and V (Rutka et al, 1988). Giese and colleagues evaluated astrocytoma migration as a function of integrin adhesiveness on various ECM proteins (collagen IV, fibronectin, laminin and vitronectin) (Giese et al, 1994). Based on the examination of eight different astrocytoma cell lines, the group concluded that the migration of glioma cells was subject to alteration depending on tumor expressed integrins and the availability of complementary matrix proteins. Furthermore, even though laminin frequently enabled tumor cells to adhere and migrate with increased adhesion, overall it was stated that there was no specific ECM protein that would always result in increased astrocytoma binding (Giese et al, 1994).

Friedlander and colleagues examined the migration trends of twenty-four excised human astrocytomas, ten glioblastoma cell lines, and three medulloblastoma cell lines on nine different ECM protein coated culture dishes (Friedlander et al, 1996). The comparative migration of astrocytomas (grades I, II and III), glioblastomas and MBs demonstrated that most tumor cells, regardless of their grade, were capable of migrating on fibronectin and laminin at rates exceeding 30 μm over 16 hours. A closer comparison between low-grade and high-grade tumor migration on all tested substrates revealed that, on average, high-grade tumors migrated approximately 14 μm more than low-grade tumor cells under similar conditions. Specifically, type IV collagen substrates induced a 4-fold increase in distances traveled by high-grade tumor cells over low-

grade cells. Collagen IV coated substrates also stimulated approximately 100 μm migration over 16 hours of thirteen excised glioblastomas and eight well studied glioblastoma cell lines, with cell lines being more motile than the excised tumors (Friedlander et al, 1996). Finally, monoclonal antibodies specific for the α_v and β_1 integrins were used to reduce the migration of four glioblastoma cell lines (U-373 MG, U-118 MG, U-251 MG and U-87 MG) on several migration enhancing ECM substrates, including collagen type IV (Friedlander et al, 1996). These results illustrate that brain tumor-derived cells can migrate remarkably large distances within the brain, often to varied regions of the brain. However, tumor cell populations are very diverse, and such studies have not identified the lineage of motile cells, or whether certain sub-populations of cells could migrate farther than others within brain.

MB samples revealed type I collagen present in the leptomeninges, and in the ECM surrounding blood vessels and tumor cells (Liang et al, 2008). Expression of both type I collagen and β_1 integrin, a subunit of a known type I collagen receptor, localized to the same area of MB. This same study also showed that the adherence of MB cells to type I collagen matrix in vitro depends on the presence of β_1 integrin (Liang et al, 2008).

A study by Corcoran and Del Maestro revealed that MB cell lines do not defer cell proliferation for migration across an uncoated surface or invasion of a type I collagen matrix, contrary to the "Go or Grow" hypothesis (Corcoran & Del Maestro, 2003). The "Go or Grow" hypothesis proposes that cell division and cell migration are temporally exclusive events and that tumor cells defer cell division to migrate (Giese et al, 1996). Migrating and invading MBs continued to proliferate and migrate/invade, irrespective of the number of divisions that took place (Corcoran & Del Maestro, 2003). These findings emphasize the need to evaluate the effect

of future therapies on both biological events and, if possible, to identify intracellular signaling proteins that negatively regulate MB migration/invasion and proliferation.

Matrix-degrading proteases are involved in the hydrolytic breakdown of ECM proteins and have been shown to regulate tumor cell progression and invasion (Levicar et al, 2003; Rao, 2003; Rooprai & McCormick, 1997). Additionally, proteases have been well-studied and shown to display differential expression and activation patterns, correlated to their invasion-associated effects, i.e. angiogenesis (Forsyth et al, 1999; Thorns et al, 2003). These proteases are either located in the membrane of the cell or secreted into its surroundings, respectively denoted as MT-MMP and MMP. Diffusely invasive glioma cells express MMPs that enable them to catabolize ECM proteins that have been shown to prohibit the migration of other cells that lack these MMPs. For instance, specific membrane proteins expressed by CNS myelin have been shown to have anti-spreading functionality on neurite outgrowth, astrocytes and fibroblasts (Schwab & Caroni, 1988; Spillmann et al, 1998).

The migration of glioma-, MB- and meningioma- cell lines on CNS myelin was found to be tumor grade-dependent and to involve active unspecified MMPs (Amberger et al, 1998). Culture dishes were coated with 15 μg/well rat spinal cord myelin, a concentration shown to reduce by 80% the migration of fibroblasts, followed by the seeding with various cell lines and the recording of cell ability to adhere and spread (Amberger et al, 1998). The results conclude that high grade glioblastomas, like U-251 MG, were able to strongly attach and spread, while low grade gliomas and MB exhibited poor attachment and inhibited spreading (Amberger et al, 1998). Additionally, spreading of GBM and Anaplastic Astrocytomas (AA) cells on CNS myelin was strongly blocked when cells were treated with the MMP blocker O-phenanthroline (Felber et

al, 1962), and temporarily inhibited with carbobenzoxy-Phe-Ala-Phe-Tyr-amide (Amberger et al, 1997) confirming the role played by MMPs in ECM modification as a precursory for migration.

Belien and colleagues studied the role of MT1-MMP in enhanced spreading and migration of gliomas (Belien et al, 1999). As a substrate, they utilized myelin-coated culture dishes, since it was previously shown that invasion of gliomas predominantly occurs along the white matter of the CNS (Giese et al, 1996; Pedersen et al, 1995), which is heavily composed of myelin (Baumann & Pham-Dinh, 2001; McLaurin & Yong, 1995), to seed both gliomas and MT1-MMP-transfected fibroblast. In this case, MT1-MMP was shown to be responsible for altering the cellular environment to enable migration of gliomas and the transfected fibroblasts (Belien et al, 1999).

When the invasiveness of five MB cell lines within a 3D in vitro collagen I or IV-based model was studied, the data showed that within hours of implantation, individual cells readily detached from the surface of the cell aggregates and invaded the collagen matrix, to distances of up to 1,200 μm and at rates of up to 300 μm per day (Ranger et al, 2010). Furthermore, MB invasiveness within this 3D model appears to depend upon a combination of metalloproteinase (MMP-1 and -2, TIMP-1 and -2) and cysteine protease activity (Ranger et al, 2010).

The receptor tyrosine kinases, like integrins, function as signal mediators of extracellular proteins yet in a different way. Integrins, as mentioned above, interact primarily with static, structural ECM proteins that are the composite materials of the cellular environment (Tucker, 2006). Meanwhile, RTKs interact with soluble macromolecules present in the environment, e.g. growth factors, that trigger a cascade of events in the cells spanning from the extracellular surface of the plasma membrane to the nucleus, to elicit various cellular responses (Konopka & Bonni, 2003; Mueller et al, 2003; Teodorczyk & Martin-Villalba, 2010). Additionally,

genetically modified and overexpressed RTKs are capable of eliciting cellular signals in the absence of ligand binding, thus bypassing the need for an extracellular trigger (Akbasak & Sunar-Akbasak, 1992; Dong et al, 2011; Strommer et al, 1990; Torp et al, 2007). Ding and colleagues employed U-87 MG cells grown on coated cultured dishes to demonstrate a strong adhesion to vitronectin, as opposed to collagen or laminin, which was mediated through the $\alpha_v\beta_3$ and $\alpha_v\beta_5$ integrins (Ding et al, 2003). Additionally, the group was able to link the specific cooperative interaction between the RTK PDGFRβ and the $\alpha_v\beta_3$ integrin to induce migration of U-87 MG cells into the wounded area in a scratch-wound assay after treatment of the culture with a 83 pM concentration of PDGF (Ding et al, 2003). Therefore, these results suggest the direct correlation between the ability of RTKs to transmit extracellular signals into the cell and to convert these signals into direct and measurable cellular response.

As an improvement upon the simple use of cell culture dishes for study of tumor cell migration, micropipette turning assays have been used to create gradients within culture dishes that enable changes in cell migration with micropipette position. Gradients, defined as fields where biochemical concentrations are varied along a specific distance, are generated via simple diffusion of biological molecules from the micropipette into the culture medium. Gradient formation and stability are functions of the molecular properties of the stimulant being used (i.e. diffusivity constant and molecular weight) as well as pipette mechanics (i.e. dimensions and flow rates) (Lohof et al, 1992), and for these reasons make gradient measurement difficult. Wyckoff et al. used the micropipette method to collect subpopulations of motile mammary carcinoma and macrophage cells into microneedles filled with Matrigel™ and a range of EGF concentrations from confluent culture dishes (Figure 6) (Wyckoff et al, 2000). The Matrigel™ matrix is a solubilized basement membrane preparation extracted from Engelbreth-Holm-Swarm (EHS)

mouse sarcoma (Ohashi et al, 2006; Reed et al, 2009), commonly used in cell-matrix interaction studies. The contents of the microneedles were then emptied into new culture dishes and allowed to grow for at least 6 days before quantifying cell populations. A bell-shaped curve of normalized cell numbers was reported and had the maximal number of collected cells for 25 nM EGF, 8-fold greater than controls (Wyckoff et al, 2000). Such results illustrate that growth factor concentration gradients, or differences in concentrations along given distances, stimulate brain tumor cell migration.

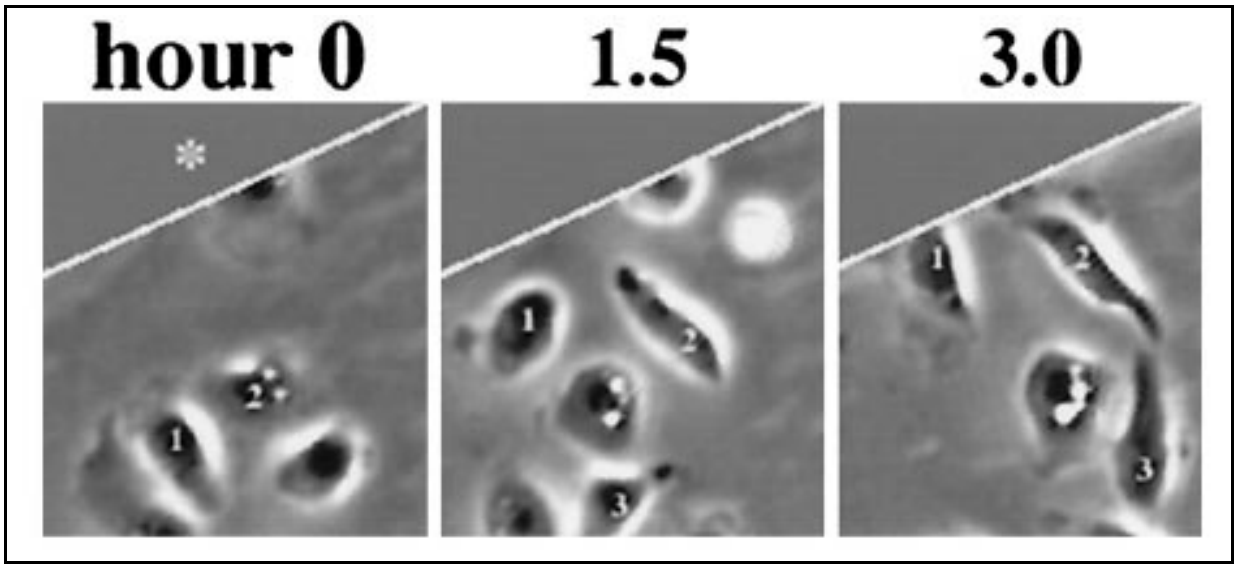

Figure 7: Tumor cells chemotax toward needles containing EGF. Cells are seen orienting and moving toward a needle containing matrigel and 25 nM EGF. By 1.5 h after the needle was placed in the culture dish, cells 1 and 2 have already oriented themselves toward and have moved in the direction of the needle, whereas cell 3 has entered the field of view. By 3 h, cells 1 and 2 have reached the matrigel edge. The edge of the matrigel (*) is delineated by the white line and shown in gray. Only motile cells within the field are numbered. The average velocity of the cells is 0.32 ± 0.03 μm/min. (Courtesy of Wyckoff et al., 2000).

1.1.5.2. Spheroids

A key question regarding cancer cell migration and invasion is based on determining the reason why tumor cells detach from the bulk tumor mass. Some studies have suggested that lack of contact-inhibition may be responsible for cell migration away from the bulk (Pedersen et al, 1995). While normal cells go into a quiescent state that allows apoptosis during nutrient depleted states, cancer cells do not rely on contact-dependent growth and therefore can detach and venture out to diffusely invade the parenchyma. The Spheroid Model utilizes the natural tendency of cancer cells to form colonies and to grow into localized spheres (Santini & Rainaldi, 1999; Zhang et al, 2005). This model mimics the 3D characteristics of cell migration, while culture dish experiments described in the previous subsection provide important data concerning 2D cell migration. As a result, the spheroid model has been used to study the directional migration of tumor cells from the bulk spheroid mass in response to specific motogens and chemotherapeutic agents, as well as to measure the penetration of various molecules into the tumor (Carlsson & Nederman, 1983; Nederman et al, 1983).

Spheroids grown from several different GBM cell lines were placed on uncoated 24-well dishes and treated with EGF, which triggered a strong stimulation of cellular invasion and increased growth (Lund-Johansen et al, 1990). Similarly, spheroids grown from several human glioma cell lines exhibited enhanced growth and directional migration when cultured in 10 ng/ml EGF or 10 ng/ml bFGF concentration, compared to control and other growth factors, such as PDGF-BB (Engebraaten et al, 1993). When MB cultures were induced to generate spheroids, gene expression of CD133 (a hallmark of the brain cancer stem cells and radio-resistant tumors), membrane type-1 matrix metalloproteinase (MT1-MMP), and MMP-9 were induced and correlated with increased invasiveness of the spheroid cells (Annabi et al, 2008). Additionally,

Corcoran and Del Maestro revealed that MB cells from an established cell line, UW228-13, could exhibit elevated levels of invasion into a 3-dimensionsal matrix of type I collagen compared to biopsied DAOY cells (Figure 8) (Corcoran & Del Maestro, 2003).

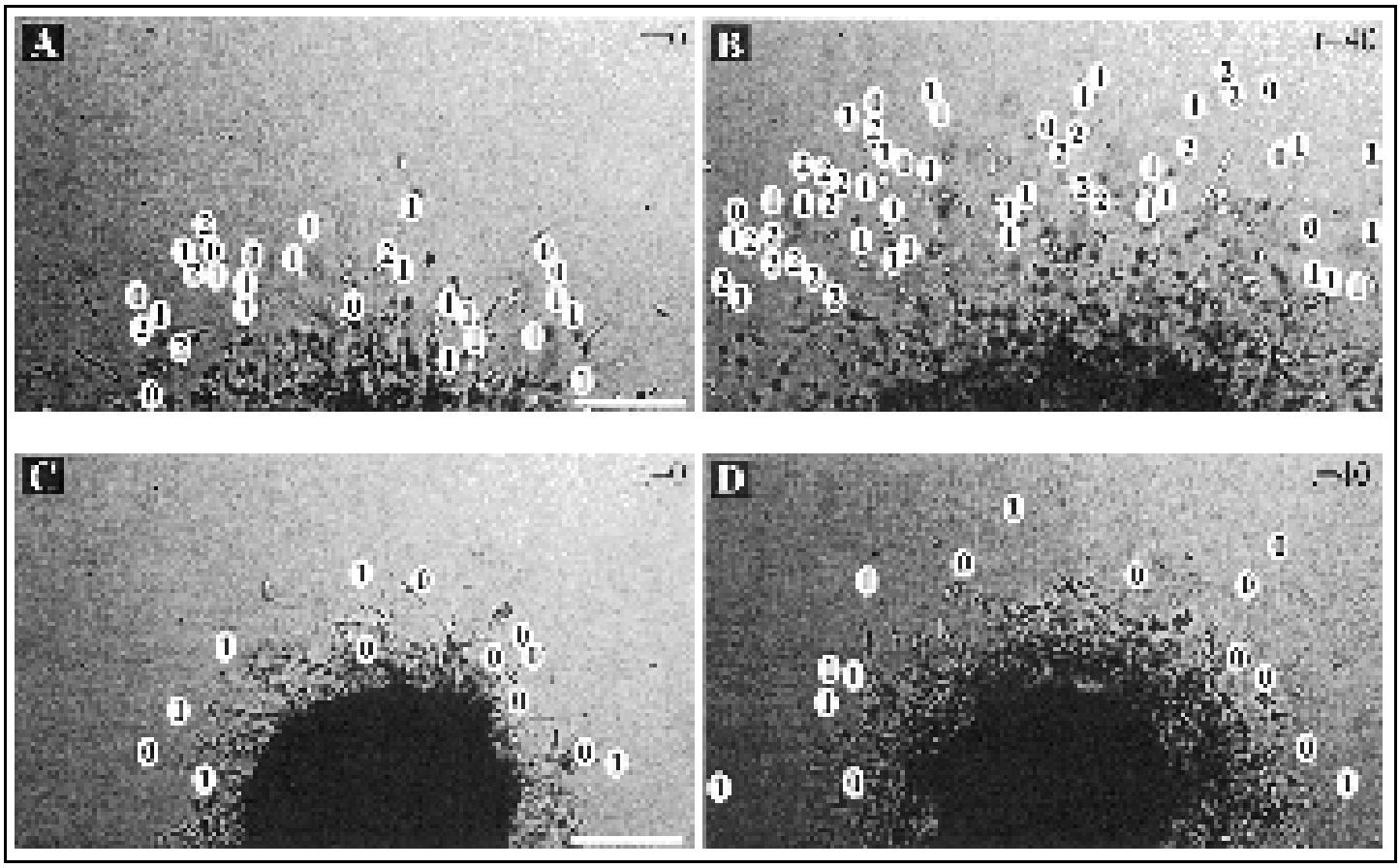

Figure 8: First and last images extracted from time-lapse videos of DAOY (A and B) and UW228-3 (C and D) spheroids invading Type I collagen matrices. Spheroids were recorded 48 hours after implantation. The numbers identify cells that divided zero, one, or two times in 40 hours; parent cells are labeled in A and C and daughter cells in B and D. The number of hours elapsed from the start time of the videos (t) are indicated at the top right corner of images. Scale bars, 250 μm. (Courtesy of Corcoran et al., 2003)

Wild-Bode and colleagues grew glioma spheroids on agar base-coated culture flasks until they were ~200 μm in diameter, followed by their transfer to 96-well plates (Wild-Bode et al, 2001). In order to examine the cause of glioma relapse in close proximity to the excised lesion, they measured the radial distance of migration as function of irradiation at 3 Gy. Irradiation led to increased migration of all cell lines, compared to non-irradiated cells, a phenomenon that was linked to increased expression and activation of MMP-2, MMP-9 and MT-1-MMP (Wild-Bode et al, 2001).

Just as the spheroid model employs a 3D environment in order to better mimic in vivo conditions, other in vitro technologies were developed to imitate the biochemical environment of the brain. In particular, transwell assays were developed in order to expose tumor-derived cells to different concentration gradients of cytokines present within brain.

1.1.5.3. Transwell Migration Assays

The transwell migration assay is a commonly-used test to study the migratory response of cells to inducers or inhibitors. This assay is also known as the Boyden or modified Boyden chamber assay, and was originally used to evaluate leukocyte chemotaxis (Boyden, 1962). In this assay, a chamber is separated into two compartments by a polyethylene terephthalate (PET) membrane in which cells are placed into the upper compartment and allowed to settle, while the solution being tested for a specific chemotactic activity (chemoattractant, neutral, or chemorepellant) is placed in the lower compartment. The membrane contains randomly distributed pores through which the cells migrate, in response to the chemoattractant from the bottom compartment. Different ECM components can be used to coat the membrane in order to mimic the basement membrane that cells must penetrate while invading in vivo (Figure 9), while

exposing the cells to various chemicals for different lengths of time. The main advantage of this assay is its detection sensitivity. Migration through the permeable membrane can be caused by very low levels of chemoattractants (Kreutzer et al, 1978). Prolonged studies are difficult, due to the fact that the chemoattractant concentration will quickly equalize between the compartment below the membrane and the compartment above the membrane. Another disadvantage is the relative difficulty in setting up the transwells. Despite these disadvantages, transwell assays are commonly the test of choice for high-throughput migration and invasion studies.

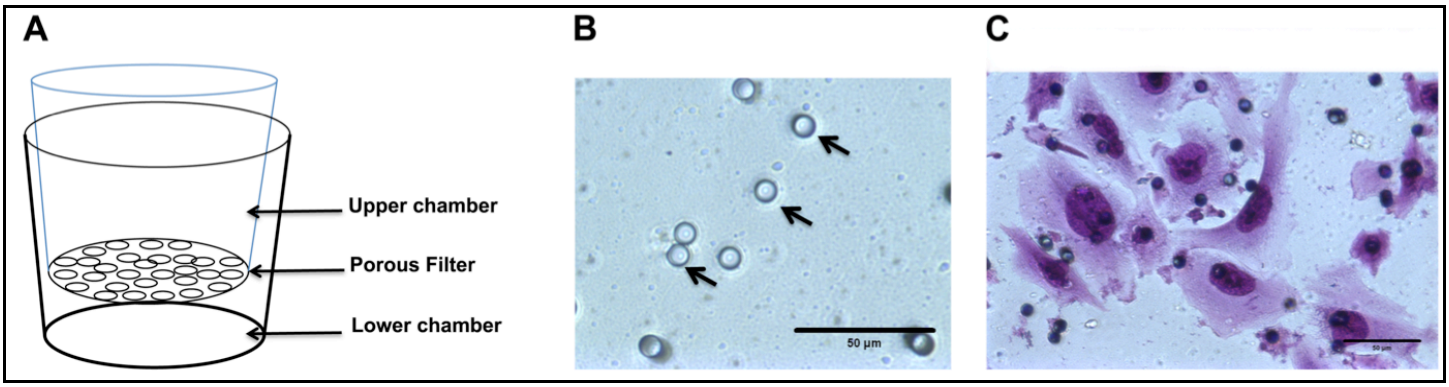

Figure 9: Boyden chamber assay. (A) Transwell migration assays are composed of a well insert with a porous filter bottom that temporarily separates the cell solution from the test solution. (B) The filter has randomly distributed microscale diameter pores as shown by arrows. (C) Invasive Daoy cells on the underside of the filter stained and imaged for migration analysis. Scale bar = 50 µm.

Over the last 50-years, several modifications have been implemented to this technology by various research groups in order to circumvent difficulties encountered with its use. For instance, upon crossing the membrane and reaching the lower surface of the chamber, cells may detach from the filter, thus resulting in an underestimate of transmigrated cells (Li & Zhu, 1999). Albini and colleagues were among the first researchers to use filters coated with ECM. They used radiolabeled proteins to demonstrate an 8-10 hour gradient stabilization period within the Boyden chamber, and showed that cell invasion time was very much dependent on the volume of the coated matrix barrier (Albini et al, 1987). Li and Zhu pioneered the use of different cell populations to attract other cells, by growing a monolayer of bovine aortic endothelial cells (BAEC) on filters, and investigating the transendothelial migration of six cell lines of different human tumors (Li & Zhu, 1999).

Chemotactic migration of GBM cells in response to several growth factors, predominately Platelet-derived growth factor (PDGF), Epidermal growth factor (EGF), and Hepatocyte growth factor (HGF), has been extensively studied (Hoelzinger et al, 2007). These studies have demonstrated dosage-dependent motogenic responses to various concentrations and combinations of these cytokines (Brockmann et al, 2003). For example, Moriyama and colleagues demonstrated, through a checkerboard analysis of various HGF concentrations, that a dose-dependent response to HGF induces both chemotaxis and chemokinesis of U-251 MG cells (Moriyama et al, 1996). In this study the concept of an "optimal concentration" was introduced, and the authors reported a decline in the chemotactic activity of U-251 MG cells at concentrations exceeding the reported optimal concentration of 50 ng/ml (Moriyama et al, 1996). Similarly, Koochekpour and colleagues used transwell assays to show dose-dependent migration and invasion of five different human glioma cell lines toward various concentrations of, in

addition to reducing basal migration of these cells using an anti-HGF neutralizing antibody (Koochekpour et al, 1997). Brockmann and colleagues reported increases in U-87 MG migration, as high as 33-fold greater than controls, in the presence of 100 pM HGF concentrations. In the same study, 1 nM TGF-α and 50 nM FGF-1 stimulated U-87 MG migration 17- and 4-fold, respectively (Brockmann et al, 2003). Transwell assays were used to demonstrate the chemotaxis of metastatic breast adenocarcinomas toward bone and brain extracts, rather than extracts from liver or lung (Hujanen & Terranova, 1985). Interestingly, it was found that C6-GFP rat glioma cells could extend their leading cytoplasmic processes through membrane pores, as a function of actin dynamics alone, but they required myosin IIA/B to generate additional cytoplasmic contractile forces to push the nucleus through pores having a smaller diameter (Beadle et al, 2008).

A study that looked at the inhibitory effect of dietary-derived flavonols on the HGF receptor Met activity suggests that such an effect may contribute to the chemopreventive properties of these molecules (Labbe et al, 2009). The authors showed that the flavonols quercetin, kaempferol, and myricetin inhibited HGF/Met signaling in MB, preventing the formation of actin-rich membrane ruffles and resulting in the inhibition of Met-induced cell migration in Boyden chambers (Labbe et al, 2009). Furthermore, quercetin and kaempferol also strongly diminished HGF-mediated Akt activation (Labbe et al, 2009).

While investigating the effect of ionizing irradiation (IR) on the invasiveness of glioma cells via transwell assays, Park et al. reported increased Matrigel™ invasion of PTEN null gliomas, U-251 MG and U-373 MG, as a result of elevated levels IR treatment, which the group suggested correlates with increases in MMP-2 secretion (Park et al, 2006). Similarly, Wild-Bode and colleagues found that the sublethal irradiation doses of 1, 3, and 6 Gy increased the

chemotactic migration and invasion of three different human glioma cell lines with increasing dosage (Wild-Bode et al, 2001). Similarly to glioma, radiation enhanced invasion and migration of 7 Gy irradiated MB compared to non-irradiated MB cells, as assessed via Boyden chamber assays (Nalla et al, 2010). Increased expression of urokinase-type plasminogen activator (uPA) and its receptor, uPAR, focal adhesion kinase (FAK), N-cadherin and integrin subunits (e.g., α_3, α_5 and β_1) was detected in irradiated cells. Conversely, down-regulation of uPAR reduced the radiation-induced adhesion, migration and invasion of the irradiated cells, primarily by inhibiting phosphorylation of FAK, Paxillin and Rac-1/Cdc42 (Nalla et al, 2010).

Transwell assays were also used to study the activated RTK-dependent MB migration. These studies have shown that MB migration is dependent on estrogen-receptor (Belcher et al, 2009), c-Met (Guessous et al, 2010), and PDGF-receptor beta (PDGFR-β) activation (Yuan et al, 2010). Via a combination of wound-healing assays and modified Boyden chamber assays, two groups showed that PDGF-induced overexpression of Rac1, a Rho GTPase, is involved in MB cell migration and invasion, whereas knockdown of Rac1 expression dramatically inhibited migration and invasion of MBs (Chen et al, 2011; Yuan et al, 2010). These findings may promote the evaluation of Rac1 as a novel therapeutic agent impairing medulloblastoma PDGF-induced migration/invasion. Additional work has demonstrated that PDGFR-β activity may guide the migration of MB by transactivating the EGF receptor (EGFR) (Abouantoun & MacDonald, 2009**).** These results are of particular interest, since EGFR is known to be expressed in GNPCs of the human cerebellum, participating in its normal development and function (Seroogy et al, 1995). Recently, the multifunctional signaling protein neurotrophin receptor $p75^{NTR}$ was shown to be a central regulator for GBM (Johnston et al, 2007) and MB spinal

invasion while γ-secretase inhibitor, which blocks $p75^{NTR}$ proteolytic processing**,** significantly abrogates $p75^{NTR}$ induced MB migration and invasion in vitro and in vivo (Wang et al, 2010).

The transwell assays, even though used commonly for cell migration experiments, often yield inconsistent results across research groups due to the experimental individual assay modifications made by each group. For example, the ECM component used for filter coating can serve as a chemoattractant via integrin signaling (triggered by the interaction with laminin contained in the matrix), or via the release of growth factors embedded in the matrix itself. Although a reduced-growth factor form of Matrigel™ is generally used (i.e. reduced amounts of the above mentioned molecules are present in the matrix), there are a plethora of extracellular matrix proteins and growth factors, reconstituted along with Matrigel™, whose concentrations may vary with each batch purchased, and cause variations in the results. Yet, perhaps the largest shortcoming of transwell assays with respect to quantifying migration is that the cytokine microenvironments they create are very complex to model mathematically. Diffusion gradients of molecules across the membrane pores are difficult to measure or predict analytically, with or without matrix coating. Among in vitro approaches, microfluidics has proven to be a powerful technology to study cell migration over the past few years, due to the ability to generate a precise cell microenvironment that can be both predicted by analytical models and validated experimentally (Kong et al, 2010), as summarized further on.

1.1.6. Microdevices

Advances in microfabrication have made microfluidics systems easier to design and manufacture. Currently, the majority of devices are constructed of polydimethylsiloxane (PDMS) via soft lithography pioneered by the Whitesides group (McDonald & Whitesides, 2002). The polymer allows the construction of systems with high transparency and low thickness that are highly-compatible with biological microscopy. As dissemination of glioma cells can often follow the path of white matter tracks or other heterogeneous structures, mechanical properties of the microenvironment play significant roles in tumor cell locomotion (Guck et al, 2010). PDMS microsystems pre-define the cell migratory path within microsized channels that mimic in vivo conditions. As such, cell motility and directionality can be examined and measured via conventional time-lapse imaging. Pioneering applications of microdevices for cancer cell study utilized microchannels coated and filled with various extracellular matrixes in 2D and 3D (Schoen et al, 2010; Sung et al, 2009) to illustrate the selectivity of cancer cell migration on distinct ECM, as well as to measure traction forces and leading edge protrusions of a variety of cancer cell types (Li et al, 2009). More recently, biomedical engineers have begun to develop systems that generate linear and non-linear cytokine gradients in order to more accurately investigate the chemotactic behavior of cells derived from primary tumors.

Establishment of steady-state gradient profiles has been examined using flow-based gradient generators, diffusion-based gradient generators, as well as hybrid generators (mixture of convection and diffusion). One of the original microdesigns for migration study was developed by Jeon and colleagues, in a gradient mixer design initially used for neutrophil chemotaxis (Li Jeon et al, 2002). This device contains multiple inlets that enable the loading of different ligand solutions that are then mixed in channels perpendicular to the flow direction (Figure 10A). A

subsequent Star shaped generator was then developed for further chemotaxis study (Kim et al, 2010). In such flow-based designs, two concentrations of biomolecules flow separately into a network of microchannels, where mixers are patterned to combine adjacent streams via convection in order to generate a chemical gradient. While flow-based devices are able to finely control the spatiotemporal resolution of the gradient, they require constant flow rates of reagents that remove molecules secreted from cells that are critical to regulation of tumor cell migration (Huang et al, 2011).

Subsequent microdevice designs now often generate soluble gradients by using passive diffusion. These systems can eliminate fluid flow near the surroundings of cells by using 3D hydrogels or high resistance channels so that transport occurs predominantly via diffusion (Beebe et al, 2002). Here, two reservoirs are typically used to maintain given chemical concentrations in a specified sink and source. Diffusion along adjoining microchannel(s) then facilitates the formation of a concentration gradient between the reservoirs that enables cells to migrate along the defined gradient (Paguirigan & Beebe, 2008a). While these systems eliminate the flow stresses imposed upon cells in flow-based devices, they require several hours to generate desired gradients, and rapid adjustment to the gradient profile is often difficult if not impractical. As a result, hybrid microsystems have been developed to enable the use diffusion with a minute level of convection to bolster formation of a desired gradient. For example, our group was able to generate steady-state gradients that were stable for 2-3 days using a bridge design and by exploiting the ultra-low bulk velocities generated by density differences between the reagents used (Figure 10B) (Kong et al, 2010).

The development of microfluidic platforms that incorporate real-time control of cell imaging and measurement of chemotactic concentration gradients is highly needed for

understanding the dynamics of brain tumor interactions, an area which remains relatively unexplored when the majority of microfluidic studies focus on measurement of end-point cellular responses.

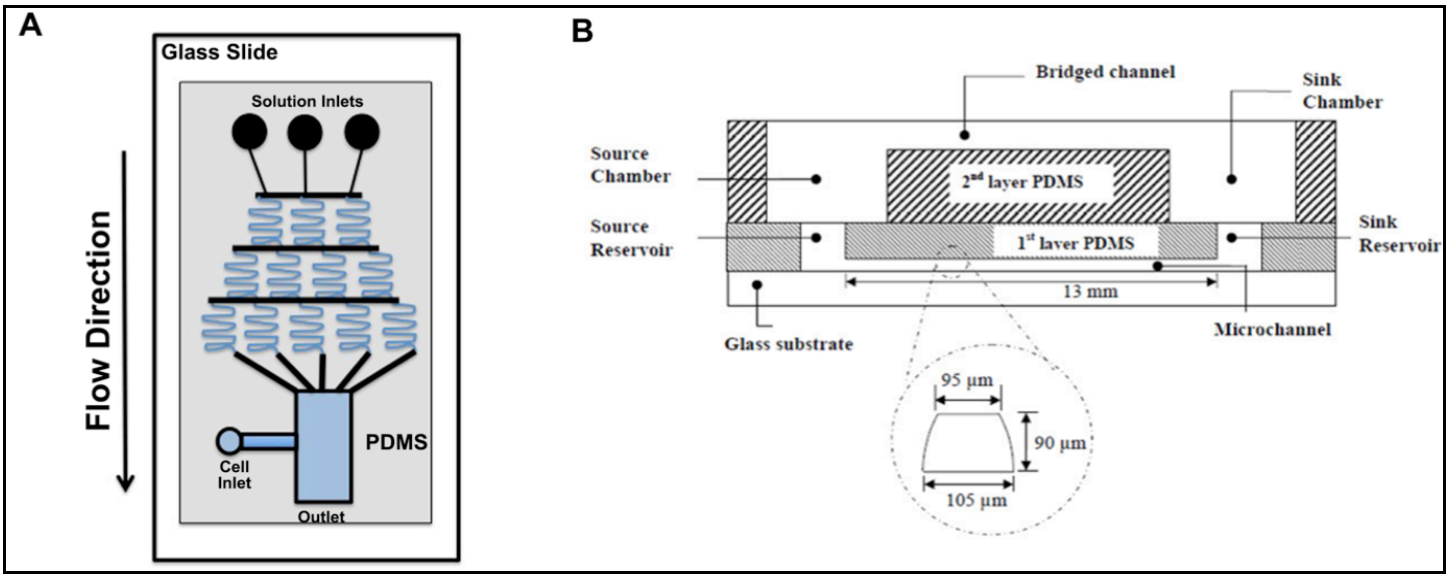

Figure 10: Schematics of microdevices currently used to generate concentration gradients (not to scale). The flow mixer device was first proposed by Li Jeon and colleagues to create highly controllable concentrations along specific distances via continuous convective flow. (A) Schematic representation of a premixing gradient generating device pioneered by Li Jeon and colleagues. (B) A hybrid microlane system uses interconnected reservoirs to create concentration gradients via both convection and diffusion. The microchannel approximately measures 13 mm in length, 90 µm in depth and 100 µm in width (averaged with the upper side of 95 µm and the lower side of 105 µm), as its semi-hemispherical cross-section shown in inset. (Courtesy of Kong et al., 2010)

1.1.7. Future prospects of anti-invasive brain tumor therapy

The impetus for the development of anti-migratory therapeutic agents for brain tumors has been the desire to ease the manageability of the disease, by arresting tumor cells to their primary local environment. Such strategies can reduce the need to utilize the so-called "Search and Destroy" approach that is the currently suggested clinical necessity. Elucidation of possible mechanisms used by diffusely infiltrative brain cells will enable a better understanding of how to render these cells static, while providing targets for the development of pharmacological products capable of such a task.

More recently it has been suggested that enhancing the recruitment of endogenous progenitors toward tumor masses will aid in restoring the brain regions that have been resected or lost via necrosis (Cayre et al, 2009). Neural stem cells (NSCs) have aroused attention in the field of neurooncology as delivery vehicles of therapeutic genes. In addition to their multipotential capabilities that allow them to differentiate into neurons, astrocytes and oligodendrocytes, NSCs are also characterized by their remarkable capability to migrate through the brain (Gage, 2000; Yandava et al, 1999). The ability of implanted NSCs to distribute themselves throughout the tumors and follow invasive glioma cells has raised the idea of their therapeutic potential in targeting invasive glioma cells in vivo (Aboody et al, 2000; Staflin et al, 2009). Shimato and colleagues demonstrated in vitro that human NSCs exhibited extensive tropism for MB cells (Shimato et al, 2007). Using leptomeningeal dissemination mouse models, they confirmed in vivo that NSCs were able to distribute diffusely to MB cells that had spread throughout the entire spinal cord after implantation in the cisterna magna and that genetically transformed NSCs functioned effectively in killing MB cells (Shimato et al, 2007). Similarly, genetically-modified NSCs were delivered intra-cranially and shown to target MBs (Kim et al,

2006). Recently, it was shown that human umbilical cord blood-derived stem cells (hUCBSCs) can integrate into human MB after local delivery, and that MMP-2 expression by the tumor cells mediates this response through the SDF1/CXCR4 pathway (Bhoopathi et al, 2011). These results offer a new promising therapeutic modality that uses human stem cells for targeting intra-cranial as well as leptomeningeal dissemination of medulloblastomas.

Although significant results are being generated from the stem cell community, brain tumor researchers have only recently begun to reflect on the specifics of glial progenitor recruitment as a form of treatment for the disease. Glial progenitor cells have shown increased healing potential after supplementing the cultures with exogenous concentrations of Vascular Endothelial Growth Factor D (VEGFD) when compared to controls (Kranich et al, 2009). Using transwell assay a dose dependent response of murine neural stem cells towards human glioma conditioned media (Heese et al, 2005) and bi-potential O-2A progenitors toward Platelet-Derived Growth Factor (PDGF) (Gallo et al, 1996) has been displayed.

Ideally, as has been the case in previous years, the focus should be to target cytokines and their cognate receptors involved in glioma chemotaxis signaling events. Moving forward, the community is in great need of technologies and strategies that can both approximate the chemical microenvironment present in the in vivo brain, and replicate this environment in vitro. In doing so, migration strategies can be developed that examine how combinations of cytokine and/or pharmacological cocktails can be used to limit the diffusive migration of tumor-derived cells into healthy brain.

The migration of glioma and medulloblastoma tumor cells into healthy brain tissue is a critical, yet poorly-understood, component of the tumor invasion and metastasis that contributes to poor patient prognosis. Extensive in vivo study of brain tumors has generated invaluable data

to elucidate the molecular alterations and genetic backgrounds present in diseased cells, the signaling mechanisms cells use to communicate with their surrounding microenvironment, and the characteristic patterns of dissemination used by specific tumor cell types. In complement, in vitro study of brain tumor-derived cells has established the chemotactic potential of various cytokines and extracellular matrixes, evaluated the effectiveness of pharmaceutical cocktails on tumor growth, as well as enabled fundamental measurement of motility and directionality in tumor cell samples. While the majority of research efforts to date have focused on the origin and nature of tumorigenesis in glioma and medulloblastoma, the community is now beginning to examine the integrated role of cell migration in tumor growth and dissemination. Future research is needed to examine the existence and characteristics of tumor cell populations with highly motile phenotypes in order to establish cell migration as a viable therapeutic target, and start designing treatment regimens based on cell migratory behaviors.

Here, we approach the problem of tumor cell dissemination by focusing on the role that specific cytokines may play in stimulating the migration of not only the characteristically invasive brain tumor cells but also that of the glial progenitors that seemingly aid in their malignant progression. By examining the chemotaxis of various brain tumor and glial progenitor cell lines via traditional transwell assays in response to predetermined exogenous growth factor concentration gradients and tumor conditioned media, we have been able to demonstrate the selective dosage-dependent response of each group of cells. Additionally, our ability to develop modifiable microfluidic devices (**Chapter 3**) that can be utilized to visually examine the migratory response of human MB-derived Daoy cells (**Chapter 4**), and neonatal glial progenitors (**Chapter 5**) in vitro has further led to the characterization differential invasion

patterns that each cell line utilizes when exposed to various growth factor concentration gradients.

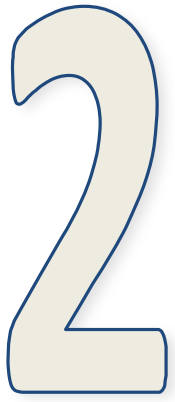

CHAPTER 2. Detailed Materials and Methods

Cell Lines

The three mouse cell lines derived from the RCAS/Ntv-a model were obtained from the laboratory of Dr. Eric C. Holland at Memorial Sloan Kettering Cancer Center (MSKCC). The system is comprised of two components, retroviral vectors and mice transgenic for cell type specific expression of the retroviral receptor. The RCAS viral vectors are avian-specific and will infect mammalian cells only if they are engineered to express the RCAS receptor, tv-a. The Ntv-a transgenic mouse line was constructed expressing tv-a as a transgene from the nestin promoter, which is expressed in neural cells early in the glial cell lineage. The Ntv-a system accomplishes glial-specific gene transfer, in vivo, which permits determination of the role of single and multiple mutations in mouse gliomas. The three different cell types used were: (1) RCAS-PDGF infected cells, driven by a PDGF autocrine loop; (2) RCAS-Ras infected cells, whose downstream Ras pathways are constitutively activated; and (3) RCAS-LacZ cells, which lack engineered mutations to receptors or signaling pathways and instead expresses the reporter gene, β-galactosidase.

Cell Culture

Cell pellets of each cell line obtained from MSKCC were suspended in 100 µl of Dimethyl Sulfoxide (DMSO) plus 900 µl of Dulbecco's Modified Eagle Medium (DMEM) (Mediatech Inc., VA) supplemented with 10% fetal bovine serum (FBS) and 1% L-glutamine and stored at -80°C for 48 hours and then transferred to liquid nitrogen tank at -196°C for long term storage. First, the pellet/DMSO was thawed in a 37°C water bath and then pipetted into a 50

ml tube that contained 10 ml of DMEM with FBS. The cell solution was centrifuged for 15 minutes at 1,600 RPM at 20°C. The supernatant was then aspirated, and 10 ml of DMEM was added to disrupt the cell pellet. The cell solution was displaced three times through a cell strainer with membrane pores of 40 μm diameter (BD Falcon, MA). Furthermore, in order to ensure that the DMSO has been washed away completely, the cell solution was then centrifuged a second time, the supernatant was aspirated off, and the solution was displaced through the strainer three more times. The cell solution was then pipetted into a 250 ml T-75 tissue culture flask (BD Falcon, MA), and maintained at 37°C. The cells were fed during culturing with 10 ml of supplemented DMEM every two days. The cells were passed when reaching approximately 80% confluence, by cleaving cell integrins with a three-minute treatment of 0.05% trypsin- 0.53 mN EDTA (Mediatech Inc., VA) at 37°C. The suspension was then diluted with equal volumes of serum-containing growth medium, and cells were collected via centrifugation, suspended in growth medium, and sub-cultured. The human malignant glioma cell lines, U-87 MG and U-251 MG, were handled in an identical manner. The MB-derived Daoy cell line (#HTB-186, purchased from ATCC, Manassas, VA) was established from a tumor biopsy of a 4-year-old boy. Cells were cultured with sterile Eagle Minimum Essential Medium (EMEM) without phenol red (pH 7.1-7.4) (Mediatech Inc., Herndon, VA), supplemented with 2% L-Glutamine (Mediatech Inc., Herndon, VA), 1% Penicillin-Streptomycin-Amphotericin B - 100x solution (Mediatech Inc., Herndon, VA), and 10% fetal bovine serum (FBS) (Gemini Bio-Products, West Sacramento, CA). The cells were grown onto sterile polystyrene tissue culture flasks (BD Biosciences, Franklin Lakes, NJ) and incubated at 37^{o}C with 5% CO_2. Cells were not serum-starved for any experiments in this study.

Chemotaxis and Invasion Transwell Assay

The migration of cells in response to signaling triggered by different concentrations of growth factors was analyzed via transwell assays as described previously (Brockmann et al, 2003). Briefly, experimental growth factor solutions were added to the lower chamber of a 24-well BD Falcon Companion TC Plate (Cat#: BD353047, BD Bioscience, MA), using serum-free DMEM as a control. Cell solutions were added to the upper chamber culture inserts (Cat#: BD353097, BD Bioscience, MA) at a density of 1.5 x 10^6 cells/ml of supplemented DMEM. Migration was allowed for 12 hours at 37^{o}C. Upon migration experiment completion, excess cell solution was aspirated from culture inserts. Cells on the upper side of the filter were removed, and the cells that migrated to the underside of the filter were fixed and stained with Diff-Quick® Stain Set (Dade Behring, DE) to enable cell counting. The nuclei of cells that migrated to the underside of the filter were counted using an inverted light microscope with a 20x objective (Nikon TE300, Morrell Instruments, NY). Cells located within five areas of the culture inserts were counted for each filter using a checkerboard pattern, for a total of five rectangular locations of 0.58 mm x 0.44 mm, used to gather representative cell counts per experiment.

For the invasion assays, a modified thick coating volume of 200 µl of 0.5 mg/ml Matrigel™ (Cat#: 356230, BD Bioscience, MA) was used to coat the filters in all invasion assays (Brockmann et al, 2003; Ohashi et al, 2006). After an incubation period of three hours at 37^{o}C, uncovered culture plates were placed into a class II biological flow hood for 48 hours. Upon drying, plates were wrapped in aluminum foil and stored at 4^{o}C for future migration experiments. Coated filters were used within seven days, but prior to their use they were rehydrated with 200 µl serum free DMEM and incubated at 37°C for one hour. For chemotaxis assays filters remained non-coated.

Growth Factor Stimulated Chemotaxis

Four different growth factors were used for these experiments: Epidermal Growth Factor (EGF), Platelet Derived Growth Factor-BB (PDGF-BB), Hepatocyte Growth Factor/Scatter Factor (HGF/SF), and Transforming Growth Factor α (TGF-α). A quantity of 5 µg of powdered Hepatocyte Growth Factor/Scatter Factor (HGF/SF) within a 110 µl volume of 0.35 M NaCl and 0.01 M Phosphate solution was diluted in Dulbecco's Modified Eagle Medium (DMEM to a 1 µg/mL concentration and stored at -20°C. A 10 µg quantity of Platelet Derived Growth Factor-BB (PDGF-BB) lyophilized powder was reconstituted in 10 ml Phosphate Buffered Saline (PBS), 4 mM Hydrochloric and 0.1% BSA to yield a concentration of 1 µg/ml, and stored at -20°C. The lyophilized 20 µg TGF-α was reconstituted in 10 mM acetic acid, 0.1% BSA and stored at -20°C. All resulting growth factor solutions were diluted with DMEM to obtain the concentrations specified for each experiment: 0.01 pM, 1 pM, 10 pM, 100 pM, 1 nM, and 10 nM.

Cell Counting

The migrated cells were imaged at 20X in a Nikon TE2000-U microscope. For each cell culture insert, the nuclei of the cells were counted in a checkerboard fashion using the NIS-Elements BR software. The relative chemoattractant factor (RCF) was determined by dividing the number of migrated cells (cells towards growth factors or cells) by the control (cells toward DMEM or DMEM + 10% FBS). The percentage of invasion was calculated by dividing the mean number of cells invading through Matrigel™ coated insert membrane by the mean number of cells migrating through non-coated insert membrane (based on BD's Matrigel™ guidelines).

Statistical Analysis

The experiments were performed in triplicates. Results are expressed as mean ± standard error of mean. Statistically significant differences were determined using the Student t-test (two-tailed) and one-way analysis of variance (ANOVA). Differences with $P < 0.05$ were considered statistically significant.

Cell Lysates

The GPC^{LacZ}, GPC^{PDGF}, GPC^{kRas}, XFM^{PDGF}, U-87 MG, and U-251 MG were each plated in 100-mm culture plate (Becton Dickinson, MA). Once 80-95% confluence was reached, the cells were serum starved overnight. The next day, the 100-mm plates were placed on ice. The serum free media was aspirated and the cells were washed with 5 ml of cold 1X DPBS.

Cells were lysed in lysis buffer (Sigma, MO) containing protease and phosphatase inhibitors (Sigma, MO) on the Orbital shaker for 15 minutes at room temperature. The cells were scraped off the surface of the dish in 1 ml of lysis buffer and transferred to pre-chilled conical tubes (BD Falcon, MA). The cell debris were spun down for 15 minutes at 16,000 rpm. The cell lysates (supernatant) was transferred to chilled eppendorf tubes and stored at -80°C or -20°C depending on the storage period.

Filtering Low Molecular Weight Proteins

The supernatant containing the proteins from the different cell samples was transferred to an Eppendorf tube containing a microcon YM-10 (Millipore, MA). The microcon YM-10 was used to remove salt and proteins with a molecular weight of < 10 kDa. The samples were centrifuged at 10,000 rpm for 30-60 minutes.

Protein Concentration Determination

Protein density was determined using the Bio-Rad DC Protein Assay (Bio-Rad, CA). The absorbance of proteins reacting with alkaline copper tartrate and Folin solution were measured at 750 nm. In this colorimetric assay, the measured intensities of lysate samples were compared to those of Bovine Serum Albumin standards to determine protein density (in mg/ml).

Protein Electrophoresis & Western Blot

A total cell lysate density of 40 μg/well was loaded onto a 8-16% Tris-Glycine Precise Pre-Cast Protein Gel (Pierce, IL). After electrophoresis at 115 V for 90 minutes at 25°C, proteins were transferred onto a nitrocellulose membrane, which was then blocked for 30 minutes in 5%-BSA-TBS. Primary and secondary antibodies were diluted in 5%-BSA-TBS according to manufacturer's recommendation. The membrane was incubated with primary antibody overnight at 4°C, followed by TBST washing and incubation with secondary antibodies for 60 minutes at 25°C in the dark. Additional TBST washing proceeded membrane scanning with the Li-Cor's Odyssey Infrared Imaging System in the infrared spectrum.

Antibodies and Immunocytochemistry

Sequential double immunofluorescence was performed as described previously (Dudu et al, 2008). Briefly, cells grown on coverslips were fixed for 15 minutes at room temperature with paraformaldehyde (Cat#: P6148, Sigma, St. Louis, MO) and labeled with rabbit polyclonal anti-β-actin (1:1000) (Cat#: ab8227, Abcam, Cambridge, MA), rabbit monoclonal anti-phosphorylated-EGF-R (1:500) (Cat#: ab40815, Abcam, Cambridge, MA), rabbit polyclonal anti-phospho-c-Met (1:500) (Cat#: 44888G, Invitrogen, Camarillo, CA), rabbit polyclonal anti-phospho-PDGFR-α (1:500) (Cat#: 44-1006, Invitrogen, Camarillo, CA), rabbit polyclonal anti-

phospho-PDGFR-β (1:500) (Cat#: ab16862, Abcam, Cambridge, MA), followed by anti-rabbit AlexaFluor® 488 or 594 antibodies (Cat#: A11034 and A11037, respectively, Invitrogen, Camarillo, CA).

μLane System

Systems are comprised of a 5-cm-long glass microscope slide bonded to a polydimethyl siloxane (PDMS) elastomer as discussed previously (Kong et al, 2010; Kong et al, 2011). Channels used for this study were 1.5 cm in length, and approximately 100 μm by 100 μm in cross-section. Channels were filled with a solution of 2 μg/mL of Matrigel™ (BD Bioscience, MA) containing a desired cytokine concentration. Systems were then incubated at 37°C for 1.5 hours to allow Matrigel™ polymerization. Afterwards, a rectangular section of PDMS was cut out to generate a larger reservoir, called New Reservoir. A cell solution having a density of 1.5 x 10^6 cells/ml was added into the New Reservoir. The system was imaged immediately using an inverted microscope (Nikon TE200, Morrell Instruments, NY) to verify the locations of viable cells at the new reservoir-microchannel interface, and then incubated at 37°C. Images of cells within the microchannel were taken at various time intervals to record the migration of cells within the channel.

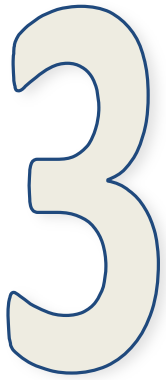

CHAPTER 3. A Microfluidic Device to Establish Concentration Gradients Using Reagent Density Differences

Qingjun Kong[1], Richard A. Able, Jr. [1,2], Veronica Dudu[1], and Maribel Vazquez[1,*]

[1]Department of Biomedical Engineering, The City College of The City University of New York (CCNY), 160 Convent Avenue, Steinman Hall Room 403D, New York, NY 10031

[2]Department of Biochemistry, The City Graduate Center of The City University of New York (CCNY) 365 Fifth Avenue, New York, NY 10016

J. of Biomechanical Engineering, 2010 Dec;132(12):121012 PMID: 21142326

Vazquez@ccny.cuny.edu

Phone: 212.650.5209 Fax: 212.650.6727

*Corresponding Author

Keywords: microfluidic device, concentration gradients, Dextran

Abstract

Microfabrication has become widely utilized to generate controlled microenvironments that establish chemical concentration gradients for a variety of engineering and life science applications. To establish microfluidic flow, the majority of existing devices rely upon additional facilities, equipment, and excessive reagent supplies, which together limit device portability as well as constrain device usage to individuals trained in technological disciplines. The current work presents our laboratory-developed bridged μLane system, which is a stand-alone device that runs via conventional pipette loading and can operate for several days without need of external machinery or additional reagent volumes. The bridged μLane is a two-layer poly-dimethylsiloxane (PDMS) microfluidic device that is able to establish controlled chemical concentration gradients by relying solely upon differences in reagent densities. Fluorescently-labeled Dextran was used to validate the design and operation of the bridged μLane by evaluating experimentally-measured transport properties and experimentally-determined molecular diffusivity within the microsystem in conjunction with numerical simulations and established mathematical transport models.

3.1.0. Introduction

Microfabrication techniques have been widely adapted to develop systems that generate specific spatial chemical concentrations and concentration gradient profiles in real time (Atencia & Beebe, 2005; Folch, 2007; Keenan & Folch, 2008; Mosadegh et al, 2007; Paguirigan & Beebe, 2008a; Paguirigan & Beebe, 2008b; Whitesides, 2006). Microfluidics is often considered a central technology for miniaturized systems developed for chemical, biological and medical applications, due in large part to their proven ability to increase throughput and reduce experimental cost (Kamotani et al, 2007; McDonald et al, 2000; Paguirigan & Beebe, 2008b; Weibel & Whitesides, 2006). Various groups have developed microfluidic devices that generate linear (Motoo et al, 2008; Tanaka et al, 2006; Yang et al, 2009) and non-linear concentration gradients (Ahmed et al, 2010; Balagadde et al, 2005; Chung et al, 2009; Crowe et al, 2001) via conventional forced fluid flow (Dertinger et al, 2001; Jeon et al, 2002; Tourovskaia et al, 2005; Zaman et al, 2006; Zhao et al, 2001), as well as via diffusion across laminar streams (Haibo et al, 2008; Yamaguchi et al, 2004), diffusion along interconnecting channels (Chung et al, 2009; Jeon et al, 2000), or in combination with electroporation (Du et al, 2009) and numerous other methods (Beebe et al, 2002; Izquierdo et al, 2010).

While researchers have increasingly begun to combine multiple design features to achieve greater gradient control (Bernard et al, 2000; Delamarche et al, 1997; Frevert et al, 2006; Goulpeau et al, 2007; Irimia et al, 2006; Kamholz et al, 1999; Tan et al, 2010), the ultimate goal is often to manufacture devices that are easy to produce, minimize convective fluid flow, and maintain controlled gradients for extended periods of time (Abhyankar et al, 2006; Fosser & Nuzzo, 2003; Goulpeau et al, 2007; Keenan & Folch, 2008; Kobel & Lutolf, 2010; Millet et al, 2010). One of the most common methods for generating steady-state gradients has been through

free-diffusion of molecules between source and sink fluids separated by either a membrane or 3D gel (Abhyankar et al, 2006; Mosadegh et al, 2007; Tan et al, 2010; Wu et al, 2006), or geometric obstructions (Li et al, 2007; Paliwal et al, 2007). These methods impede convective fluid flow, thereby enabling stable gradient formation over the life of the reagents. A comparable number of systems have achieved gradient control via microfluidic interfaces that are perpendicular to parallel flowing fluids (Kamholz et al, 1999; Kamholz & Yager, 2001). Systems that generate such gradients directly (Breckenridge et al, 2010; Irimia et al, 2006; Kamotani et al, 2007; Lee et al, 2005) or indirectly (Jeon et al, 2002) are able to maintain stable gradients for extended periods of time so long as desired input flow rates remain constant (Keenan & Folch, 2008; Velve-Casquillas et al, 2010).

A large drawback of many microfluidic designs is their dependence on multistage flow control and complex 3D transport phenomena in order to rapidly generate desired concentration gradients (Saadi et al, 2007). In addition, most microsystems continue to rely upon costly facilities and equipment for device fabrication, sample handling and/or operation, including 3D photolithographic layering (Yang et al, 2009), piezoelectric microactuators (Tanaka et al, 2006), and external power supplies (Balagadde et al, 2005; Kanegasaki et al, 2003; Lin, 2004). As a result, an additional microfluidic design goal has been to produce systems that eliminate the need for external parts, while maintaining methods of generating gradients with distinctly different profiles (Abhyankar et al, 2006). Hence, there remains a bioengineering need for user-friendly systems that maintain given microenvironments via a combination of gradients and flow control in order to examine the numerous biological phenomena that occur across long time scales and confined spatial distances (Adler et al, 2009; Park et al, 2009).

The current study has developed a microfluidic device, called the bridged μLane system, which is a stand-alone device that operates continuously and autonomously without need of external equipment, power supplies, computerized apparatus, or clean room facilities. Instead, our system is fabricated in a conventional fume hood and sustains steady-state concentration gradients over a period of 2-3 days by exploiting the ultra-low bulk velocities generated by density differences between the reagents used. In so doing, the bridged μLane can generate gradient profiles that span over 5 orders of magnitude, over hour-long time scales that approach the microenvironments generated in vivo. In brief, the bridged μLane consists of two layers of the biocompatible material poly-dimethylsiloxane (PDMS). The top layer serves as a user interface to maintain consistent experimental conditions within large volume reservoirs that are fluidically connected to a closed bottom layer, where samples are transported and examined within a single microchannel. This work presents the design and fabrication of the bridged μLane system alongside experimental, numerical, and mathematical validations of stable concentration gradients generated therein using fluorescently-labeled Dextran as a test molecule.

3.2.0. Materials and Methods

3.2.1. Design

The bridged μLane system consists of two layers of PDMS with a closed microchannel and two fluidic reservoirs on the first layer, and two larger fluidic chambers and an open bridge channel on the second, or user interface layer. As shown in Figure 1A, the first layer contains two, 9.0-μl-volume reservoirs, called the source reservoir (SRR) and sink reservoir (SKR), connected by a single, closed microchannel, or μLane, of 13,000 μm length and 95 μm hydraulic diameter, using $D_h=4A/P$ (Crowe et al, 2001) where A is the cross-sectional area and P is the perimeter. The system's 2nd layer of PDMS is the user interface layer, and consists of two cylindrical chambers, defined as the source chamber (SRC) and sink chamber (SKC), and a semi-circular, open channel, known as the bridge channel (Figure 1B). The SRC and SKC chambers are of 6-mm-diameter and 6-mm-height each (170 μl), and are vertically and fluidically connected with the SRR and SKR reservoirs in the 1st layer of the system, respectively. In addition, the SRC and SKC are connected to each other via the open bridge channel of 9-mm-length and 2-mm-depth. The overall system works by using the large volume chambers and bridge channel on the 2nd layer to generate concentration gradients within the smaller volume microchannel on the first layer. Solution is manually loaded into the SRC until it has filled the SRR reservoir, microchannel, SKR reservoir, SKC chamber, and bridge channel. Sample is then loaded into the SRC, drop wise and slowly, until the sample makes contact with solution within the bridge channel to initiate system operation. The volume of each chamber (170 μl) is designed to be much larger than the volume within each reservoir (9 μl) and μLane (0.1 μl), in order to facilitate manual loading via conventional pipette or syringe to initiate gradual transport into the microchannel with minimal channel entrance effects. The large ratio of

chamber volume (170 µl) to µLane volume (0.1 µl) facilitates modeling of constant reagent concentration in the chambers during transport analysis. Further, the ratio of µLane length to diameter is substantially large (L/D_h=137) so as to enable computational modeling of one-dimensional transport within the microchannel. Lastly, the ratio of each reservoir volume (9 µl) to the µLane volume (0.1 µl) is also large, ($V_{SRR}/V_{\mu Lane}$=27), in order to sustain continuous transport between each reservoir and the microchannel over long experimental time scales.

Without the bridge channel, the µLane channel readily facilitates transport via convection, as even small differences in the liquid levels of the SRR and SKR reservoirs will generate hydrostatic pressure gradients known to cause microfluidic flow (Paguirigan & Beebe, 2008b; Tanaka et al, 2006; Whitesides, 2006). The advantage of the so-called Bridged µLane system is that the bridge channel is used to balance solution volumes within the SRC and SKC chambers in order to eliminate hydrostatic pressure differences between the chambers. As such, the addition of sample and/or reagent with a different density into the SRC chamber on the second layer then provides the driving force to generate a small microfluidic flow within the µLane channel in the first layer, which facilitates transport via convective diffusion. The large differences in volume ratios between chambers, reservoirs and channels on the 1st and 2nd layers of the device provide the dual advantage of enabling the modeling of transport processes as one-dimensional in the microchannel, as well as generating fluidic processes with very different time scales for achieving steady-state transport.

3.2.2. Manufacturing

System fabrication was performed via three different conventional manufacturing processes: i) Fabrication of microchannel-patterned mold using proximity photolithography; ii)

Fabrication of the 1st layer PDMS using elastomeric molding and bonding; and iii) Fabrication of the 2nd layer PDMS using elastomeric molding.

i) Photolithography: A pre-cleaned glass substrate was coated with an adhesion promoter, Surpass 3000, (DisChem Inc., Ridgway, PA) and an 100-µm-thick layer of negative photoresist, SU-8 2075, (MicroChem Inc., Newton, MA) using a spin coating apparatus (Laurell Tech. Corp., North Wales, PA). The substrate was baked on a hot plate and irradiated with UV light using a laboratory-fabricated photomask containing desired microchannel patterns (intensity: 21700-8900 µW/cm^2 at 2-10 inches, Model B-100AP, UVP Inc., Upland, CA). Substrates were then re-baked, allowed to cool at room temperature (25°C), and immersed in SU-8 developer (MicroChem Inc., Newton, MA) until photoresist patterns were visible. The patterned substrate exhibited dimensions of 13.0±0.1-mm-length (mean ± SD) by 100±5-µm-width by 90±1-µm-height as measured via surface profilometer (Model SJ-301, Mitutoyo America Corp., Middlesex, NJ) and optical microscope (Nikon TE2000, Morrell Instrument Company Inc., Melville, NY).

ii) Fabrication of the 1st layer PDMS: Liquid-state poly-dimethylsiloxane (PDMS) mixed with silicone elastomer curing agent (Dow Corning Corp., Midland, MI) was degassed and poured onto the photoresist-patterned substrate described above. After polymerization, the PDMS elastomer was peeled from the patterned substrates resulting in open microchannels of 13.0±0.1-mm-length by 100±5-µm-width and 90±1-µm-depth. Subsequently, it was punctured with 2-mm-diameter pipette tips (Model 9-inch Pasteur Pipette, Fisher Scientific Co., Agawam, MA) on both ends in order to generate two reservoirs with approximately 9 µl volume each, defined as the source (SRR) and sink reservoirs (SKR). The PDMS elastomer was bonded onto a pre-cleaned glass substrate (unpatterned) by applying ozone generated via a high-frequency

generator (Electro-Technic Products, Inc., Chicago, IL) onto both the PDMS and glass surfaces for 30 seconds each. The 1st layer PDMS was then generated, as shown in Figure 1A. Cross-section uniformity of the closed microchannel itself within this 1st layer was verified using an optical microscope (Nikon TE2000). Since large machines, such as deep reactive-ion etching (DRIE) apparatus, were not used in the microfabrication, the cross-section was semi-hemispherical (Lee et al, 1998; McKnight et al, 2004; Vazquez et al, 2002; Vazquez et al, 2001) with a hydraulic diameter of D_h=95μm as examined via optical microscope and profilometer, shown in Figure 1C. This profile is of note because high aspect ratio, rectangular channels are extremely difficult to manufacture via this protocol (Holden et al, 2003).

iii) Fabrication of the 2nd layer PDMS: For the second layer of PDMS, or user interface layer, a laboratory-made acrylic mold was manufactured via milling machine, to match the larger dimensions of the SRC, SKC and bridge. After the acrylic mold was aligned on top of the 1st layer PDMS, the mixed solution of liquid-state PDMS and curing agent were poured around the acrylic mold to form a 6-mm-thick 2nd layer PDMS. After the PDMS was polymerized, the acrylic mold was removed. The 2nd layer PDMS consisted of two cylindrical chambers, and a semi-circular, open channel, or so-called bridge channel (Figure 1B). The two chambers, of 6-mm-diameter and 6-mm-height each, were defined as the source chamber (SRC) and sink chamber (SKC). The SRC and SKC chambers were vertically and fluidically connected with the SRR and SKR reservoirs, respectively, in the 1st layer (Figure 1C).

The complete bridged μLane system is thus composed of an open bridge channel that connects the open SRC and SKC chambers on the second or user interface layer, as well as a closed microchannel that connects the SRR and SKR reservoirs on the 1st layer.

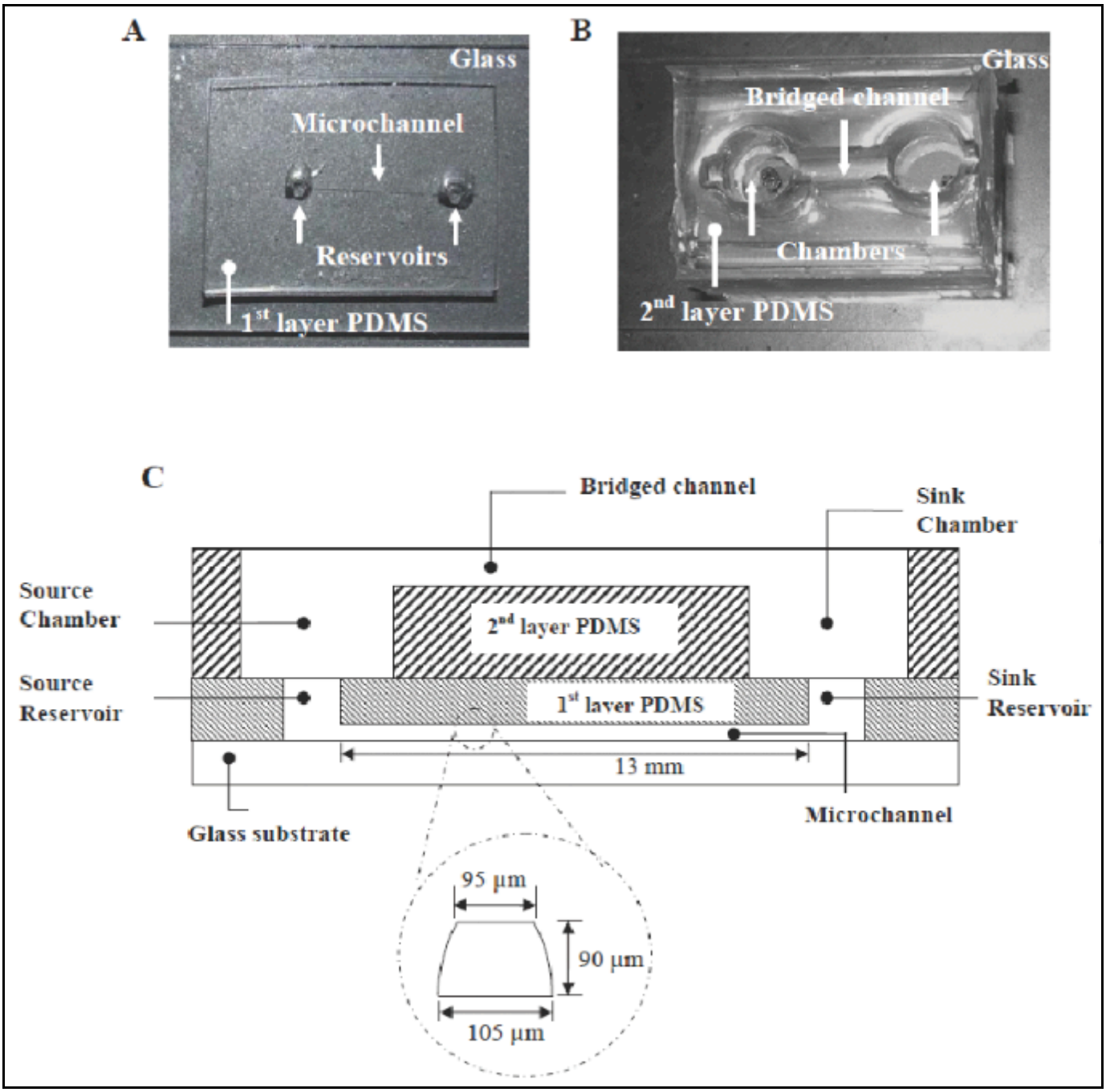

Figure 1: Images and schematic of the bridged µLane system. After photolithography and elastomeric molding, a microchannel with two reservoirs was fabricated in polymerized PDMS, defined as the 1st layer PDMS of the bridged µLane system. This PDMS layer was then bonded onto an ultrasonically-cleaned microscope glass slide (A). A second layer of PDMS, consisting of a bridge channel and two chambers, was molded on top of the 1st layer PDMS (B). This layer of PDMS was defined as the 2nd layer PDMS, or user interface layer, of the system. The chambers in the 2nd layer PDMS were fluidically connected with the reservoirs in the 1st layer PDMS, as shown in the bridged µLane system schematic (C) (not to scale). The microchannel approximately measures 13

mm in length, 90 μm in depth and 100 μm in width (averaged with the upper side of 95 μm and the lower side of 105 μm), as its semi-hemispherical cross-section shown in inset.

3.2.3. Mathematical modeling

Two-dimensional numerical simulations of the bridged μLane system were performed in order to model the transport within entire the microsystem, i.e. the microchannel, both the SRR and SKR reservoirs in the 1st layer PDMS, the bridge channel, and both the SRC and SKC chambers in the 2nd layer PDMS. The mass transport within the entire microsystem was modeled using the 2-D continuity equation (Equation 1), convective-diffusion equation (Equation 2), momentum equation (Equation 3), and hydrostatic equation (Equation 4), as shown below (Bird et al, 2002):

Continuity equation: $$\frac{\partial \rho}{\partial t} + \underline{\nabla}(\rho \cdot \underline{u}) = 0 \qquad (1)$$

Convective-diffusion equation: $$\frac{\partial C}{\partial t} + \underline{u} \cdot \underline{\nabla} C = D\nabla^2 C \qquad (2)$$

Momentum equation: $$\rho(\frac{\partial \underline{u}}{\partial t} + \underline{u} \cdot \underline{\nabla}\underline{u}) = -\underline{\nabla} p + \mu\nabla^2 \underline{u} \qquad (3)$$

Hydrostatic equation: $$-\underline{\nabla} p + \rho \underline{g} h = 0 \qquad (4)$$

where r (kg/m^3) is reagent density, $\underline{u}$ (m/s) is fluid velocity, y (m) is the vertical direction, x (m) is the horizontal direction, C (g/L) is solution concentration, D (m^2/s) is the diffusion coefficient, or diffusivity, of the reagent molecule, p (Pa) is hydrodynamic pressure, and h (m) is the height of the 1st and the 2nd layer PDMS (m). These coupled equations were solved using finite element

methods. Note that all physical boundaries of the microsystem were regarded as insulated boundaries of mass transfer and momentum transport because only trace amounts of Dextran were observed to permeate through PDMS wall boundaries during experimental time scales of up to 7 days. Transport within PDMS across 1-2 days is therefore neglected in this analysis (Feng et al, 2010). For ease of explanation, mathematical modeling will be described within four separate control regions: (i) The source chamber (SRC) in the 2nd layer and the source reservoir (SRR) in the 1st layer; (ii) The microchannel in the 1st layer; (iii) The sink reservoir (SKR) in the 1st layer and the sink chamber (SKC) in the 2nd layer; and (iv) The bridge channel in the 2nd layer. Finite-element-analysis (FEA) software FEMLab Version 3.4 (Comsol Inc., Burlington, MA) was used to solve these 4 coupled equations simultaneously within the four interconnected regions described above. A fine mesh of 1504 elements was used, which confined the distance between nodes to approximately 8 μm and computational time of less than 3 minutes. Note that simulation results remained approximately unchanged (<1%) when finer meshes were used.

(i) SRC to SRR: The initial reagent concentration within the SRR reservoir was set to 0 μg/ml because no sample reagent (only buffer or deionized water) was directly added into the reservoir, while the initial molecule concentration within the SRC chamber was set to 40 μg/ml to reflect the sample reagent concentration used during experiments. The concentration within the SRC was held constant throughout simulations because the large chamber to reservoir volume ratio (140:1) maintained an approximately constant reagent concentration during experiments. As a result, the molecule concentration at the interface between the SRC chamber and the SRR reservoir was fixed at C=40 μg/ml. The reagent concentration at the interface between the SRR reservoir and the entrance of the microchannel ($C_{x=0-}$) was modeled as equal to

the reagent concentration at the interface within the microchannel ($C_{x=0+}$), i.e. $C_{x=0-}= C_{x=0+}$, indicative of a continuous boundary.

The initial velocity entering from the SRC chamber and within the SRR reservoir was assumed to be zero. Lastly, the boundary condition of velocity at the interface between the SRR reservoir and the microchannel was set $V_{x|x=0-}= V_{x|x=0+}$, as a continuous boundary. The hydrodynamic pressures within the SRC and SRR were calculated using the hydrostatic equation (Equation 4).

ii) Microchannel: The transport within the microchannel from the SRR reservoir to the SKR reservoir was modeled as one-dimensional because of the large ratio between the microchannel length and its hydraulic diameter (137: 1). The initial concentration of reagent within the entire microchannel was set to C=0 μg/ml, as no reagent was applied in the beginning of experiments. The boundary at the entrance of the microchannel was set as continuous boundary ($C_{x=0-}= C_{x=0+}$) as mentioned. Similarly, the boundary at the exit of the microchannel (x=L) was also set as a continuous boundary, i.e. $C_{x=L-}= C_{x=L+}$, as the concentration within the SKR reservoir at the interface between the microchannel and the reservoir ($C_{x=L-}$) was regarded to be equal to the concentration within the SKR reservoir at the interface ($C_{x=L+}$). The initial velocity within the microchannel was zero, while the boundary conditions at the entrance of the microchannel and the exit of the microchannel were regarded as continuous boundaries, i.e. $V_{x|x=0-}= V_{x|x=0+}$ and $V_{x|x=L-}= V_{x|x=L+}$.

iii) SKR to SKC: The initial reagent concentration within the SKR reservoir and SKC chamber was set to C=0 μg/ml, as no reagent was added at the beginning of experiments. The concentration at the boundary between the SKC chamber and the SKR reservoir was set to C=0 μg/ml and the boundary between the SKR reservoir and the microchannel (x=L) was regarded as

a continuous boundary, i.e. $C_{x=L-}= C_{x=L+}$. The velocity within the SKR reservoir was initially zero. The velocity at the interface between the SKC chamber and the SKR reservoir was set to be zero, while the boundary condition of velocity at the interface between the microchannel and the SKR reservoir was set as continuous boundary, i.e. $V_{x|x=L-}= V_{x|x=L+}$. The pressure in the SKR reservoir was calculated via hydrostatics.

iv) Bridge channel: The initial concentrations of the SRC chamber and the SKC chamber were set to 40 μg/ml and 0 μg/ml, respectively, and maintained constant during simulations. The initial reagent concentration within the bridge channel was also 0 μg/ml, as no reagent was added. The concentrations at the boundaries of the interface between the SRC chamber and the bridge channel, and the interface between the SKC chamber and the bridge channel were also set to 40 μg/ml and 0 μg/ml, respectively.

3.2.4. Experimental Measurement

Fluorescently-labeled Dextran solutions (Cat. # D22910, 10 kDa, Molecular Probes, Eugene, OR) and 1.9-μm-diameter fluorescent beads (Duke Scientific, Cat # G0200, Palo Alto, California) were added into the system in order to explicitly measure Dextran transport within the bridged μLane system. First, phosphate buffer saline (PBS) solution (Mediatech Inc., Herndon, VA) containing the 1.0-μm-diameter fluorescent beads with concentration of 10^4 beads/ml was injected into the microchannel using a 1-ml syringe (Becton, Dickinson and Company, Franklin Lakes, NJ). These beads were used to optically measure bulk flow velocity within the reservoirs, microchannel, and chambers of the system. PBS solution was then pipetted into the SKC chamber and the bridge, respectively. Note that the PBS solution was added drop wise, and slowly, into the bridge and the SKC chamber so as to prevent dilution of the

fluorescent source. Afterwards, solutions of Dextran at a concentration of 40 μg/ml were added drop wise into the SRC chamber, only, until it contacted the PBS solution present in the bridge. After the contact was made, solutions of fluorescent beads and solutions of Dextran were observed to migrate significantly more slowly within the microchannel from the SRR reservoir to the SKR reservoir. The systems were then placed in a fluorescent microscope for fluorescent intensity measurement. The fluorescent detection positions within the microchannel were set at 3 mm, 5 mm, 8 mm, and 11 mm away from the entrance of the microchannel.

3.2.5. Microscope Imaging and Fluorescent Measurement

An inverted epi-microscope (Nikon TE2000) with a 20X microscope objective (Nikon Plant 20X, Morrell Instrument Company Inc., Melville, NY) was used to image the μLane systems via a cooled CCD camera (CoolSNAP EZ, Photometrics, Tucson, AZ) with Nikon software (Nikon Instrument Element 2.30 with 6D module, Morrell Instrument Company Inc., Melville, NY). A shutter (HF204, Prior Scientific Inc., Rockland, MA) mounted in the Nikon TE2000 was used to control the exposure time.

An excitation light of wavelength of 488 nm was applied onto the channel during Dextran transport so that emitted fluorescence was collected via microscope objective. The intensity values of fluorescence collected at detection positions 5 mm, 8 mm and 11 mm away from the SRR reservoir were plotted over time. Meanwhile, movement of fluorescent beads within the microchannel was recorded in order to measure the mean bulk flow velocity. Experiments were repeated four times. In each repeated experiment, a new bridged μLane system was used to measure the fluorescent intensity and bulk flow velocity at different detection positions over time. The results were processed using the Student's t test and presented in the format of average ± standard deviation.

3.2.6. Data processing and plotting

The experimental data of fluorescent intensity (8 bit values between 0 and 256) as a function of time, and the simulation data as a function of time were normalized to values between 0 and 1, and plotted in the same diagram using Origin 7.5 software (Origin Lab Corp., Northampton, MA). Note that some dimensionless normalized experimental data slightly exceeded 1 because of experimental noise. The normalized experimental data were fitted into a curve ($R^2 \geq 99.8\%$), using the Hill function, a category of Sigmoidal functions provided by the software, in order to better compare with the simulated data. The Hill function is given as:

$$y = V_{\max} \cdot \frac{x^n}{k^n + x^n} \tag{5}$$

where the V_{max} is the asymptotic value of the experimental data, k and n are empirical constants given by the software, and x and y are axis coordinates. The residual difference, defined as the absolute difference between each individual data point from the Hill-function fit curve and each individual data point from the simulation curves at the same corresponding time point, was analyzed using the Student's t-test in order to identify the simulation curve that was closest to the Hill-function fit curve of the experimental data. The simulation curve with the least standard deviation of residual difference (<2%) and the least average residual difference at all the data points (<1%) was considered to be characteristic of the diffusion coefficients in free solution.

3.3.0. Results

The bridged μLane system was designed to generate steady-state concentration gradients within microchannels via reagent concentration difference without relying upon external equipment, power, or reagent volumes. A fluorescent reagent, mathematical modeling, and numerical simulations were used to examine the concentration gradients generated within the microsystem. Results compared experimentally-measured values of bulk velocity, diffusivity and concentration to those predicted mathematically and derived numerically.

3.3.1. Mathematical Predictions

FEMLab simulations generated concentration distributions within the bridged μLane system, as illustrated in Figure 2. As seen, SRC and SKC chamber concentrations remained approximately constant, while significant reagent concentration distributions were seen within the SRR and SKR reservoirs. Importantly, FEM analysis predicted that reagent concentration varied by two orders of magnitude along the microchannel length. The time response of Dextran via FEM analysis shown in Figure 2B illustrates how the reagent concentration reaches steady-state within 11 hours mid-channel, at approximately 5 mm. Bulk flow present in the microchannel was examined via Reynolds number (Re) and Peclet number (Pe) to analyze its fluidic properties. The Reynolds number (Re) is a dimensionless number that measures the ratio of inertial forces to viscous forces, defined as (Bird et al, 2002):

$$\mathrm{Re} = \rho V d / \mu \qquad (6)$$

where ρ is fluid density (kg/m^3), V is flow velocity (m/s), d is characteristic length (m) and μ is fluid viscosity (Pa.s). This value was predicted to be less than 10^{-3} in our model, indicative of viscous, laminar flow within the microchannel, with a bulk velocity of 0.17 μm/s. The Peclet number (Pe) is a dimensional number that measures the ratio of convective bulk flow to diffusion, defined as (Bird et al, 2002):

$$Pe = VL / D \qquad (7)$$

where V is fluid velocity (m/s), L is the length of channel (m) and D is the diffusion coefficient (m/s^2). Using the diffusion coefficient of Dextran reported in the literature to range from 0.8×10^{-6} cm^2/s to 0.84×10^{-6} cm^2/s (Gennerich & Schild, 2002; Haller & Saltzman, 1998; Hiemenz & R., 1997; Loan et al, 2000; Saltzman et al, 1994) and the average bulk flow velocity estimated from the mathematical models, the Pe was predicted to be between 16 and 25. Such values illustrate that bulk flow dominated the Dextran transport within the microchannel even at the low Re and velocities predicted mathematically via the Poiseuille flow model (Bird et al, 2002; Crowe et al, 2001).

Figure 2 also illustrates concentration differences within the bridge channel near the SRC chamber after 23 hours. However, the volume of the bridge is over 10^4 times larger than the volume of the microchannel, such that there is no backflow as a result of microchannel transport. In addition, concentration gradients within the bridge are diffusion dominated, and as such the bridge does not equilibrate concentrations within the SRC and SKC chambers within experimental time scales of 5-7 days given the large chamber volumes and absence of

measurable bulk flow. FEMLab analysis indicates reagent equilibration within the 2nd PDMS layer requires upwards of 200 hours given the system volumetric dimensions.

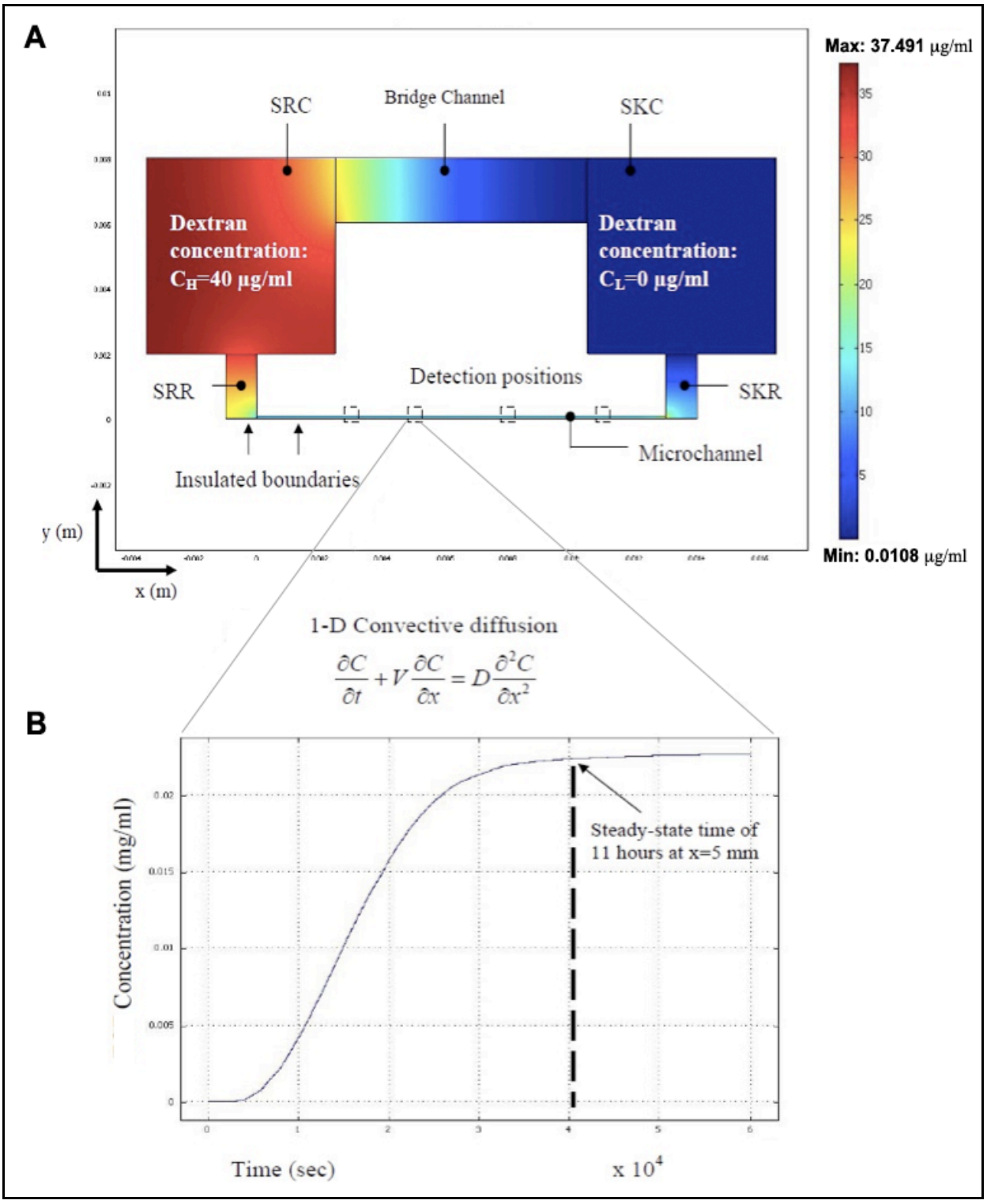

Figure 2: Simulation of Dextran transport within the bridged µLane system. The source chamber (SRC), source reservoir (SRR), microchannel, sink reservoir (SKR), sink chamber (SKC) and bridge channel were modeled using finite element software (A). The Dextran concentration in the SRC chamber was set to a maximum of C_H

= 40 ng/ml, while the Dextran concentration in the SKC chamber was set to a minimum of C_L = 0 ng/ml. The bulk velocity within the microchannel was measured using fluorescent beads, and inputted into the Dextran transport model for numerical simulation. All of the boundaries of the bridged μLane system were modeled as insulated from mass transfer. Dextran transport at different positions within the microchannel, x = 5 mm, x = 8 mm and x = 11 mm, respectively, was examined over time. One-dimensional convective diffusion equation was used to model the transport of Dextran within the microchannel, where C represents concentration, V is bulk velocity and D is the diffusion coefficient. The simulation illustrates that the Dextran concentration at a representative microchannel position of x = 5 mm increases over time and reaches steady-state in 11 hours (B).

3.3.2. Experimental Measurement of Transport

Experimental measurements of the fluorescent intensity of Dextran samples and fluidic flow of fluorescent microbeads within the bridged μLane were performed in order to verify the transport parameters predicted by our model. No significant change of fluorescent intensity (<1%) was measured within the SRC and SKC chamber, indicative of approximately constant concentrations during experiments, i.e. 40 μg/ml and 0 μg/ml, respectively. Transport of solutions of fluorescent Dextran and fluorescent beads was imaged within the system and observed to displace along the SRR reservoir, microchannel and SKR reservoir with increasing fluorescent intensity by time, as shown in Figure 3 and Figure 4, respectively**.** As seen, Dextran fluorescence intensity was measured at different channel positions over a 20-hour period and plotted to illustrate the time response within the bridged μLane system. The experimental data shown is within 9% of the response predicted via FEM simulation, indicating a steady-state Dextran concentration is experimentally reached mid-channel after approximately 12 hours (as per Figure 3).

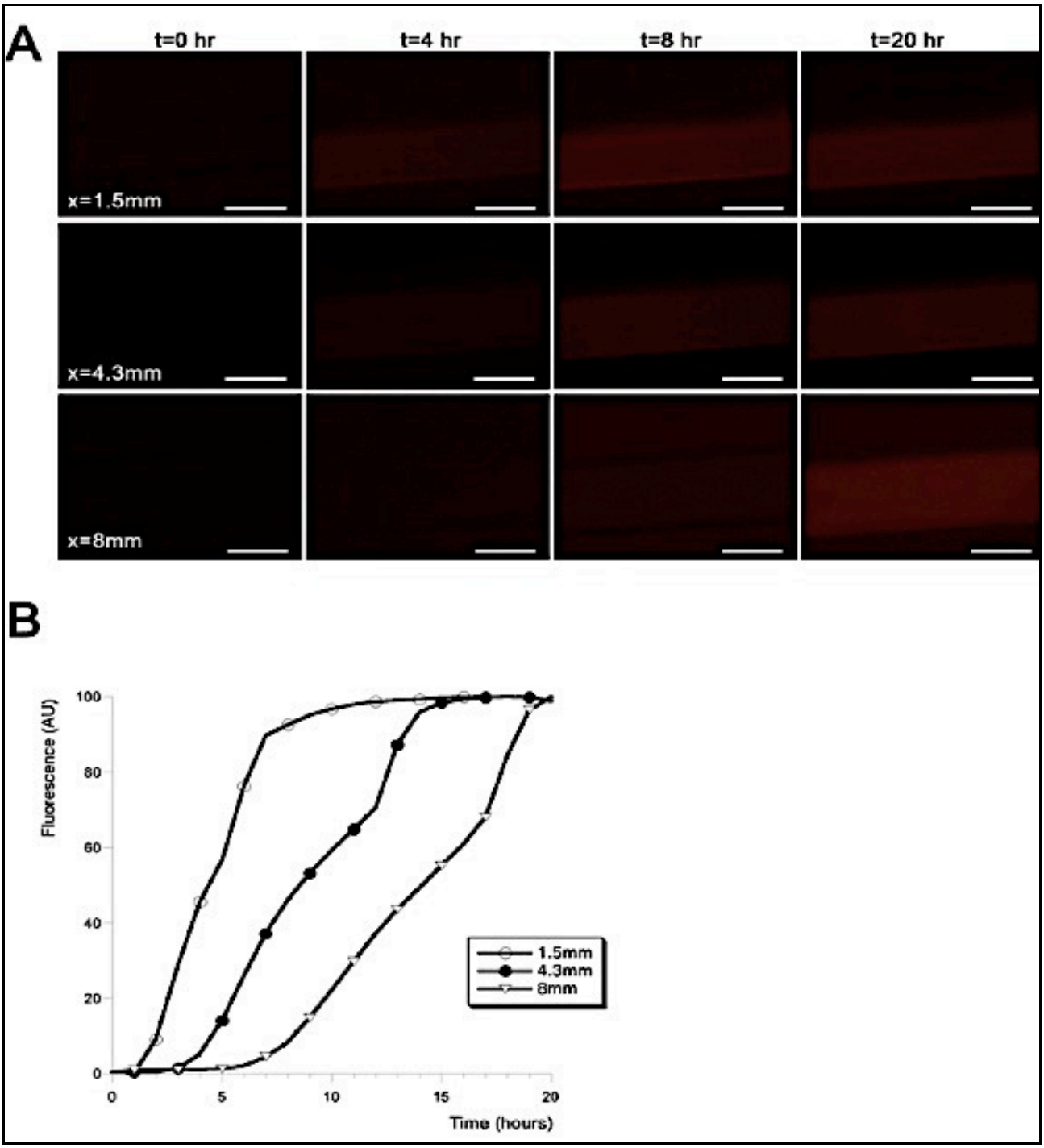

Figure 3: Images of Dextran transport within the microchannel at three representative positions over time (A). Fluorescence was initially observed throughout the microchannel in approximately 4 hours with increasingly fluorescence intensity measured for up to 20 hours. Average intensity values measured every hour across 3 different channel sections are plotted to illustrate the Dextran concentration profile obtained experimental at steady state (B). Scale: 100 μm.

In addition, bulk flow within the system was examined using fluorescent beads with and without the use of the bridge channel. As shown in Figure 4, beads were seen to migrate with different velocities in the microsystem with and without the bridge channel. An average bulk velocity of V_{avg}=92.3±1.4 μm/s was measured within the μLane system in the absence of the bridge channel (n=12), but an average velocity of V_{avg}=0.37±0.11 μm/s was measured within the bridged μLane system (n=16). In addition, no bulk flow was measured within the bridge channel when beads were used, confirming that Dextran transport within the bridge was diffusion-dominated and did not significantly affect the transport of Dextran within the microchannel nor alter concentrations of the large volume SRC and SKC chambers over experimental time scales.

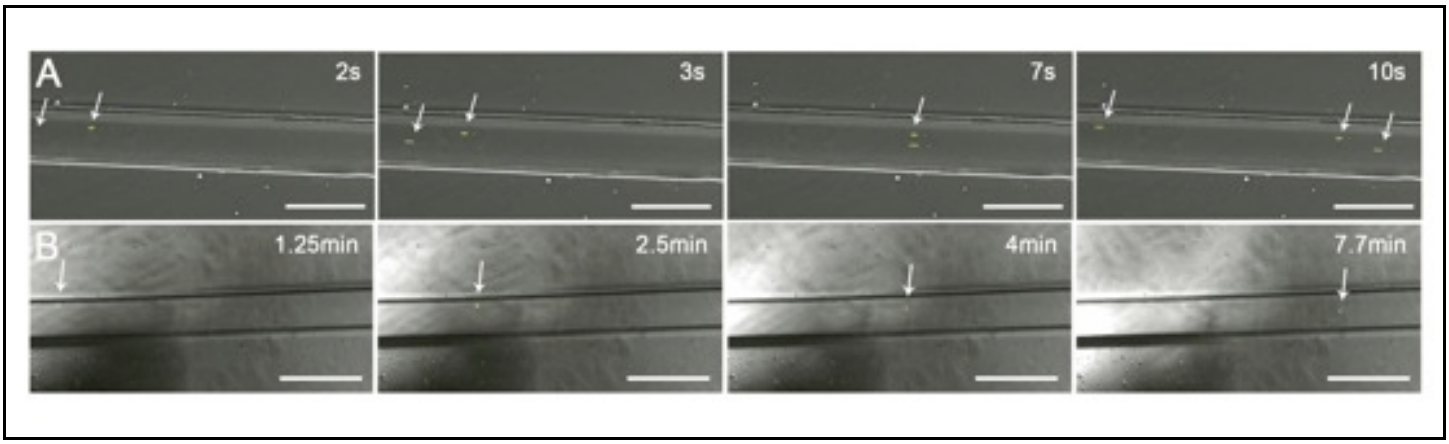

Figure 4: Images of the bulk flow of beads within a µLane device in the absence of the bridge channel (A) and within the bridged µLane system (B). Images illustrate the motion of individual beads across a fixed, representative channel section. Scale: 100 µm.

As a validation experiment, the diffusion coefficient of Dextran was measured using the bridged μLane system by comparing the transport imaged at four different detection positions within the microchannel, x = 3 mm, x = 5 mm, x = 8 mm, and x = 11 mm. Fluorescent intensity of Dextran measured experimentally over 96 hours at these four specific detection positions were normalized and shown in Figure 5. In addition, normalized FEM computer-modeled predictions of Dextran concentration at the corresponding detection positions were computed and plotted alongside the experimental data in this figure. In the simulations, numerical predictions utilized Dextran diffusivity values between $D=1.0 \times 10^{-6} cm^2/s$ and $D=0.7 \times 10^{-6} cm^2/s$ and a measured bulk velocity of $V_x=0.37$ μm/s for a wide range of examination. Computer-generated predictions from our numerical model were within 6% of each experimentally measured intensity. Using these corroborating results, we illustrate that Dextran transport within the bridged μLane system occurred with a diffusivity of $0.82 \pm 0.01 \times 10^{-6} cm^2/s$. This value is in line with the measured diffusivity of Dextran in vitro and in vivo reported to be between $0.80 \times 10^{-6} cm^2/s$ and $0.84 \times 10^{-6} cm^2/s$ (Gennerich & Schild, 2002; Haller & Saltzman, 1998; Hiemenz & R., 1997; Loan et al, 2000; Saltzman et al, 1994).

Using the bridged μLane-derived diffusivity of Dextran and the average bulk velocity, the time to reach steady-state for the entire microchannel length of L = 13 mm was computed to be 40 hours. In addition, the concentration gradient profile, G, within the system microchannel at steady-state spanned five orders of magnitude with minimal, shallow gradients of $G=10^{-3}$ μg/(ml.mm) near the SRR reservoir and larger, highly non-linear gradients of $G=10^{1}$ μg/(ml.mm) near the SKR reservoir.

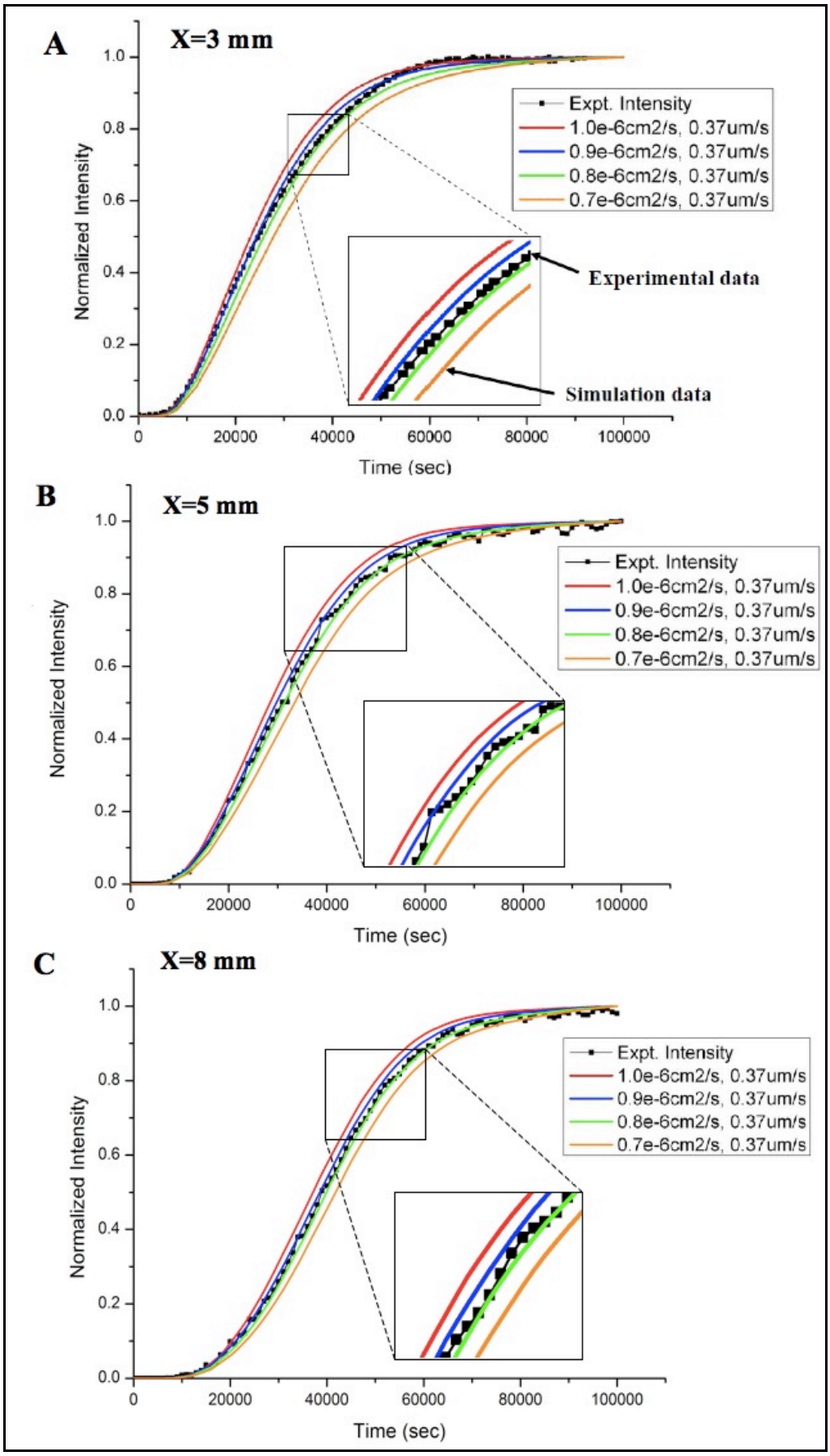
A
X=3 mm
Normalized Intensity
Time (sec)
Expt. Intensity
1.0e-6cm2/s, 0.37um/s
0.9e-6cm2/s, 0.37um/s
0.8e-6cm2/s, 0.37um/s
0.7e-6cm2/s, 0.37um/s
Experimental data
Simulation data
B
X=5 mm
Normalized Intensity
Time (sec)
Expt. Intensity
1.0e-6cm2/s, 0.37um/s
0.9e-6cm2/s, 0.37um/s
0.8e-6cm2/s, 0.37um/s
0.7e-6cm2/s, 0.37um/s
C
X=8 mm
Normalized Intensity
Time (sec)
Expt. Intensity
1.0e-6cm2/s, 0.37um/s
0.9e-6cm2/s, 0.37um/s
0.8e-6cm2/s, 0.37um/s
0.7e-6cm2/s, 0.37um/s

Figure 5: Graph of normalized experimental data obtained from Dextran transport experiments at detection positions within the bridged μLane system, compared against normalized simulation data generated from the 1-D convective diffusion equation. These normalized data were plotted as a function of time. A range of Dextran diffusion coefficients between 0.7 x 10^{-6} and 1.0 x 10^{-6} cm^2/s, and the experimentally measured mean bulk velocity for Dextran of V=0.37μm/s, were used in the numerical simulation to generate the Dextran concentration profiles shown at different detection positions over time.

3.4.0. Discussion

The ability to produce mathematically-validated, chemical concentrations and concentration gradients is essential for the study of micro and nano-scale transport within microfluidic devices. The bridged μLane system generates spatially-distributed concentration gradients within microenvironments by exploiting the density difference between the reagents used. Although these differences are minimal, they are the driving forces that generate pressure differences between the source (SRR) and sink (SKR) reservoirs to result in bulk flow along the connecting microchannel. Importantly, the bridge channel was incorporated into the system in order to diminish bulk flow in the microchannel to ultra-low levels that enabled autonomous operation for several days without need of replenished reagent volumes, external pumps, or power supplies.

The bridged μLane system utilizes ultra-low bulk flow as an advantage, as convective transport rapidly decreases the time required for reagent concentration to reach steady-state along the microchannel length. In the absence of the 2nd Layer PDMS for hydrostatic balance, for example, experiments illustrated that a submicroliter volume difference generated bulk flows within the microchannel on the order of 92.3 μm/s, which would rapidly deplete the system within one hour. In the absence of bulk flow, however, Dextran transport via diffusion alone (using the average of cited Dextran diffusivities, 0.82 x$10^{-6}$$cm^2/s$) would require over 470 hours

to reach a steady-state gradient within a 13-mm-long microchannel, instead of the 40 hours reported here. These minute bulk flows helped generate concentration gradients that spanned five orders of magnitude within the same experimental device. Larger bulk flows would have generated smaller differences in concentration gradients, perhaps requiring multiple systems to examine a range of gradients, as well as required additional reagent volumes and/or pumping per experiment.

Lastly, while other devices rely upon machined parts and complex 3D assembly, our system accomplishes microfluidic transport via inexpensive PDMS layering to accent the device's ease of use. Fabrication does not require clean room facilities with conventional, but costly, equipment such as reactive ion etchers, contact aligners, or UV steppers. Instead, microfabrication was performed within a fume hood using routine laboratory equipment such as table top stands, ovens, and hand-machined plastic carriers made to fit bench top mechanical dimensions. This large benefit eases the adaptability of the bridged μLane to laboratories that are not microfluidics-based, for use with a variety of samples and applications that range from examining particle distributions in environmental (Yamada & Seki, 2006) to the study of cell (Kim et al, 2009) and bacterial chemotaxis (Englert et al, 2010).

In summary, we have developed the bridged μLane system to achieve autonomous and defined chemical transport within microenvironments using inexpensive fabrication and straightforward operation protocols. The bridged μLane system is a novel and user-friendly platform with which to generate and examine the effects of reagent concentration gradients in a multitude of scientific and engineering studies.

Acknowledgements

This work was supported by the National Institutes of Health (GM071702-02), the National Science Foundation (CBET0428573) and PSC-CUNY.

4

Chapter 4. Role of Epidermal Growth Factor-triggered PI3K/Akt signaling in the Migration of Medulloblastoma-derived Cells

Veronica Dudu[1], Richard A. Able, Jr.[1,2], Veronica Rotari[1] ,Qinjun Kong[1], and Maribel Vazquez[1]

[1]Department of Biomedical Engineering, The City College of The City University of New York (CCNY), 160 Convent Avenue, Steinman Hall Room 403D, New York, NY 10031

[2]Department of Biochemistry, The City Graduate Center of The City University of New York (CCNY)365 Fifth Avenue, New York, NY 10016

Submitted to the Biomedical Engineering Society (BMES) Journal Cellular and Molecular Bioengineering (CMBE) August 2011

Running title: Role of EGF in medulloblastoma migration

Footnotes: Person to whom reprint requests should be sent: Dr. Maribel Vazquez, The City College of New York, Department of Biomedical Engineering, Steinman Building ST-403D, 160 Convent Avenue, New York, NY 10031, Phone: (1) 212-650-5209, Fax: (1) 212-650-6727, E-mail: vazquez@ccny.cuny.edu

Abstract

Medulloblastoma (MB) is the most common brain cancer diagnosed among children. The cellular pathways that regulate MB invasion in response to environmental cues remain incompletely understood. Herein, we examine the migratory response of human MB-derived Daoy cells to different concentration profiles of Epidermal Growth Factor (EGF) using a microfluidic system. Our findings provide the first quantitative evidence that EGF concentration gradients modulate the chemotaxis of MB-derived cells in a dose-dependent manner via the EGF receptor (EGF-R). Data illustrates that higher concentration gradients caused increased numbers of cells to migrate. In addition, our results show that EGF-induced receptor phosphorylation triggered the downstream activation of phosphoinositide-3 kinase (PI3K)/Akt pathway, while its downstream activation was inhibited by Tarceva (an EGF-R inhibitor), and Wortmannin (a PI3K inhibitor). The treatment with inhibitors also severely reduced the number of MB-derived cells that migrated towards increasing EGF concentration gradients. Our results provide evidence to bolster the development of anti-migratory therapies as viable strategies to impede EGF-stimulated MB dispersal.

Key words: chemotaxis; EGF; microfluidics; Daoy; PI3K/Akt

4.1. Introduction

Medulloblastoma (MB) is the most common malignant brain tumor in children, with a 60% survival rate 5 years after diagnosis (Duffner et al, 1999; Reddy, 2001). The disease is difficult to treat via surgery because of high tumor invasiveness and tumor re-occurrence following resection and/or irradiation (Menon et al, 2006). Despite the well-known metastatic potential of these pediatric tumors, the chemotactic migration of MB remains surprisingly understudied. The directed migration of brain tumor-derived cells is highly complex, involving interactions with extracellular matrix and chemoattractants that either diffuse from blood vessels or are produced by neighboring cells (Condeelis & Segall, 2003; Sahai, 2005). The migration of cells derived from glioma, the most common malignant tumor in adult brain, has been extensively studied and shown to be highly dosage-dependent on signaling from three primary growth factors: Hepatocyte Growth Factor (HGF), Platelet-Derived Growth Factor (PDGF), and Epidermal Growth Factor (EGF) (Brockmann et al, 2003). By contrast, MB migration has been shown to depend on c-Met, the HGF receptor (Guessous et al, 2010), as well as the PDGF-receptor β (PDGFR-β), but EGF-R-dependent migration in MB has only recently been examined.

EGF-R, also known as ErbB1 or HER1, is a primary oncogene (Kim & Muller, 1999; Salomon et al, 1995; Yarden, 2001) whose over-expression is recognized as a significant step in the progression and pathology of brain tumors. Multiple mechanisms are involved in EGF-R activation, including expression of EGF and EGF-R by neighboring tumor or stromal cells, enhanced cell sensitivity for EGF-like ligands, and constitutively active EGF-R mutations that lead to ligand-independent activation of the receptor (reviewed in (Hirata et al, 2002)). The role of EGF-R in MB is highly significant, as the receptor is known to be expressed in the cerebellar granule neuron precursor cells (GNPCs) (Seroogy et al, 1995) whose dysregulation is suspected

in MB tumorigenesis (Wechsler-Reya & Scott, 2001). One quantitative study has illustrated that engineered over-expression of the EGF-R homolog, ErbB2, increased the migration of MB in vitro (Hernan et al, 2003). Another study demonstrated that trans-activation of EGF-R via PDGFR-β activity was able to guide MB migration in vivo (Abouantoun & MacDonald, 2009). Further, EGF-mediated migration has been shown to be concentration gradient-dependent, as both breast cancer cells (Saadi et al, 2006) and fibroblast cells (Kong et al, 2011) responded to increasing gradients of EGF via higher motility in vitro.

In the present work, we utilize a microfluidic system (Kong et al, 2010) to examine the chemotactic migration of MB-derived cells towards EGF. We examine MB chemotactic dependency on EGF-R phosphorylation, consequent motility in response to a range of EGF concentration profiles, as well as activation of downstream phosphoinositide-3 kinase (PI3K)/Akt pathway. Our results illustrate that EGF-initiated MB migration relies on the PI3K/Akt signaling pathway, and is ligand-dependent despite constitutive, basal EGF-R signaling. In addition, we demonstrate that larger concentration gradients of EGF stimulate increased numbers of MB cells to become motile. Our results comprehensively point to the significance of EGF-mediated invasion of MB, and highlight how targeting of the molecular triggers that drive MB migration may represent means to improve outcome, reduce relapse and impede metastasis.

4.2. Materials and Methods

Cell Culture

The MB-derived Daoy cell line (#HTB-186, purchased from ATCC, Manassas, VA) was established from a tumor biopsy of a 4-year-old boy. Cells were cultured with sterile Eagle Minimum Essential Medium (EMEM) without phenol red (pH 7.1-7.4) (Mediatech Inc., Herndon, VA), supplemented with 2% L-Glutamine (Mediatech Inc., Herndon, VA), 1% Penicillin-Streptomycin-Amphotericin B - 100x solution (Mediatech Inc., Herndon, VA), and 10% fetal bovine serum (FBS) (Gemini Bio-Products, West Sacramento, CA). The cells were grown onto sterile polystyrene tissue culture flasks (BD Biosciences, Franklin Lakes, NJ) and incubated at 37^{o}C with 5% CO_2. Cells were not serum-starved for any experiments in this study.

Antibodies and Immunocytochemistry

Immunocytochemistry was performed as described previously (Dudu et al, 2008). Briefly, Daoy cells grown on coverslips were fixed with paraformaldehyde (Sigma, St. Louis, MO) and labeled with mouse anti-phosphorylated-EGF-R (1:500) (Meridian Life Sciences, Saco, ME), mouse anti-internal-EGF-R (1:500) – recognizing an internal epitope (Meridian Life Sciences, Saco, ME), rabbit anti-phosphorylated-Akt (1:200) (Cell Signaling, Danvers, MA), rabbit anti-phosphorylated-ERK-1/ERK-2 (1:200) (Cell Signaling, Danvers, MA), anti-mouse and anti-rabbit AlexaFluor® 488 or 594 antibodies (Invitrogen Molecular Probes, Eugene, OR). Transferrin AlexaFluor® 594 conjugate (Tf) and Cholera toxin subunit B AlexaFluor® 594 (CT-B) (both from Invitrogen Molecular Probes, Eugene, OR) were used to label the clathrin-mediated and clathrin-independent endocytic pathway, respectively. A 20 μg/mL solution of Tf

or a 10 μg/mL solution of CT-B were applied and incubated with Daoy cells for 1 hr at 37°C. Afterwards, the cells were fixed with paraformaldehyde and mounted in glycerol. Each experiment was performed at least three times.

Stimulation and inhibition of EGF-R and Akt

The stimulation of signaling pathways was adapted from the literature (Fukazawa et al, 1996). Briefly, monolayer cultures were separately incubated with 10, 100 and 1000 ng/ml EGF or EGF-Alexa 488 (Invitrogen Molecular Probes, Eugene, OR) for 20 minutes or 1 hour at 37°C. The active EGF-R was inhibited by incubating stimulated Daoy cells for 30 minutes or 1 hour at 37°C with 1 μM Tarceva, kindly provided by Dr. Eric Holland (Memorial Sloan-Kettering Cancer Center, New York, NY). In a similar manner, the active PI3K was inhibited by incubating stimulated Daoy cells for 1 hour at 37°C with 0.5 μM Wortmannin (EMD-Calbiochem, Gibbstown, NJ). All cell samples were fixed and stained immediately following experimental protocols.

Confocal Microscopy and Image Analysis

Confocal laser scanning microscopy imaging was performed using a Leica TCS SP2 instrument with a 63X oil immersion objective (NA 1.4). Identical imaging conditions were used for each set of experiments. Image analysis of fluorescence level was performed using ImageJ software (NIH, Bethesda, MD). Briefly, for each image, fluorescence intensity per cell was measured and then normalized by the cell area. The data was averaged for each condition.

Statistical significance was analyzed by performing Anova t-tests with the InStat software (GraphPad Software Inc., La Jolla, CA).

MTT assay

The Vybrant MTT Cell Proliferation Assay Kit (Invitrogen Molecular Probes, Eugene, OR) was used according to the protocol to determine cell growth rates. Briefly, MB-derived cells stimulated with multiple concentrations of EGF (0, 10, 100, and 1000 ng/ml) were treated with MTT reagents, and incubated for additional 56 hours at 37°C. The absorbance of the samples was afterwards read at 570 nm, and normalized to that of the control, which contained plain medium. Each experiment was done in triplicate.

Controlled Microenvironment

This study utilized our laboratory-developed μLane system, whose design and testing has been previously described (Kong et al, 2010). The system was fabricated using contact photolithography, elastomeric molding of polydimethylsiloxane (PDMS), and ozone bonding of PDMS to glass microscope slides. The μLane relies on molecular diffusion to generate concentration gradients and sustain steady-state over a period of 2-3 days. The system consists of a single, closed microchannel that connects two fluidic reservoirs, called the sink and the source reservoirs, as shown in Figure 1A and 1B. The microchannel measured 7,000 μm in length and 95 μm in hydraulic diameter, while the source and sink reservoir volumes measured 9 μl and 170 μl, respectively.

Molecular transport within extracellular matrix (ECM) of the μLane was validated experimentally and computationally using fluorescent Dextran (10 kDa; Invitrogen, Eugene, OR) as a model, based on similar hydrodynamic, or Stokes radii, and molecular configurations to EGF (Cadena et al, 1994; Nicholson & Tao, 1993). Experimental measurement of Dextran diffusion was performed as described in the literature (Kim & Breuer, 2004), by tracking the displacement of the fluorescently-labeled molecule. In order to determine the concentration distribution within our system, 40 μg/ml Dextran was mixed with 2.5 mg/ml Growth Factor-Reduced Matrigel (BD Biosciences, San Jose, CA) and loaded into the microchannel. The source and sink reservoirs were subsequently filled with EMEM. Fluorescent Dextran diffusion within the microchannel was imaged at different positions along the channel via time-lapse microscopy using the Nikon TE2000 inverted microscope with a 20X long working distance dry objective (NA 0.40 /WD 3.0mm) and a cooled CCD camera (CoolSNAP EZ, Photometrics, Tucson, AZ). Images were recorded every hour for 84 hours using Nikon software (Nikon Instrument Element 2.30 with 6D module, Morrell Instrument Company Inc., Melville, NY). The fluorescence intensity was measured at all time-points using the Nikon software. Experimental measurement of Dextran transport illustrated a transient evolution of a linear, steady-state concentration gradient along the microchannel after t = 69 hrs, (Figure 1C). Computational modeling of Dextran concentration profiles within the μLane system was performed using Finite Element Modeling (FEM) (FEMLab version 3.2, Comsol Inc. Burlington, MA to model the one-dimensional diffusion equation:

$$\frac{\partial C}{\partial t} = D\frac{\partial^2 C}{\partial x^2} \qquad (1)$$

where C (mg/ml) is the concentration, and D (m^2/s) is diffusivity (Kong et al, 2011). FEM computation used an initial reagent concentration in the source chamber and microchannel of 40 μg/ml in order to match the experimental conditions, and an initial concentration in the sink chamber of 0 μg/ml. Reported diffusivity values of Dextran (Ekani-Nkodo & Fygenson, 2003; Lang et al, 1986; Payet et al, 2008; Xia et al, 1998; Yuan et al, 2010) were substituted into the model in order to generate spatial concentration profiles within the microchannel that most accurately modeled those measured experimentally. Computational predictions illustrated in a linear, steady-state gradient along the 7-mm-long microchannel after t = 70 hrs (Figure 1D). Finite Element modeling of the dextran concentration profiles generated within the microchannel and in the source and sink chambers, respectively, is shown in Figure 1E. We employed the same modeling to predict that EGF diffusion will achieve steady-state within t = 70 hours within the μLane design used in this study (Figure 1C and 1D).

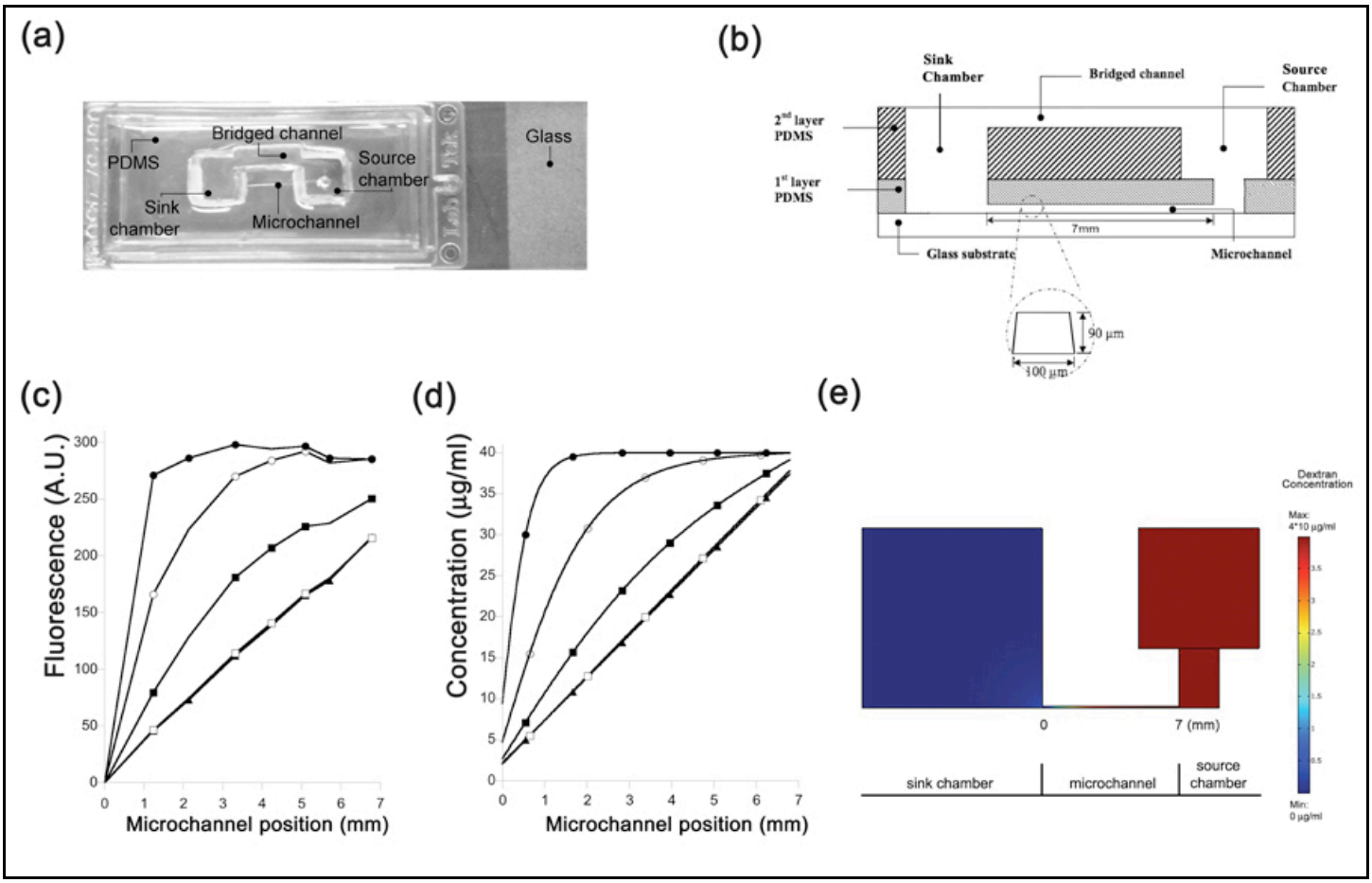

Figure 1: Characterization of the mLane system for molecular transport. (A) Image and (B) schematics of the µLane system. (C) Measurement of dextran concentration profiles within a 7-mm-long microchannel over time. The dextran fluorescence (arbitray units) decay with time is plotted against the length of the microchannel (●t=16 min, ○t= 3 hr, ■t=14 hr, □t=70 hr, ▲t=111 hr). The concentration profiles reaches a linear, steady-state at t = 70 hrs. (D) Computational simulation of dextran concentration profiles formed within the microchannel. Computationally-derived changes in dextran concentration within the channel over time are plotted against the length of the microchannel (●t=16 min, ○t= 3 hr, ■t=14 hr, □t=70 hr, ▲t=111 hr). (E) Finite Element Modeling of Dextran concentration profiles generated within the microchannel and in the source and sink chambers, respectively.

Cell Migration Experiments

EGF at different concentrations (10, 100, or 1000 ng/ml and 0 ng/ml for control) was mixed with 2.5 mg/ml Growth Factor-Reduced Matrigel™ and loaded into the microchannel and the source reservoir via syringe. μLane systems were placed in a micro-incubator (Warner Instruments LLC, Hamden, CT) that was maintained at 37ºC and mounted on a motorized stage of a Nikon TE2000 inverted microscope. MB cells at a cell density of 10^6/ml and in a solution of EMEM were added into the sink reservoir. Cells were loaded such that they adhered evenly to the bottom of the reservoir and along its microchannel interface. Cell movement from the sink reservoir into the microchannel was monitored through light microscopy, using a 20X long working distance dry objective and a cooled CCD camera. Images of cells moving from the sink reservoir into the microchannel were recorded for 72 hours using Nikon software (Nikon Instrument Element 2.30 with 6D module, Morrell Instrument Company Inc., Melville, NY). The total number of migrating cells into the microchannel was counted, and the total distance migrated by each of those cells was measured using the Nikon software.

Lastly, migration experiments were performed using known inhibitors of EGF and PI3K pathways. Cells were separately treated for 1 hour with 1 μM Tarceva (EGF-R inhibitor), or with 0.5 μM Wortmannin (PI3K inhibitor). Treated cells were loaded into the sink reservoir of the μLane and their migration imaged and analyzed as described above. Note that inhibitor experiments were only performed using the gradients generated under experimental conditions of 1000 ng/ml EGF. For all migration experiments, the data was plotted and statistical significance was analyzed via Anova tests with InStat software (GraphPad Software Inc., La Jolla, CA).

Cell Cytoplasmic Extensions and Cell Shape Index

Cells were cultured within 2.5 mg/mL of Matrigel, with or without 100 ng/ml EGF for up to 100 hours. Images of the cells were recorded using the Nikon TE2000 microscope and Nikon software. The cytoplasmic extensions of cells were counted and their numbers were averaged at the focal plane illustrating the maximum cell area. The average cell morphology was analyzed using the cell shape index (CSI) (Shen et al, 2006), as done previously by our group (Kong et al, 2011):

$$CSI = \frac{4\pi A}{P^2} \qquad (2)$$

where A represents the cell projected area, and P denotes the cell perimeter. Statistical significance of data differences was analyzed via Student t-tests using InStat software.

4.3. Results

4.3.1. Basal and ligand-activated EGF-R in MB

In order to examine EGF-induced migration of MB, we first investigated EGF-R activation, inhibition, and localization. The total EGF-R population within the MB cells studied was detected via an antibody that recognized the intracellular region of the receptor, iEGF-R. Here, iEGF-R was labeled in non-stimulated cells (Figure 2A), in cells stimulated with EGF (Figure 2B), and in cells where the activating effect of EGF was inhibited with Tarceva (Figure 2C). Tarceva is a commercial compound known to inhibit EGF-R auto-phosphorylation without affecting EGF-R expression or surface receptor density (Herbst, 2005). No significant difference in total intensity levels of iEGF-R between stimulated and Tarceva-inhibited cells were measured with respect to controls (Figure 2D). Next, immunolabeling was performed with an antibody that recognized phosphorylated EGF-R (pEGF-R). Results illustrated that MB-derived cells exhibited basal levels of activated EGF-R (Figure 2E). Interestingly, EGF stimulation of MB increased cellular levels of pEGF-R (Figure 2F) by 2.8 fold (Figure 2H), indicative of a ligand-dependent EGF-R response regardless of basal EGF-R signaling. Treatment with Tarceva consistently abolished ligand-induced EGF-R phosphorylation (Figure 2G), as levels of phosphorylated EGF-R were similar to those detected in non-stimulated cells (Figure 2H). Next, MB-derived cells were incubated with Transferrin (Tf), a marker of the clathrin-mediated endocytic pathway and Cholera Toxin Subunit-B (CT-B), a marker of the clathrin-independent endocytic pathway, to visualize endocytic compartments. In MB-derived cells, iEGF-R was seen to co-localize predominantly with Tf: 92% ± 3% (Figures 2I1-3 and 2J), but only 14% ± 4% with CT-B (Figure 2J).

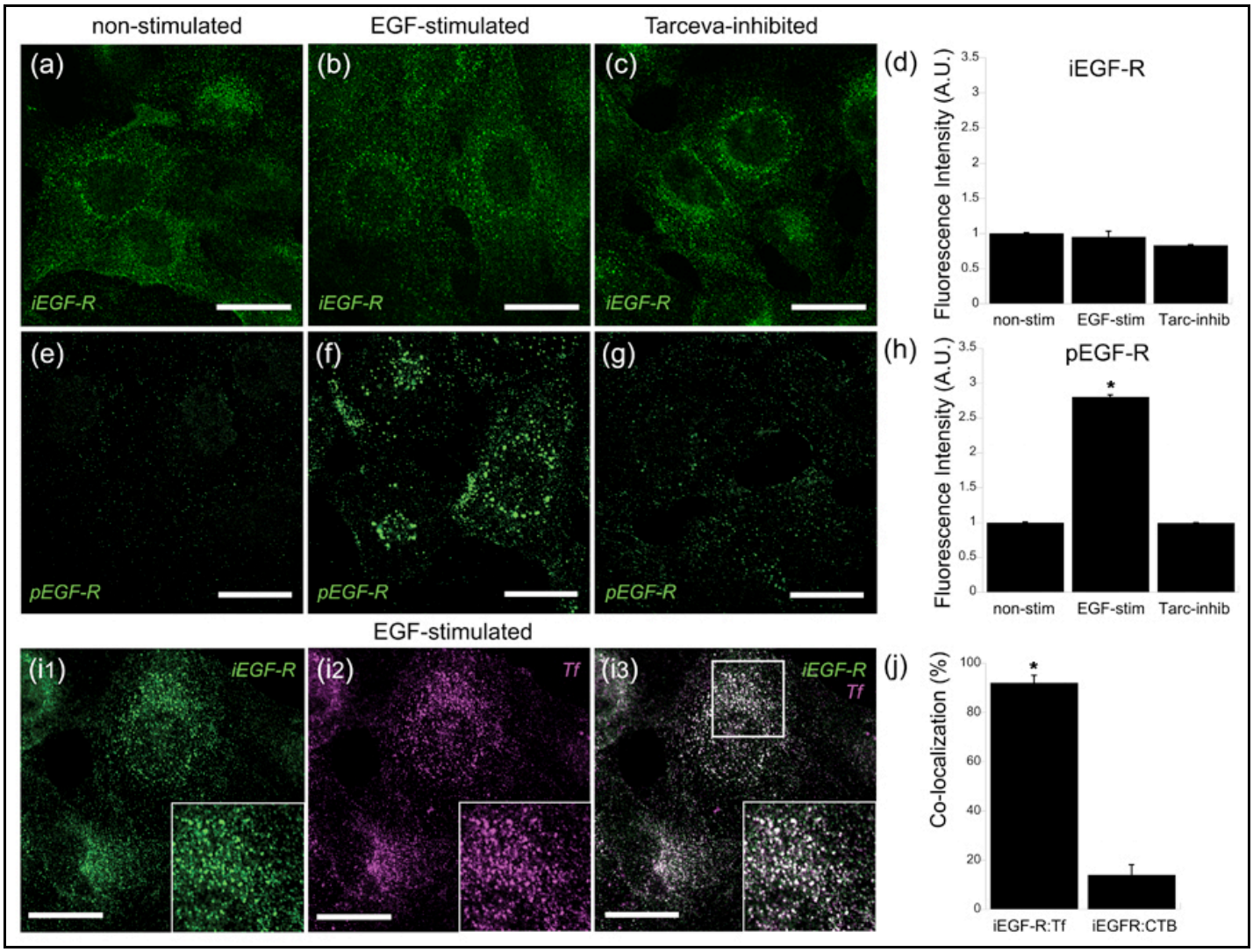

FIGURE 2: EGF-R phosphorylation levels and localization are mediated by EGF pathway stimulation and inhibition in MB-derived cells. (A) Localization of total EGF-R (iEGF-R) in non-stimulated cells. (B) Localization of iEGF-R in cells stimulated with 1000 ng/ml EGF. (C) Localization of iEGF-R in cells in which EGF signaling was inhibited by 1 μM Tarceva. (D) Average fluorescence intensity of total (iEGF-R) and in non-stimulated; EGF-stimulated and Tarceva-inhibited cells. (E)Localization of phosphorylated EGF-R (pEGF-R) in non-stimulated cells. (F) Localization of pEGF-R in cells stimulated with 1000 ng/ml EGF. (G) Localization of pEGF-R in cells in which EGF signaling was inhibited by 1 μM Tarceva. (H) Average intensity of phosphorylated EGF-R (pEGF-R) in non-stimulated; EGF-stimulated and Tarceva-inhibited cells. (I) iEGF-R (green) (I1) accumulates in Transferrin (Tf)-positive vesicles (purple) (I2) in EGF-stimulated cells; merged channels (I3). Insert shows higher magnification of the boxed area and co-localization between EGF-R and Tf. Scale bars, 20 μm. (J) Co-localization of transferrin (TR) and Cholera toxin subunit B (CTB) with iEFG-R in EGF-stimulated cells.

4.3.2. EGF induces Akt phosphorylation in MB

The next set of experiments examined the role of PI3K/Akt and MAPK/ERK signaling in the EGF-R-induced response of MB, as activation and cross-talk of these pathways downstream of activated EGF-R is well-known in glioblastoma and breast cancer migration (Kruger & Reddy, 2003; Zohrabian et al, 2009). Levels of phosphorylated Akt (pAkt) in cells stimulated with EGF (Figure 3B) were seen to increase 3.32-fold with respect to those in non-stimulated cells (Figures 3A, I). Consistently, pAkt levels were drastically reduced to control levels when EGF signaling was inhibited by Tarceva (Figures 3C, I), as well as when PI3K signaling was inhibited by Wortmannin (Figures 3D, I). Levels of phosphorylated ERK-1/2 (pERK) in cells stimulated with EGF (Figures 3F) increased 1.81-fold with respect to non-stimulated cells (Figures 3E, J), and were similar to levels for which EGF signaling was inhibited by Tarceva (Figures 3G, J). In cells treated with Wortmannin, pERK levels were similar to those measured in the absence of the PI3K inhibitor (Figures 3H, J), indicating negligible, if any, cross-talk between MAPK/ERK and PI3K/Akt pathways.

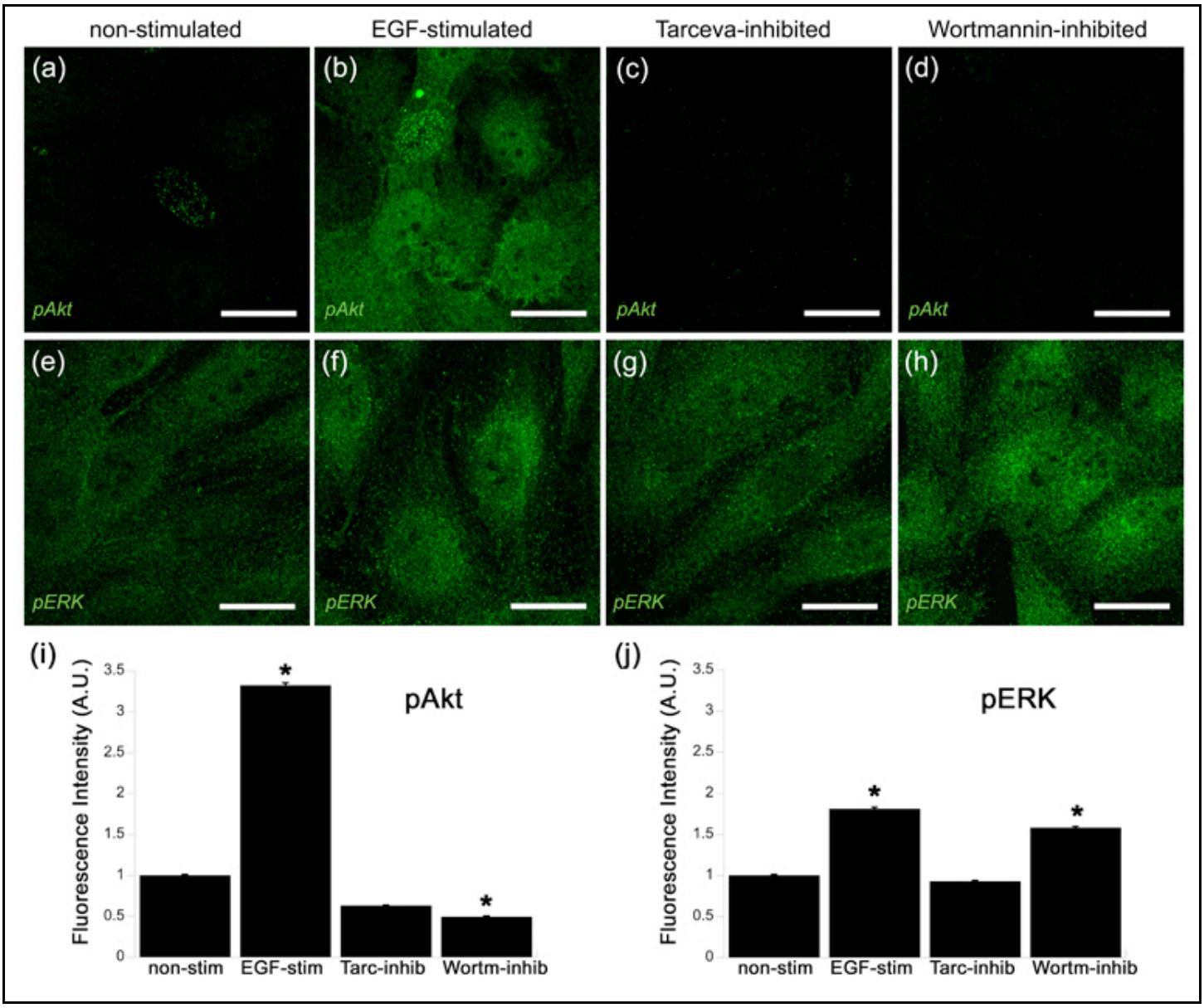

FIGURE 3: Akt phosphorylation levels and localizations are mediated by EGF pathway stimulation and inhibition in MB-derived cells. Localization of phosphorylated Akt (pAkt) in non-stimulated cells (A), in cells stimulated with 1000 ng/ml EGF (B) cells in which EGF signaling was inhibited by 1 μM Tarceva (C), and cells in which PI3K signaling was inhibited by 0.5 μM Wortmannin (D). Localization of phosphorylated pERK in non-stimulated cells (E), in cells stimulated with 1000 ng/ml EGF (F), cells in which EGF signaling was inhibited by 1 μM Tarceva (G), and cells in which PI3K signaling was inhibited by Wortmannin (H). Scale bars, 20 μm. (I) Average fluorescence intensity of activated Akt (p-Akt) in non-stimulated; EGF-stimulated; Tarceva-inhibited; and Wortmannin-inhibitied cells. (J) Average fluorescence intensity of activated activated Erk (p-Erk) in non-stimulated; EGF-stimulated; Tarceva-inhibited; and Wortmannin-inhibited cells.

4.3.3. MB morphology and proliferation within μLane system

The μLane system was next used to examine the EGF-stimulated behavior of MB-derived cells within extracellular matrix (ECM). MB cultured within ECM-alone and ECM supplemented with 100 ng/ml EGF were seen to grow, divide, and survive inside of the microchannel for 100 hours. Cellular changes were measured via the cell shape index (CSI), number of cytoplasmic extensions per cell, and observed proliferation time within the microsystem. Cells within ECM-alone exhibited rounder morphology (Figure 4A), while cells in ECM exposed to EGF exhibited elongated morphology (Figure 4B). The average, measured CSI was lower for cells exposed to EGF (Figure 4C), consistent with CSI definition, which approaches 1 for an amoeboidal cell and decreases towards zero for an elongated or branched cell (Eqn. 2). The average number of cellular extensions was not statistically different between stimulated and non-stimulated cells (Figure 4D). Lastly, MB cell division was seen to occur consistently between 42 and 46 hours in all microchannel experiments. As a result, analysis of cell behavior prior to t = 40 hrs was deemed to be primarily migratory and non-proliferative, while MB behavior post t = 40 hours was considered both migratory and proliferative in all subsequent analyses.

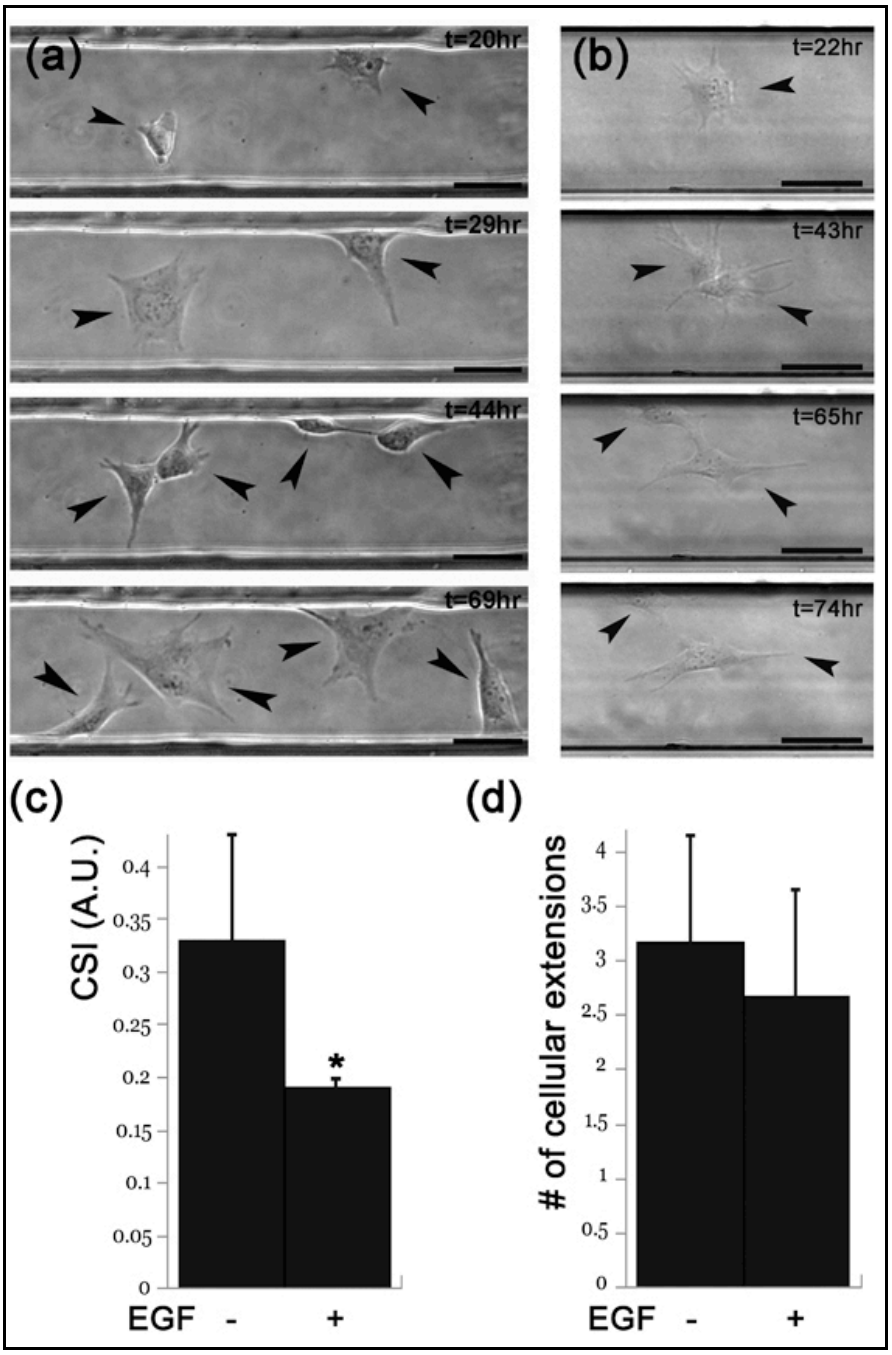

FIGURE 4: EGF induces morphological changes in MB-derived cells. (A) Cells grow and divide within 3D matrix inside of the microchannel in the absence of EGF. Arrowheads point to the dividing cells and the resulting daughter cells. (B) Cells in the presence of 100 ng/ml EGF within 3D matrix inside of the microchannel. Arrowheads point to the dividing cells and the resulting daughter cells. Scale bars, 50 μm. (C) Cellular Shape Index (CSI) of cells grown within 3D matrix in microchannels in the absence of EGF and in the presence of 100 ng/ml EGF (sample size: $n_{control}$=37, n_{EGF}=21). * $p<0.05$. (D) Number of cellular extensions in the absence of EGF and in the presence of 100 ng/ml EGF (sample size: $n_{control}$=37, n_{EGF}=21). Scale bars = 50 μm.

4.3.4. EGF concentration profiles generated within μLane system

EGF transport within the μLane generated a range of concentrations and gradients along the microchannel length over time. The concentration gradients present along the μLane from t = 0 hrs to t = 72 hrs were calculated by measuring the change in EGF concentration over a fixed microchannel distance. Mathematically, gradients can be represented by the changing slope of the curves. Note that because EGF is distributed non-linearly along the microchannel length prior to steady-state (as shown in Figure 1C), concentration gradients are also highly non-linear during this time, and encompass several orders of magnitude per experimental condition. Steady-state EGF distributions along the microchannel generated by using separate solutions of 10, 100, and 1000 ng/ml concentrations in the source reservoir each exhibited linear steady-state concentration gradients at 70 hrs.

4.3.5. EGF-mediated chemotaxis of MB within μLane system

The migration of MB-derived cells was measured in response to the separate EGF concentration profiles described above. Microenvironments generated by using 1000 ng/ml in the sink reservoir attracted the largest numbers of cells to migrate into the microchannel, both prior to and after MB proliferation (i.e. before and after t = 40 hrs, respectively). As shown in Figure 5A, the number of cells that migrated out of the sink reservoir and into the microchannel prior to 40 hours (non-proliferative) increased when exposed to increasing EGF concentrations and gradients. Number of cells observed within microchannels between t = 40 hrs and t = 70 hrs (motile and proliferative) similarly increased with EGF concentration and gradient, although in larger proportions than in experiments measuring migration alone. Larger numbers of cells were drawn into the channel when exposed to increasing EGF concentration gradients generated by

using 10, 100 and 1000 ng/mL concentrations. In addition, the migration of MB treated with the inhibitors Tarceva and Wortmannin was examined within the μLane environment generated using 1000 ng/ml EGF. As seen, the numbers of cells that responded to EGF when EGF-R signaling was inhibited by Tarceva, and when the PI3K pathway was inhibited by Wortmannin, were less than 5% of the controls in each case (Figure 5A).

Additionally, the average cell distances traveled within the different environments of the μLane were calculated for pre-proliferative cells ($t < 40$ hrs) and for cells undergoing both migration and proliferation ($t = 40$ hrs and $t = 72$ hrs). As seen in Figure 5B, the average cell distances traveled prior to $t = 40$ hrs (i.e. migration only) and between $t = 40$ hrs and $t = 72$ hrs (migration and proliferation) were lowest for controls, and increased slightly with EGF concentration and gradient. However, no statistical difference in average distance traveled was measured between the different EGF concentrations. Finally, in experiments where cells were stimulated and treated separately with Tarceva and Wortmannin, average distances traveled were reduced by 70% and 57%, respectively.

We lastly utilized the precisely-defined environment of our microfluidic system to measure the sub-populations of MB that migrated in response to specific concentrations and gradients of EGF prior to proliferation. In Figure 5C we illustrate the average numbers of cells that migrate separate 100 μm-segmented distances in relation to the explicit values of EGF concentration and gradient to which cells were exposed at $t = 40$ hrs. By measuring the average numbers of cells that migrate specific distances, the data illustrate that approximately 60-70% of cells in all experiments were observed to travel less than 200 μm into the microchannel prior to $t = 40$ hrs. Further, sub-populations that migrated less than 200 μm in response to EGF were not statistically different from one another and were lower than the average numbers recorded for the control

experiments. Furthermore, cells exposed to gradients generated by using the lowest EGF concentration examined here, 10 ng/ml, contained sub-populations that traveled up to 600 μm. In contrast, no cells were observed to migrate past 400 μm when exposed to higher EGF concentrations. Overall, the portion of cells that migrated distances greater than 300 μm in the microsystem was a minimal 7% or less of MB exposed to 100 ng/ml and 1000 ng/ml of EGF. By contrast, this sub-population was an appreciable 20% of MB exposed to the lowest EGF concentration of 10 ng/ml (Figure 5C).

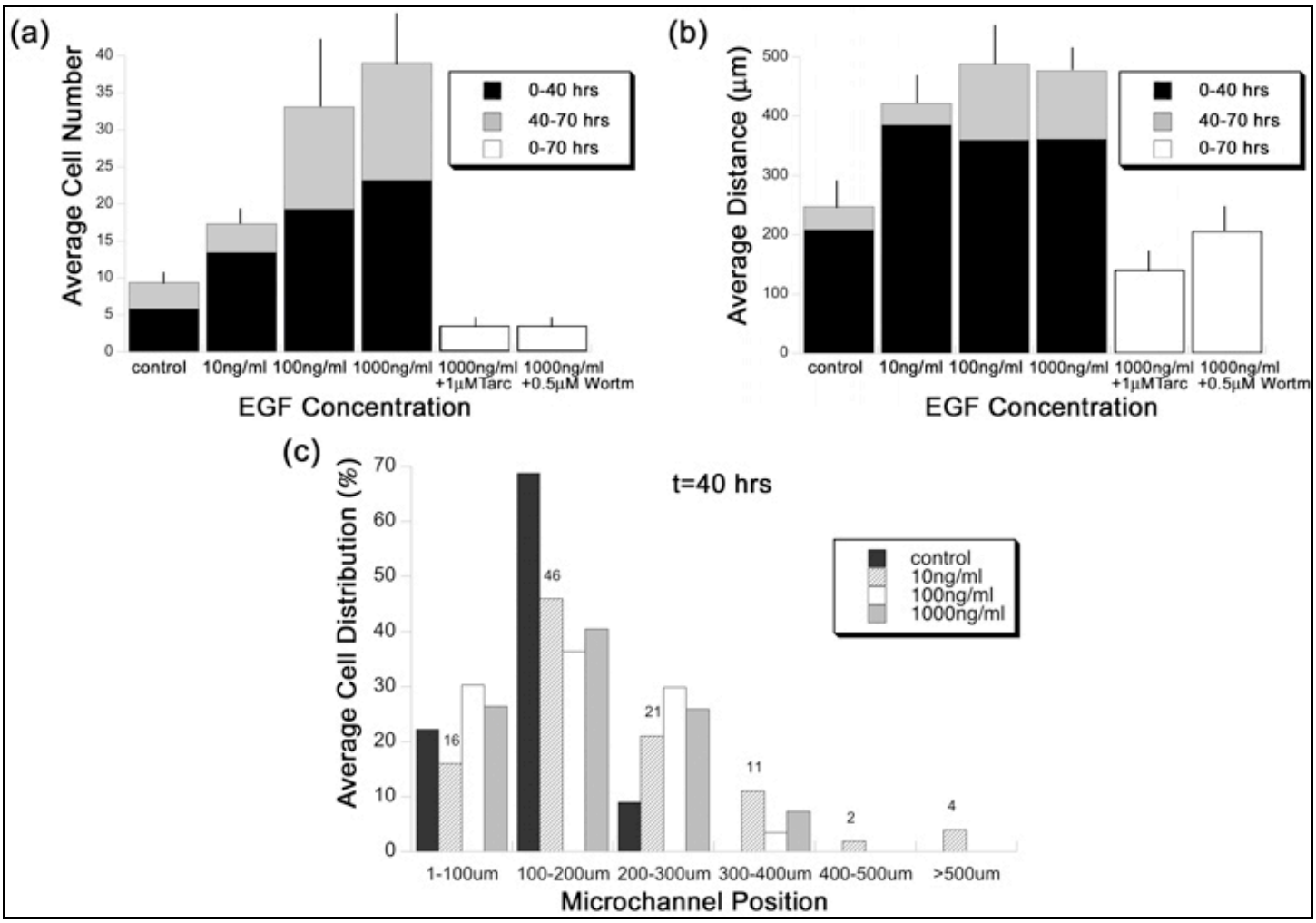

FIGURE 5. Increasing EGF concentration profiles target the invasion of a large number of MB-derived cells for longer distances. MB-derived cells were exposed 0, 10 ng/ml, 100 ng/ml, 1000 ng/ml, 1000 ng/ml EGF concentrations and 1000 ng/ml EGF + 1 μM Tarceva and 1000 ng/ml EGF + 0.5 μM Wortmannin concentration gradients for 70 hours. (A) Number of invading cells is dependent on different EGF concentration gradients. The average numbers of invading cells are represented with standard error bars. (B) Distance invaded by MB-derived cells is dependent on different EGF concentration gradients. The average distance invaded into the microchannel are represented with standard error bars (A, B sample size: $n_{control}$=6, $n_{EGF\ 10}$=6, $n_{EGF\ 100}$=4, $n_{EGF\ 1000}$= 7, n_{Tarc}=5, n_{Wort}=3). * $p<0.01$. (C) The percentage of the total number of invading cells for each experimental condition is plotted according to distance travelled. Distance is reported in 100 μm intervals.

4.4. Discussion

The migration of cells from pediatric brain tumors has been largely understudied despite their high tumor metastatic potential and aggressive invasion into healthy brain. While EGF-R is known to play significant roles in the chemotaxis of tumor cells within adult brain, the EGF-induced migration of MB has only recently been examined. The current study examined the activation of EGF-R-mediated pathways in MB and directly correlated MB migratory response to a range of EGF concentrations and gradients generated by using microfluidic system.

Initial immunocytochemisty experiments demonstrated constitutively-active EGF-R signaling in the MB cells studied. Interestingly, EGF-R response was also ligand-dependent, as increased EGF-R phosphorylation and co-localization with endosomes was observed upon EGF stimulation. These results confirm the findings of other studies (Meco et al, 2009), which documented basal EGF-R expression in medulloblastoma Daoy cells via quantitative PCR, as well as confirmed Daoy autocrine expression of EGF and TGF-a ligands. These data illustrate that EGF-R signaling is appreciable for MB cells even in the presence of exogenous growth factors. The finding that EGF-R in MB can respond to external EGF despite basal EGF-R signaling bolsters the hypothesis that exogenous EGF stimulation is able to stimulate chemotactic responses in MB-derived cells. When examining EGF activation of the PI3K and MAPK pathways, our data illustrated that the PI3K pathway was activated by EGF and inactivated when EGF signaling was inhibited by Tarceva, a kinase inhibitor, and Wortmannin, an Akt inhibitor. However, our data illustrated minimal effect of either compound on pERK, suggesting MAPK is only minimally involved in the EGF-R-induced chemotactic signaling of these cells. This result is in conflict with existing research, which illustrated decreased pERK activation in response to a MAPK inhibitor, gefitinib, in both serum starved and serum treated

Daoy cells (Meco et al, 2009). However, we note that the lack of inhibited pERK seen in our study could be due to a weaker sensitivity to Tarceva versus gefitinib in Daoy cells, as the gefitinib kinase inhibitor specifically targets ErbB2, which is known to be less expressed in Daoy than other MB cell lines (Calabrese et al, 2003).

We next examined EGF-mediated migration of MB in a microfluidic system, which enables precise control of the cellular microenvironment, as well as real-time cell visualization and measurement of cell behavior. While conventional systems such as transwell assays provide quantitative data to describe numbers of cells that become motile in response to a stimulus, the application of microdevices enables experiments to examine mechanistic parameters such as motility, polarization, directionality or the sensitivities of individual cells to concentration gradients and thresholds. However, we reiterate here that because our experiments were conducted continuously for over 72 hours, measurements of traveled cell distances include effects from all transient, non-linear gradients generated during the temporal evolution of each steady-state gradient examined (as shown in Fig. 1C, 1D). As a result, the data includes transient effects of higher concentrations and higher gradients present prior to steady-state at t = 70 hrs.

A first technical point of interest in this work is that Matrigel provided a suitable ECM for which to evaluate MB chemotactic migration. This is of interest because the diversity of motility modes utilized by cancer cells (Yamada & Cukierman, 2007) has called into question the use of Matrigel given the matrix's constituent, biologically-relevant molecules (reviewed in (Yuan et al, 2006)). Our data illustrate that the Matrigel effects were consistent with each experiment and every EGF concentration used, and thus did not contribute to the differences in migratory measurements recorded. In controls, a small, but measurable, number of cells were observed to migrate into the microchannel as a likely result of MB chemokinesis. But the number of cells

that responded in our system as a result of experimental conditions greatly outweighed the presumably-constant, baseline number of cells that migrated into the system as a result of the Matrigel alone.

Migration experiments in our microdevice revealed that the numbers of motile cells increased with increasing gradient, both before and after proliferation occurred within microchannels. The highest concentration gradient resulted in the largest gain in motile cell numbers. This result is significant because similar in vitro experiments have illustrated that gradient chemosensitivity is cell type-dependent. Our data becomes the first to show that the motility of MB-derived cells increases with increasing EGF concentration gradient. The data presented here is among the first to quantitatively demonstrate that gradient fields generated by ultra low concentrations of EGF may contribute to MB invasion and metastasis via stimulation of subpopulations with high motility responsiveness. While biopsies have illustrated large degrees of cellular heterogeneity in brain tumors, our results are striking because we illustrate heterogeneity in motility responsiveness using the an established cell line, which presumably is more homogeneous by its long standing culture.

4.5. Conclusion

The current report demonstrates the role of EGF-induced Akt activation in the migration of MB-derived cells in vitro. Results of microfluidic-based experiments correlated MB increased chemotactic response with gradient fields generated using ultra-low concentrations of EGF, providing additional impetus for the development of new anti-migratory strategies as therapeutic agents.

ACNOWLEDGMENTS

This work has been supported by the National Institutes of Health (R21 CA 118255 and U54 MICHOR), The Pediatric Brain Tumor Foundation, and PSC-CUNY (No. 69424).

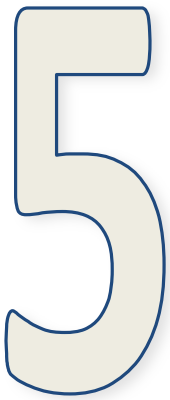

CHAPTER 5. Low Concentration Microenvironments Enhance the Migration of Neonatal Cells of Glial Lineage

Richard A. Able, Jr.[1,2], Celestin Ngnabeuye[1], Eric Holland[3] and Maribel Vazquez[1]

[1]Department of Biomedical Engineering, The City College of The City University of New York (CCNY), 160 Convent Avenue, Steinman Hall Room 403D, New York, NY 10031

[2]Department of Biochemistry, The City Graduate Center of The City University of New York (CCNY), 365 Fifth Avenue, New York, NY 10016

[3]Department of Neurosurgery, Memorial Sloan Kettering Cancer Center, New York, NY 10021

This abstract was rated as one of the top abstracts in the Cellular and Molecular Bioengineering Track submitted for presentation at the 2011 BMES meeting in Hartford, CT. Based on a peer evaluation, an invitation has been extended for submission of a full length paper in a special issue of the BMES journal "Cellular and Molecular Bioengineering" (CMBE) by November 28, 2011.

Footnotes: Person to whom reprint requests should be sent: Dr. Maribel Vazquez, The City College of New York, Department of Biomedical Engineering, Steinman Building ST-403D, 160 Convent Avenue, New York, NY 10031, Phone: (1) 212-650-5209, Fax: (1) 212-650-6727, E-mail: vazquez@ccny.cuny.edu

Abstract

Glial tumors have demonstrated abilities to sustain growth via recruitment of glial progenitor cells (GPCs), which is believed to be driven by chemotactic cues. Previous studies have illustrated that mouse GPCs of different genetic backgrounds are able to replicate the dispersion pattern seen in the human disease. How GPCs with genetic backgrounds transformed by tumor paracrine signaling respond to extracellular cues via migration is largely unexplored, and remains a limiting factor in utilizing GPCs as therapeutic targets. In this study, we utilized a microfluidic device to examine the chemotaxis of three genetically-altered mouse glial progenitor cell populations towards tumor conditioned media, as well as towards three growth factors known to initiate the chemotaxis of cells excised from glial tumors: Hepatocyte Growth Factor (HGF), Platelet-Derived Growth Factor-BB (PDGF-BB), and Transforming Growth Factor-α (TGF-α). Our results illustrate that GPC types studied exhibited chemoattraction and chemorepulsion by different concentrations of the same ligand, as well as enhanced migration in the presence of ultra-low ligand concentrations within environments of high concentration gradient. These findings contribute towards our understanding of the causative and supportive roles that GPCs play in tumor growth and reoccurrence, and also point to GPCs as potential therapeutic targets for glioma treatment.

Key words: chemotaxis; TGF- α; microfluidics; glial progenitors; glioma; concentration gradients; RCAS tv-a

5.1. Introduction

Gliomas are the most common form of primary brain cancer present in adults, affecting 10% of the worldwide cancer population and harboring a 5-year survival rate of less than 25% (Chamberlain, 2006; Stieber & Ellis, 2005; Wen & Kesari, 2008). These glial tumors pose unique clinical challenges because their aggressive migration within healthy brain tissue minimizes the effectiveness of surgical resection (Alves et al, 2011; Onishi et al, 2011; Tabatabai et al, 2011). A wealth of evidence now demonstrates that bulk tumor growth can occur via extensive cell proliferation (Dai et al, 2001; Park & Rich, 2009; Schiffer et al, 2010), as well as by aggressive recruitment of surrounding cells (Assanah et al, 2006; Charles et al, 2011; Fomchenko et al, 2011; Visted et al, 2003). Glial tumors have demonstrated the ability to recruit a variety of cells via paracrine signaling to maintain and extend tumor survival (Glass et al, 2005), including stem cells (Heese et al, 2005; Nakamizo et al, 2005), endothelial cells (Guo et al, 2003), macrophages (Wu et al, 2010) and endogenous precursors (Assanah et al, 2006; Higginbotham et al, 2011), or glial progenitor cells (GPCs).

A recent in vivo study demonstrated that GPCs were able to migrate from the brain subventricular zone (SVZ) towards pre-existing glial tumors and then surround the tumor mass (Duntsch et al, 2005; Glass et al, 2005). Such GPC recruitment by glial tumors is believed to be driven by chemotactic cues, i.e. chemical concentration gradients that stimulate cell migration towards a tumor mass (Stieber & Ellis, 2005; Ziu et al, 2006). Studies using mouse glial progenitors have demonstrated that different populations of GPCs exhibit distinct patterns of migration that are replicated in the human disease (Benedetti et al, 2000; Shih et al, 2004). For example, populations of GPCs have been seen to invade the brain as individual cells, as well as via chain cell migration along the vasculature (Rajasekhar et al, 2003; Shih & Holland, 2006).

Interestingly, such differences in migratory phenotype have been seen across cells where the intracellular signaling was accomplished via the same pathway (Rajasekhar et al, 2003; Shih & Holland, 2006). Whether distinct GPC migratory phenotypes become acquired with genetic backgrounds altered via tumor paracrine signaling is unknown. Further, how genetically transformed cells respond to extracellular cues via migration is largely unexplored, and remains a limiting factor in utilizing GPCs as therapeutic targets.

In this study we examine the in vitro migration of different populations of genetically-altered GPCs in order to examine how defined microenvironments affect the chemotaxis of the different GPC populations. We examine the growth factor-induced migration of cells derived from three primary mouse GPC types and one primary mouse tumor alongside two well-studied human glioblastoma cell lines. Our results document that despite the different migratory mechanisms employed by the GPC types, all GPCs exhibited chemoattraction and chemorepulsion by different concentrations of the same ligand, as well as enhanced migration in the presence of ultra-low ligand concentrations within environments of high concentration gradient. In addition, all GPCs studied were observed to migrate much shorter distances than their glioblastoma-derived counterparts, suggesting that glial tumors may recruit and/or transform highly localized GPCs to enhance growth. Our study provides data to merit examination of GPCs as potential drug delivery vehicles to the bulk tumor mass, and adds to the growing body of literature that points towards the study of GPC migration as a means to reduce tumor recurrence and/or growth.

5.2. Materials and Methods

Cell Culture

Three glial progenitor mouse cell types, one primary mouse tumor and two human tumor cell lines were used in this study. The GPCs of varying genetic backgrounds were chosen because they each represent a cell population that is associated with specific types of tumors present within human brain. Glial progenitor cells (GPCs) were derived from the RCAS/Ntv-a system from the laboratory of Dr. Eric C. Holland laboratory at Memorial Sloan Kettering Cancer Center, New York (Hambardzumyan et al, 2009; Holland, 2004; Orsulic, 2002). The Ntv-a transgenic mouse line is comprised of retroviral vectors and mice transgenic for cell type specific expression of the retroviral receptor, tv-a. Briefly, the Ntv-a transgenic mouse line was constructed by expressing tv-a as a transgene from the nestin promoter. The RCAS viral vectors are avian-specific and only infect mammalian cells engineered to express the tv-a receptor. The Ntv-a system accomplishes glial-specific gene transfer, which permits study of the role of single and multiple mutations in transformed cells of glial lineage.

The four mouse cell types derived from the Ntv-a system used in this study were: (a) GPC^{LacZ} cells: GPCs infected with the RCAS vector to express β-galactosidase (Lassman et al, 2004) and used as our control cell type. These cells do not express genetic abnormalities specifically associated with glial tumors, but rather represent a progenitor cell type found in different regions of the brain that can be recruited to aid in tumor growth (Dai et al, 2001) (b) GPC^{PDGF} cells: GPCs infected with the RCAS vector to develop an autocrine Platelet-Derived Growth Factor (PDGF)- Platelet-Derived Growth Factor Receptor (PDGFR) loop (Dai et al, 2001). These cells have been engineered to mimic the characteristics of cells present in

astrocytomas, where a PDGF autocrine loop is believed to be responsible for increased proliferation as well as enhanced group migration in the brain (Dai et al, 2001; Lokker et al, 2002) (c) GPC^{kRas} cells: GPCs infected with RCAS vector that generates constitutively-activated downstream Ras pathways (Holland et al, 2000). These cells are characteristic of oligodendrocytomas that present with large diffuse spreading of cells which maintain contact with one another in the brain (Holmen & Williams, 2005; Schwartz et al, 1991) and (d) XFM^{PDGF} cells: Derived from a mouse oligodendrocytoma engineered to express secreted PDGF-B in mice with a INK4a-Arf-/- background (Hambardzumyan et al, 2009; Tchougounova et al, 2007). The XFM^{PDGF} and GPC^{PDGF} cells are similar in their ability to produce and respond to their own PDGF, but XFM^{PDGF} cells have the INK4a-Arf locus deleted, disabling possible tumor suppressor capabilities. Note that GPC^{LacZ}, GPC^{PDGF} and GPC^{kRas} cells were generated via RCAS infection in culture dishes, while XFM^{PDGF} cells were harvested from an excised, induced mouse tumor as shown in Figure 1. In addition, the two human glioblastoma cell lines studied were U-87 MG (ATCC Cat # HTB-14™) and U-251 MG (ATCC Cat # HTB-17™). These cell lines were examined alongside GPCs because they have been extensively used in glioma research, both in vivo and in vitro.

All cells were cultured using sterile Dulbecco's Modified Eagle Medium (DMEM) (Cat#: 10-017-CV, Mediatech, VA), supplemented with 2% L-Glutamine (Cat#: 25-015-CI, Mediatech, VA), 2% Penicillin-Streptomycin-Amphotericin B - 100x solution (Cat#: 30-002-CI, Mediatech, VA), and 10% fetal bovine serum (FBS) (Cat#: MT35-010-CV, Mediatech, VA). The cells were grown onto sterile polystyrene tissue culture flasks (BD Biosciences, Franklin Lakes, NJ) and incubated at $37^{o}C$ with 5% CO_2.

Growth Factors

Three growth factors were used to examine chemotaxis in this study: Hepatocyte Growth Factor/Scatter Factor (HGF) (Molecular Weight = 80 kDa) (Cat#: 2207-HG/SF, R&D Systems, MN), Platelet Derived Growth Factor-BB (PDGF) (Molecular Weight = 12.4 kDa) (Cat#: 220-BB, R&D Systems, MN), and Transforming Growth Factor α (TGF-α) (Molecular Weight = 6 kDa) (Cat#: 616430, Calbiochem & Oncogene, CA). Growth factors were diluted with serum-free DMEM to obtain a concentration range for each experiment between 1 pM and 10 nM.

Chemotaxis Assays

Cellular chemotaxis in response to extracellular signaling from growth factors was analyzed via transwell assays, as described previously (Brockmann et al, 2003; Ohashi et al, 2006). Briefly, a modified thick coating volume of 200 μl of 0.5 mg/ml Matrigel™ (Cat#: 356230, BD Bioscience, MA) was used to coat the polyethylene terephthalate (PET) membranes with 8 μm-diameter pores, which separated the upper and lower chambers of the transwell system. The matrix was polymerized after a three-hour incubation period at 37^{o}C, and the uncovered culture plates were placed into a class II biological flow hood for 48 hours to dry. Upon drying, plates were wrapped in aluminum foil and stored at 4^{o}C for future experiments. Coated filters were rehydrated with 200 μl serum free DMEM and incubated at 37°C for one hour immediately prior to their use.

Growth factor solutions between 1 pM and 10 nM concentrations were added to the lower chamber of a 24-well plate (Cat#: BD353047, BD Bioscience, MA), while cell solutions at a density of 1.5 x 10^6 cells per ml of supplemented DMEM were added to the upper chamber culture inserts (Cat#: BD353097, BD Bioscience, MA). The transwell assay was incubated for 12 hours at 37^{o}C to allow cells migrate through the porous membrane, after which excess cell

solution was aspirated from culture inserts. Cells on the upper side of the membrane were removed, and cells on the lower side of the membrane were fixed and stained with Diff-Quick® Stain Set (Dade Behring, DE) to facilitate cell counting. The nuclei of cells that migrated to the underside of the membrane were counted using an inverted light microscope with a 20x objective (Nikon TE300, Morrell Instruments, NY). Cells located within five areas of the culture inserts were counted upon each filter using a checkerboard pattern (Zigmond & Hirsch, 1973) for a total of five rectangular locations of 0.58 mm x 0.44 mm. These data were used to gather representative cell counts per experiment ($n>7$).

Conditioned Media Chemotaxis Assays

Cells derived from U-87, U-251, and XFM^{PDGF} tumors were grown separately in T-75 tissue culture flasks in supplemented DMEM. Once 90-95% confluence was reached, complete media was replaced with 10 ml of serum-free DMEM and cells were incubated overnight. The next day, supernatant was collected and serially diluted in serum-free DMEM to concentration ratios of 1:0 (100% or non-diluted), 1:1 (50%), and 1:4 (25%). Conditioned media (CM) was used in lieu of growth factor solutions (Bao et al, 2006) within transwell assays for these sets of experiments ($n\geq3$).

Relative Chemoattractant Factor (RCF)

Cell migration indexes are reported here using a parameter called the Relative Chemoattractant Factor (RCF). RCF is defined as the normalized cell count per experiment, and is determined by dividing the average number of cells that migrated towards the test solutions, N_{Test}, by the average number of cells that migrated towards the control solution (in this case

serum-free DMEM), $N_{Control}$. In this way, RCF represents the fold-increase in cell migration from control experiments to experimental conditions, as described by Equation 1.

$$RCF = \frac{N_{Test}}{N_{Control}} \quad \_(1)\_$$

Statistical Analysis

RCF values calculated during migration assays were analyzed by analysis of variance (ANOVA) to determine the statistical differences between experimental groups and Student's t-test to determine the statistical differences between individual experimental groups and controls. P values less than 0.05 were defined as statistically significant.

Antibodies and Immunocytochemistry

Sequential, double immunofluorescence for detection of growth factor receptors was performed as described previously (Dudu et al, 2008). Briefly, cells grown on coverslips were fixed for 15 minutes at room temperature with paraformaldehyde (Cat#: P6148, Sigma, St. Louis, MO) and labeled with rabbit polyclonal anti-β-actin (1:1000) (Cat#: ab8227, Abcam, Cambridge, MA), rabbit monoclonal anti-phosphorylated-EGF-R (1:500) (Cat#: ab40815, Abcam, Cambridge, MA), anti-rabbit AlexaFluor® 488 or 594 antibodies (Cat#: A11034 and A11037, respectively, Invitrogen, Camarillo, CA).

Immunoblotting and Detection

Protein lysates were generated from 90-95% confluent serum starved cells grown in 100-mm culture plates and done in triplicate (Becton Dickinson, MA). All cells were serum starved

for two hours in 1X PBS at 37^{o}C and separately stimulated for 20 minutes using the specified growth factor concentrations that correlated with maximum RCF values determined from transwell assays. Cells we lysed at 4^{o}C on ice in cold lysis buffer (Cat#: 2978-50, Sigma, MO) containing 70 µl Protease Inhibitor (Cat#: 78425, Pierce IL,), 2 mM phenylmethylsulfonyl fluoride (Cat#: P7626, Sigma-Aldrich MO) and 10 µl Phosphatase Inhibitor Cocktail 2 (Cat#: P5726, Sigma-Aldrich MO) for 15 minutes. Proteins, 40 µg/well, were separated by 8-16% Tris-Glycine SDS-PAGE precast gels (CAT#58519, Lonza, Rockland, ME), then transferred to nitrocellulose membranes.

Detection of protein expression was performed using corresponding primary antibodies, the IRDye® 800CW goat polyclonal anti-rabbit secondary (Cat#: 926-32211, LiCor Biosciences, Lincoln, NE) and the Odyssey Infrared Scanner at 795 nm (LiCor Biosciences, Lincoln, NE). An average intensity measurement, I, was made by selecting a rectangular region (created via the Odyssey software's select tool) that encompassed the entire band area of a membrane to record its intensity during imaging. The identical rectangular region was then overlaid onto remaining band areas to determine the average intensity for each band. The average intensity of each experimental condition (e.g growth factor-stimulated or not) was then divided by the average intensity of the control condition. In this manner, the intensity of control bands have been normalized to I=1, such that reported values of average intensity for experimental conditions reflect a fold-increase or fold-decrease compared to controls.

Confocal Microscopy

Confocal laser scanning microscopy imaging was performed using a Leica TCS SP2 instrument with a HCX PL APO CS 63X oil immersion objective (NA 1.4). Imaging conditions

used for each set of experiments were set with Ar/HeNe Laser at 20%; a 1024 x 1024 format; gain range of 600-700 volts; 0.5% offset; and a 200-hertz scanning speed.

μLane System

The laboratory-developed μLane system used for this study has been previously described (Kong et al, 2010; Kong et al, 2011). In brief, systems are comprised of a 5-cm-long glass microscope slide bonded to a polydimethylsiloxane (PDMS) elastomer. As shown in Figure 2A and 2B, the design includes a sink reservoir (V = 200 μl), and a source reservoir (V = 10 μl). The reservoirs are connected by a single microchannel of 100 μm by 100 μm cross-section and 1.5-cm length. The system works via diffusion, whereby growth factors present in high concentration in the source reservoir and channel diffuse towards lower concentration within the sink reservoir to create concentration gradients that stimulate cell migration. In these tests, the microchannel was first filled with a solution of 2 μg/mL of Matrigel™ (BD Bioscience, MA) containing a desired growth factor concentration and incubated at 37^{o}C for 1.5 hours to enable Matrigel™ polymerization. Then, excess matrix was aspirated from the sink reservoir and replaced with cell solution at a density of 1.5 x 10^{6} cells/ml. The system was then incubated at 37^{o}C. Cell movement into the microchannel from the sink reservoir was monitored via light microscopy using a 20X long working distance dry objective and a cooled CCD camera. Images of cells moving from the sink reservoir into the microchannel were recorded at t=12 hrs, t=24 hrs, and t=36 hrs using Nikon software (Nikon Instrument Element 2.30 with 6D module, Morrell Instrument Company Inc., Melville, NY). The numbers of cells that migrated into the microchannels were counted within three regions within the channel, 0-200 μm, 200-400 μm, and 400-600 μm. Experiments were completed in triplicate using newly fabricated μLane systems for each experiment.

Mathematical Modeling

Diffusion within the μLane system was modeled using Fick's Law described by Equation 2.

$$\frac{\partial C}{\partial t} = D\frac{\partial C}{\partial x} \tag{2}$$

where C is concentration (ng/ml), t (s) is time, D (m^2/s) is the diffusion coefficient, and x (m) is distance. 1-D modeling was appropriate for this system because the channel length, L, was substantially larger than its diameter, D, with L/D >100. Equation 2 was solved using Finite-element-analysis software Matlab 7.7 (MathWorks, Natick, MA), with an initial concentration, C_0, set throughout the channel length that was either 10 pM or 100 pM, as per experiment. The boundary conditions were fixed at C=0 at x=0, i.e. entrance of the channel from the sink reservoir, and $C=C_0$ at x=L, i.e. the entrance of the channel at the source reservoir end, for all time, t. Analysis via Fick's law enabled computation of concentration profiles within the μLane for all times. The simulation revealed that the concentration distribution within the microchannel reached steady-state at t=103 hours, after which no changes in concentration with time were seen. Concentration gradients were obtained by calculating the change in concentration along the channel length as done previously (Dudu et al, 2011) via Equation 3:

$$G = \frac{\partial C}{\partial x} \tag{3}$$

where G is gradient, C is concentration (ng/ml), and x (m) is distance.

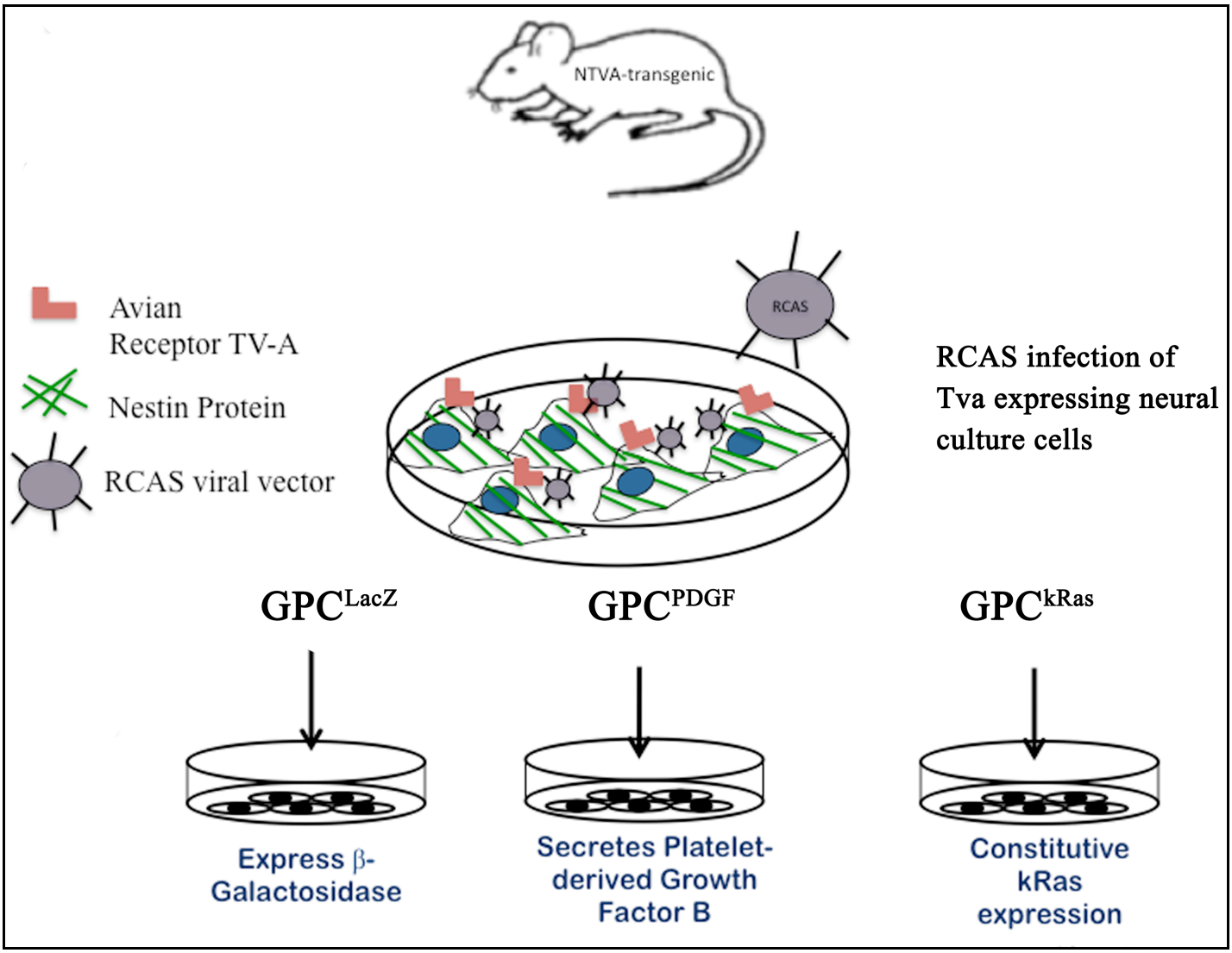

FIGURE 1: RCAS-tv-a System used to produce GPC^{LacZ}, GPC^{PDGF}, GPC^{PDGF}, and XFM^{PDGF} cells. Ntv-a transgenic mice were created by pronuclear injection with a viral construct that contained a nestin promoter region. This infection enabled the transcription of the avian glycoprotein receptor, tv-a, in Nestin-expressing murine glial progenitor cells. Cells that expressed tv-a were then infected with various RCAS retroviruses in culture to generate GPC^{LacZ}, GPC^{PDGF}, and GPC^{kRas} cells. XFM^{PDGF} tumors were generated within mice of INK4a-Arf -/- background that were injected with the RCAS-PDGF-B viral vector.

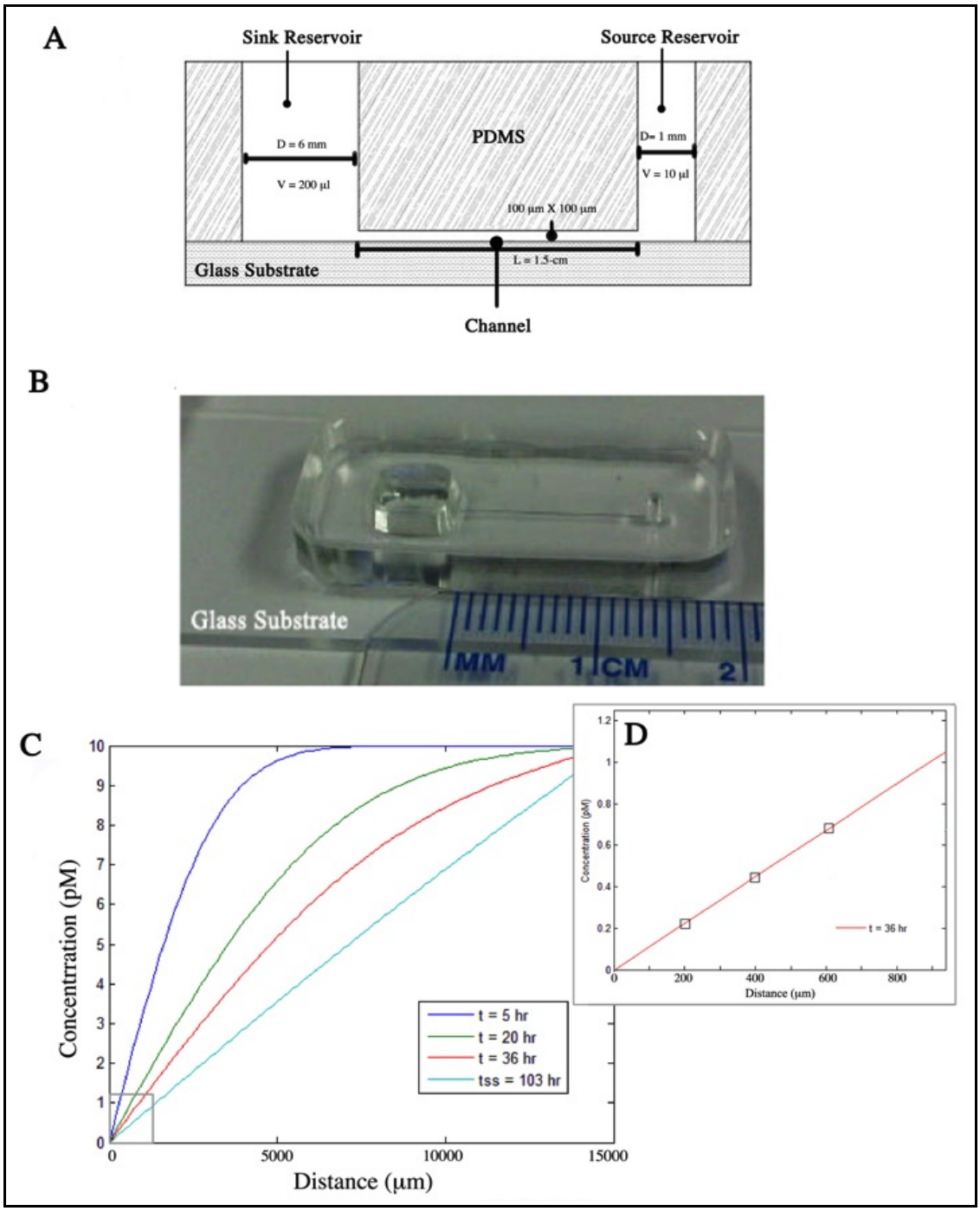

FIGURE 2: Description of the µLane system. (A) A schematic of the µLane system comprised of a sink and source reservoir connected by a microchannel of 100 µm by 100 µm cross-section. (B) Image of a µLane system fabricated in our laboratory using glass-PDMS. (C) Mathematical simulation of the distribution of ligand concentration within the microchannel over time, t. (D) Inset highlights the concentration profile present within the first 1000 µm of the channel closest to the sink reservoir at the experimental time of t=36 hours.

5.3. Results

5.3.1. Glial Progenitor Cells (GPCs) exhibit a dose-dependent response to tumor-conditioned media (CM).

In order to examine the migratory behavior of GPC^{LacZ}, GPC^{PDGF} and XFM^{PDGF} cells, we measured the number of motile cells towards serially diluted conditioned media (CM) gathered from the U-87, U-251 and XFM^{PDGF} tumor-derived cells. As shown in Figure 3, GPC^{LacZ} cells exhibited a dosage-dependent migratory response towards U-87, U-251, and XFM^{PDGF} conditioned media (CM). The highest number of motile cells was measured in response to non-diluted conditioned media, 100% or CM_{100}, and was reduced when exposed to 50% diluted conditioned, CM_{50}, and 25% diluted conditioned media, CM_{25}, from identical tumor sources. The GPC^{LacZ} cells exhibited a maximum RCF of 10 when migrating towards U-87 CM_{100} as compared to control experiments. Chemotaxis of GPC^{LacZ} cells in response to XFM^{PDGF} CM_{100} exhibited a maximum RCF of 3.9. GPC^{PDGF} cells in response to CM of U-87, U-251, and XFM^{PDGF} exhibited RCF values of 8, 5, and 6 respectively. Similarly, XFM^{PDGF} cells in response to CM of U-87 and XFM^{PDGF} exhibited RCF values of 4 (Figure 3A and C). Lastly, RCF values for all cells towards CM_{100} were reduced to 1 (i.e. level of controls) when neutralizing antibodies were used to block effects of Hepatocyte Growth Factor (HGF) and Transforming Growth Factor Alpha (TGF-α) (data not shown).

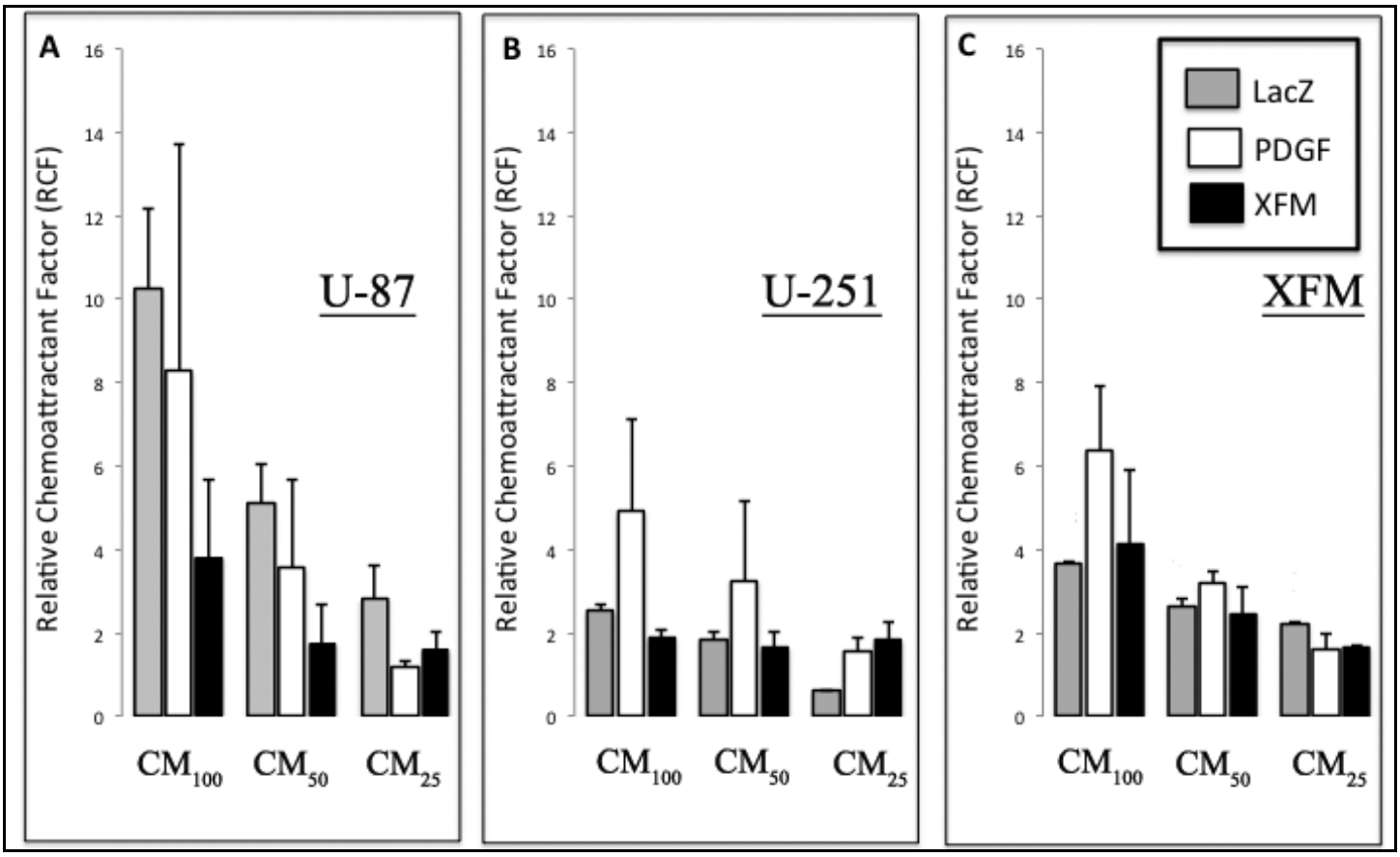

FIGURE 3: Dose-dependent response of GPC^{LacZ}, GPC^{PDGF} and GPC^{kRas} glial progenitor cells and U-87 tumor cells to glioma conditioned media (CM). Bar graphs depict values of Relative Chemoattractant Factor (RCF), defined as the number of motile cells towards experimental conditions normalized by the number of motile cells towards control conditions (in this case non-supplemented DMEM). The normalized number of motile cells measured in response to non-diluted conditioned media, CM_{100}, 50% conditioned media, CM_{50}, and 25% conditioned media, CM_{25}, of (A) U-87, (B) U-251, and (C) XFM^{PDGF}.

5.3.2. Glial Progenitor Cells (GPCs) exhibit different expression levels of cognate receptors.

We next examined GPC expression of 3 key cognate cytokine receptors known to be highly chemoattractive to cells derived from glial tumors and present within tumor CM (Chicoine & Silbergeld, 1997): cMet, the receptor for Hepatocyte Growth Factor (HGF), Epidermal Growth Factor Receptor (EGFR), the receptor for the Epidermal Growth Factor (EGF) and Transforming Growth Factor Alpha (TGF-α) ligands, and Platelet-Derived Growth Factor Receptor beta (PDGFRβ). Western blot analysis shown in Figure 4 illustrates that all GPC types express different levels of the 3 receptors, each benchmarked against the well-studied U-87 cell line in each experiment (Clark et al, 2010). As seen, GPC^{LacZ}, GPC^{kRas}, and GPC^{PDGF} express cMet to approximately the same level as U-87 cells. GPC^{PDGF} and GPC^{kRas} express PDGFR at levels similar to U-87, while GPC^{LacZ} expression of PDGFR was minimal. Lastly, GPC^{PDGF} and GPC^{LacZ} expressed EGFR at levels less than U-87 and GPC^{kRas} illustrated trace amounts of EGFR.

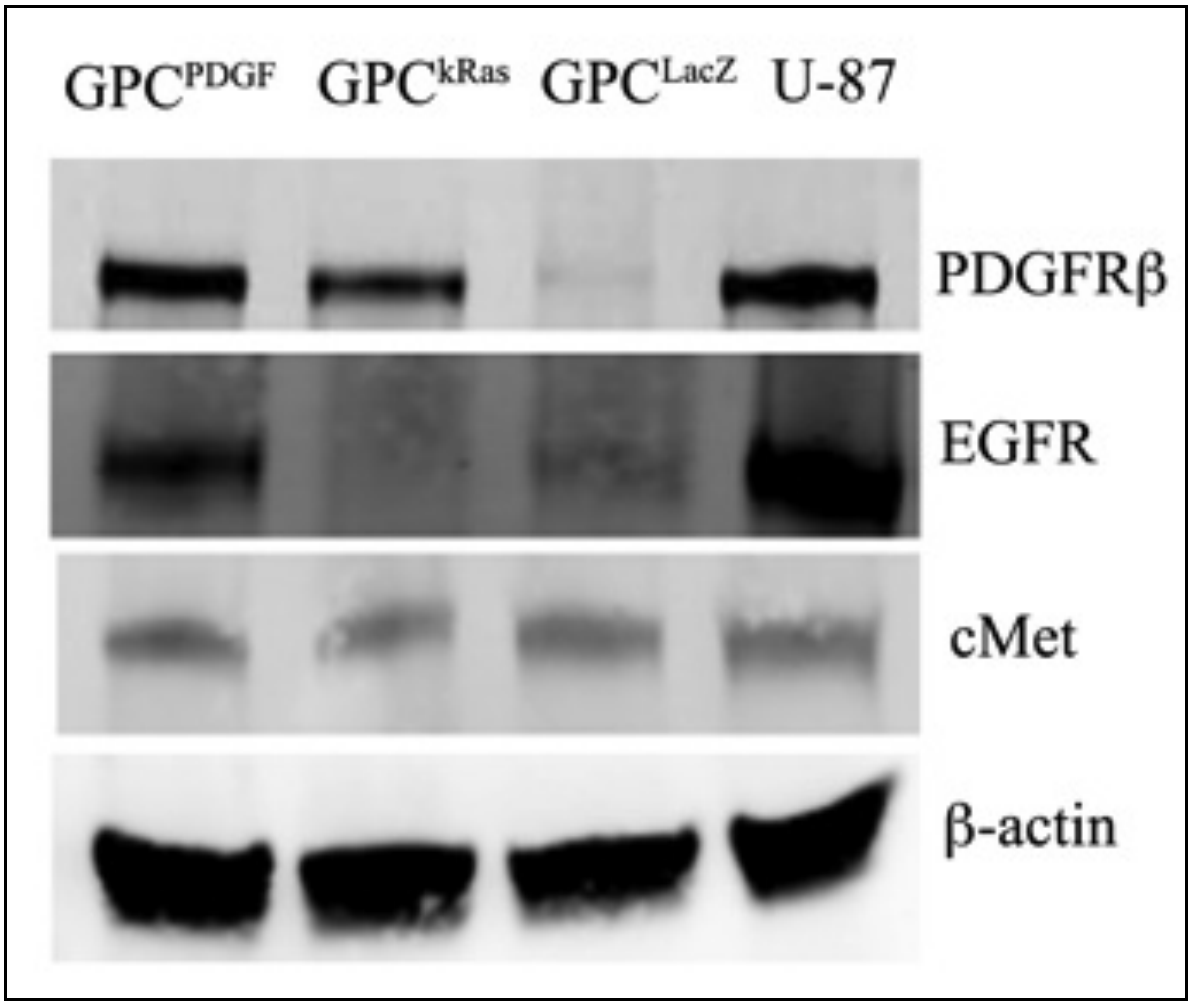

FIGURE 4: GPC^{PDGF}, GPC^{kRas}, GPC^{LacZ} and U-87 cell expression of total Platelet Derived Growth Factor Receptor (PDGFR), Epidermal Growth Factor Receptor (EGFR), and cMET (receptor for Hepatocyte Growth Factor, HGF) examined via Western blot analysis. β−actin was used as a loading control.

5.3.3. Glial progenitor cells (GPCs) exhibit increased chemotaxis in response to ultra low concentrations of exogenous HGF, PDGF, and TGF-α.

With the varying levels of GPC growth factor receptors established, the next experiments utilized transwell assays to examine the migratory responses of GPC^{LacZ}, GPC^{PDGF}, GPC^{kRas}, and U-87 cells towards different concentrations of HGF, PDGF, and TGF-α. As shown in Figure 5, GPC^{LacZ} demonstrated the highest RCF value of 58 in response to a 10 pM HGF solution, an RCF of 12.7 in response to 1 pM PDGF and an RCF of 8.75 in response to 1 pM of TGF–α. By contrast, a concentration of 1 pM HGF induced motile GPC^{PDGF} cells with a RCF value of 8, while 100 pM TGF-α induced a 9-fold migration response in GPC^{PDGF} cells over controls. The migration of GPC^{kRas} cells was highest when exposed to a solution of 1 pM TGF-α, exhibiting an RCF value of 38, an RCF value of 10 toward 1 pM HGF, and an RCF value of 4 toward 1 pM HGF. Lastly, U-87 cells exhibited their largest RCF value of 6.64 towards 1 nM HGF.

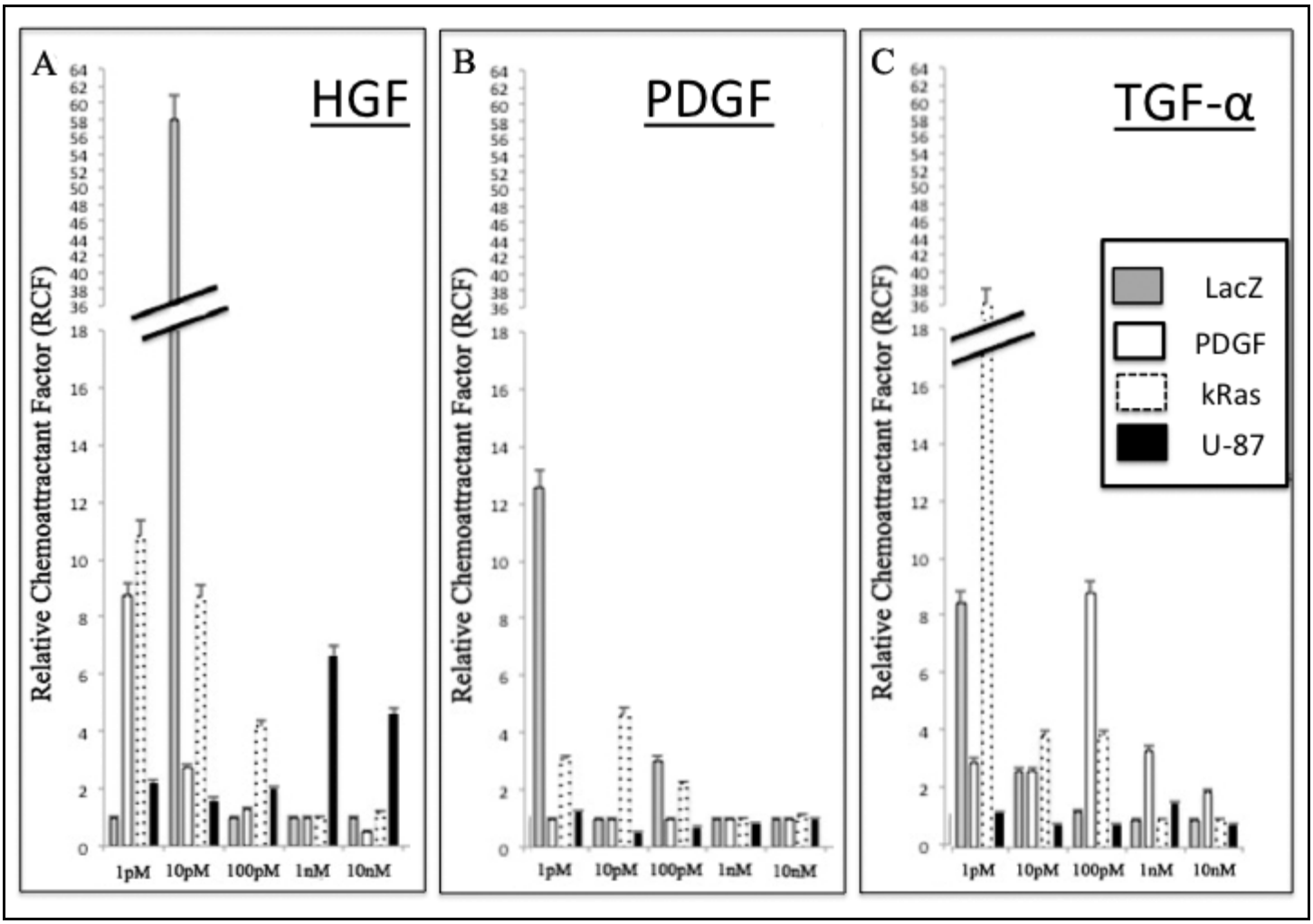

FIGURE 5: Dose-dependent response of GPC^{LacZ}, GPC^{PDGF}, GPC^{kRas} glial progenitor cells and U87 tumor cells to a concentration range of the (A) Hepatocyte Growth Factor (HGF), (B) Platelet-derived Growth Factor BB (PDGF) and (C) Transforming Growth Factor-α (TGF-α). Bar graphs depict values of Relative Chemoattractant Factor (RCF), defined as the number of motile cells towards experimental conditions normalized by the number of motile cells towards exogenous growth factors.

5.3.4. Glial progenitor cell receptor expression is up- or down-regulated when stimulated with exogenous growth factor.

While the HGF and PDGF ligands demonstrated chemotactic abilities, all subsequent experiments focused particularly on the chemotaxis induced by exogenous TGF-α because it was shown to be a chemoattractant for all of the cell types studied here and because its receptor, EGFR, is an extensively-studied oncogene present in diverse tumors of varying grade (Liu et al, 2003; Maiti et al, 2008). In the next experiments, western blot analysis was used to detect changes in phosphorylated EGFR (pEGFR) expression between cells that were stimulated and non-stimulated with TGF-α. Detection of pEGFR was positive in non-treated (control) populations of GPC^{LacZ}, GPC^{PDGF} and GPC^{kRas} cells, as shown in Figure 6. The intensity of each band was normalized to a value of I = 1 using device software as described previously. Upon stimulation with TGF-α, elevated levels of pEGFR were detected in the GPC^{LacZ} and GPC^{PDGF} cell types with average intensity values of I = 2.63 and I = 5.05, respectively. Conversely, the average intensity of pEGFR upon TGF-α stimulation in the GPC^{kRas} cell population was lower than control, at I = 0.49.

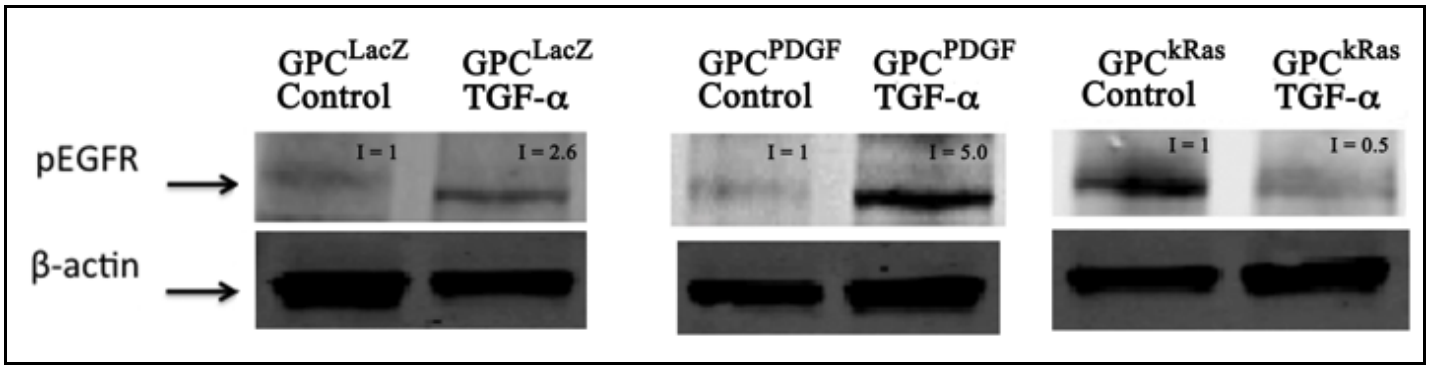

FIGURE 6: Expression of phosphorylated Epidermal Growth Factor Receptor (pEGFR) in GPC^{LacZ}, GPC^{PDGF}, and GPC^{kRas} glial progenitor cells stimulated and unstimulated with TGF-α ligand as examined via Western blot analysis. The average intensity of bands, I, was divided by the intensity of bands at control conditions using device software in order to report values that reflect a fold-increase of fold-decrease of pEGFR intensity per experiment.β-actin was used as a loading control.

5.3.4. The μLane system facilitates analysis of cell migration within controlled microenvironments.

Given the varying levels of EGFR expression and differences in its regulation in response to TGF-α stimulation, we next examined how specific microenvironments of TGF-α affected the chemotaxis of the genetically-altered GPC populations studied. We examined the migration of the GPC^{LacZ}, GPC^{PDGF}, GPC^{kRas}, and U-87 cell populations within our laboratory-developed microfluidic system, the μLane, in order to identify the different migratory phenotypes and distances traveled in response to known TGF-α concentration profiles. First, no cells were present at the start of microchannel experiments, facilitating visualization of cells migrating outwards from the sink reservoir and into the microchannel over time. Second, control experiments using U-87 cells incubated within a 3D matrix without exogenous growth factors verified that the μLane system maintained cell viability for up to 7 days (data not shown). In addition, as cells were seen to begin proliferating within the μLane after 40 hours, cell migration experiments were limited to a 36-hour period in order to exclude effects of cell division in our analysis. Last, cell distances traveled in the μLane system were measured in 200 μm increments. We determined this number to be significant because it was the average thickness of matrix-coated filters used during transwell assays, i.e. the maximum migration distance in those initial experiments.

Figure 7 illustrates the migration of GPC^{LacZ}, GPC^{PDGF}, GPC^{kRas}, and U-87 cells within μLane microenvironments generated by using 0 pM, 10 pM and 100 pM TGF-α within 3D matrix. No GPC^{LacZ} or GPC^{PDGF} cells were seen to migrate into the channel within 36 hours when no additional exogenous growth factors were added within the matrix (i.e. control experiments). In contrast, the GPC^{kRas} and U-87 cells were seen to migrate within the channel in

low numbers during control experiments (Figure 7A1-7A4). When cells were exposed to gradients generated by an initial TGF-α concentration of 10 pM, all cell populations displayed enhanced migration into the channels (Figure 7B1-7B4). In addition, each cell type exhibited a distinct migratory phenotype. GPC^{LacZ} cells migrated as single cells, GPC^{PDGF} cells exhibited group migration, while GPC^{kRas} and U-87 MG cells migrated in close association to each other resembling chains of migrating cells. Lastly, experiments recorded that GPC^{LacZ}, GPC^{kRas}, and GPC^{PDGF} appeared chemo-repulsed from the channel entrance when exposed to a microenvironment generated using 100 pM TGF-α, while the U-87 cells remained migratory (Figure 7C1-7C4).

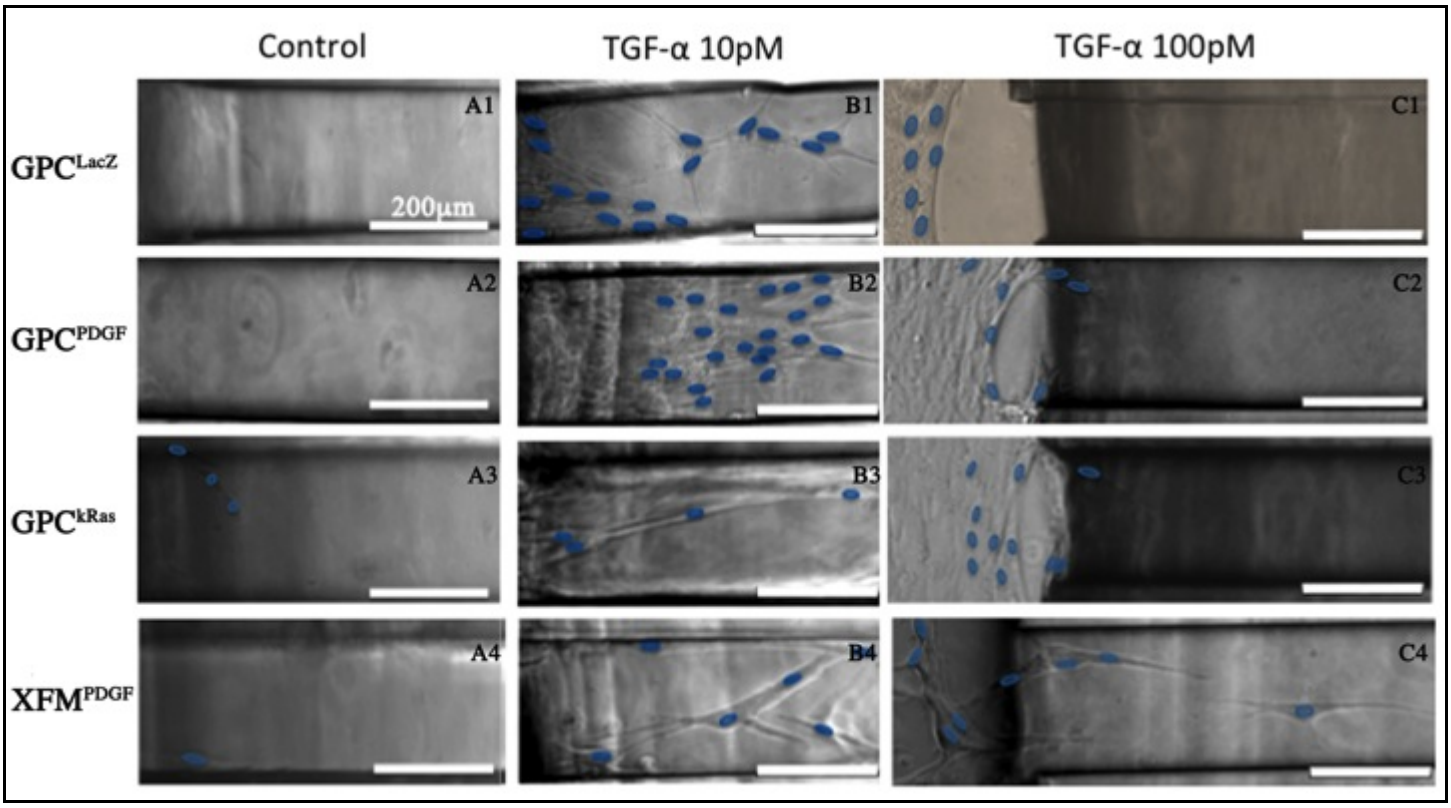

FIGURE 7: Migration of GPC^{LacZ}, GPC^{PDGF}, GPC^{kRas}, and U-87 cells within the µLane system after 36 hours in response to concentration gradients generated by using initial concentrations of (A1-A4) 0 pM (control), (B1-B4) 10 pM and (C1-C4) 100 pM of TGF-α in the sink reservoir. The left hand side of images A1-A4 and B1-B4 represent the interface between the sink reservoir and the microchannel. The nuclei of representative cells are indicated by blue ovals. Scale bars = 200 µm.

The concentrations and concentration gradients experienced by cells within the μLane were then determined via mathematical modeling, as shown Table 1. As seen, the TGF-α concentration within the first 600 μm of the μLane was between 0 pM and 0.67 pM (4.02 pg/ml of TGF-α) when 10 pM (60 pg/ml of TGF-α concentration) was used, and an order of magnitude higher, between 0 pM and 6.7 pM (40.2 pg/ml of TGF-α), when 100 pM TGF-α was used (600 pg/ml) for chemotaxis experiments. Similarly, the concentration gradient within these same regions of the channel was approximately 6.8 pg/ml· per mm of channel when 10 pM was used, and 68 pg/ml per mm of channel when 100 pM was used. We note that because the distribution of concentrations along the channel length does not reach steady-state in the system until t=103 hours, cells were exposed to highly non-linear and transient concentration profiles during all experiments.

Distance (μm)	Co = 0 pM		Co = 10 pM		Co = 100 pM	
	Co (pM)	**G** ($pg \cdot ml^{-1}$ per mm)	**Co** (pM)	**G** (pg.ml-1 per mm)	**Co** (pM)	**G** ($pg \cdot ml^{-1}$ per mm)
0-200	0	0	0-0.22	6.8	0-2.2	68
200-400	0	0	0.22-0.45	6.8	2.2-4.5	68
400-600	0	0	0.45-0.67	6.8	4.5-6.7	68

TABLE 1: Concentrations and concentration gradients present within specified positions of the microchannel 36 hours after different initial concentrations, C_0, of TGF-α were used to generate ligand concentration profiles.

Finally, the average number of cells that migrated between three regions within the channel, i.e. 0-200 μm, 200-400 μm, and 400-600 μm, was measured in response to microenvironments generated using 10 pM TGF-α as shown in Figure 8. As seen, between 70-80% of total migratory GPC cells exhibited maximum migration between 0-200 μm in the presence of the lowest concentration of less than 0.22 pM (1.32 pg/ml of TGF-α), located at the interface between the channel entrance and the sink reservoir. GPC^{LacZ}, GPC^{PDGF}, and GPC^{kRas} cells demonstrated that the remaining 20-30% of total migratory cells were able to migrate between 200-400 μm in the presence of a concentrations between 0.22 pM and 0.45 pM (2.7 pg/ml of TGF-α). The majority of U-87 cells, 70%, were also seen to migrate within the first 200 μm of the microchannel, while 19% of these cells were observed to migrate between 200 μm and 400 μm into the channel. U-87 were the only cell type able to migrate distances greater than 400 μm in the channel, with total of 11% of motile cells observed at this distance.

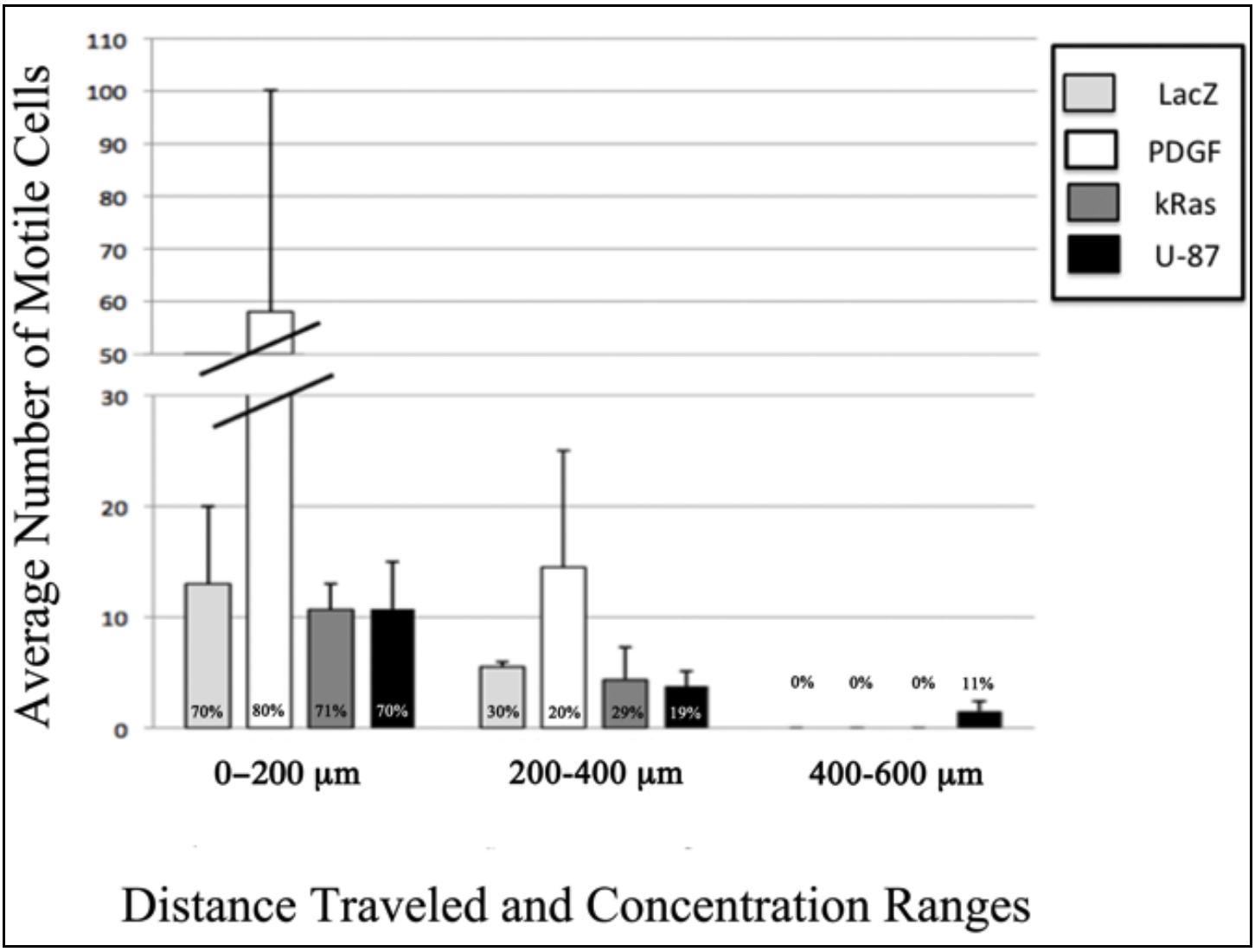

FIGURE 8: Average numbers of migratory cells and the average maximum distances traveled within the μLane. Data was calculated using microenvironments generated 36 hours after using 10 pM TGF-α in the source reservoir. The percentage of each cell type observed to migrate distances between 0-200 μm, 200-400 μm and 400-600 μm are shown.

5.4. DISCUSSION

The current study utilized in vitro systems to examine the chemotactic migration of genetically engineered GPCs toward cytokines known to be secreted by glial tumors for enhanced tumor growth and dispersal in vivo (Chicoine & Silbergeld, 1997; Mueller et al, 2003; Pedersen et al, 1995).

Initial experiments first verified that GPCs of different genetic backgrounds were chemoattracted to conditioned media (CM) obtained from cultures of different tumors, as well as to different growth factors present within those CM. Our results were in agreement with the wealth of data demonstrating tumor ability to recruit a diversity of cells by varying the type and concentration of factors secreted (Guo et al, 2003; Heese et al, 2005; Kleihues & Sobin, 2000; Werbowetski et al, 2004; Xu et al, 2010). However, it was surprising to observe that all GPC types migrated preferentially towards ultra-dilute solutions (e.g. picomolar (pM) concentrations) of growth factors when the majority of studies utilize much higher concentrations to induce the chemotaxis of glioma-derived cells (Brockmann et al, 2003; Heese et al, 2005; Masui et al, 2010; Pollack et al, 1991; Qazi et al, 2011; Sampetrean et al, 2011; Wells, 1996) To examine this further, we examined the migratory responses of each genetically-altered GPC population in response to different concentrations and gradients of TGF-α.

Our study focused primarily on this EGFR binding ligand because of the well-documented role of EGFR signaling in glioma (Liu et al, 2003; Lo, 2010; Ronellenfitsch et al, 2010; Ye et al, 2010) and the lack of genetic EGFR alteration in any of the GPCs studied. Interestingly, while the upregulation of pEGFR observed reinforced the well-established positive signal transduction required for enhanced migration (Grotendorst et al, 1989; Wong et al, 1989), pEGFR downregulation was also seen to result in enhanced GPC migration. This was

unanticipated because it suggests a negative-feedback suppression mechanism that was not observed in the cell migratory response. We then utilized a controlled microfluidics environment to quantitatively examine the migratory response of GPCs to known concentration profiles of TGF-α.

TGF-α microenvironments generated via our μLane system revealed significant findings about the migratory behavior of the GPCs examined. First, despite differences in their genetic backgrounds, all GPC populations were observed to migrate readily into the microchannel when exposed to low TGF-α concentrations, but then become largely chemorepulsed by higher concentrations of the same ligand. The microchannel images illustrate classic examples of negative feedback in migration, whereby excess ligands present when receptors have become saturated and bound eliminate or reverse the biochemical effect (Amit et al, 2007; Wyckoff et al, 2000). This migratory behavior is consistent with the picomolar chemoattraction measured in our initial transwell assay experiments, and is previously unreported with GPCs or glioma. This corroborating data implies that the stimuli which produce migratory behavior in glial tumors may differ from those that attract GPC populations towards the bulk tumor mass. Differences in the effects of such external cues remain unexamined, and carry significant consequences for how constituent and/or recruited GPC populations respond to glioma therapies (Dancey & Sausville, 2003; Zhang et al, 2009).

Second, mathematical analysis of the concentration profiles generated within the μLane illustrated that GPCs were most chemoattracted by environments of both ultra low concentration and high concentration gradient. While gradients are well-accepted as chemotactic driving forces (Lauffenburger & Horwitz, 1996; Wang, 2009) published studies illustrate that chemotaxis is very cell type specific: Some cell types migrate more readily at higher concentration and gradient

(Kong et al, 2011; Wang et al, 2004), while others migrate best in shallow gradients with higher concentration (Jeon et al, 2002). Moreover, all GPCs in our study were observed to migrate much shorter distances in the microchannel than their tumor cell counterparts. These results seem divert from the characteristic patterns of GPCs capable of migrating long distances in the brain (Farin et al, 2006; Kakita & Goldman, 1999). Rather, because GPCs become stimulated by high concentration gradients at low concentration, our data implies that GPCs may become most chemoattracted during initial gliomagenesis, where small numbers of cells express low concentrations of cytokine, rather than by larger tumors seeking to increase their heterogeneity and potential nourishment.

Last, experiments using μLane systems illustrated distinct patterns of GPC migration that were surprisingly similar to what has been reported for different types of glial tumor cells in vivo. Cells of oligodendrogliomas and astrocytomas have been seen to typically invade normal brain parenchyma by migrating through the white matter tracts as individuals (Duffau et al, 2004; Pedersen et al, 1995), similar to the single cell migration exhibited by GPC^{LacZ} cells in our study. By contrast, gliomas with sarcoma characteristics have been reported to invade the brain primarily by tracking along blood vessels (Kanamori et al, 2004; Schwartz et al, 1991) such that each cell is in close contact with its motile neighbors, i.e. exhibiting the chain cell migration observed by GPC^{kRas} cells in our study. These similarities suggest that perhaps tumors of different types and grade recruit or/or transform neighboring GPCs into cells with preferred genetic backgrounds, which then regulate cell migration mechanisms that best enhance tumor dispersal and/or growth. Such novel research direction is provocative and exciting, as GPCs have remained relatively unexplored as therapeutic agents in the treatment of glioma.

5.5. CONCLUSION

The current study is among the first to examine the in vitro migratory responses of GPC populations with different genetic backgrounds present in the human disease. Our novel findings of uniform GPC chemoattraction at ultra-dilute ligand concentrations coupled with short migration distances underscore the need for a more comprehensive examination of glioma dispersal and growth mechanisms that incorporates tumor interactions with localized GPC populations. In addition, analysis of differences in the migratory responses of these genetically-altered cells advocate study of GPCs as potential therapeutic targets for glioma treatment.

BIBLIOGRAPHY

Abhyankar VV, Lokuta MA, Huttenlocher A, Beebe DJ (2006) Characterization of a membrane-based gradient generator for use in cell-signaling studies. *Lab Chip* 6: 389-393

Aboody KS, Brown A, Rainov NG, Bower KA, Liu S, Yang W, Small JE, Herrlinger U, Ourednik V, Black PM, Breakefield XO, Snyder EY (2000) Neural stem cells display extensive tropism for pathology in adult brain: evidence from intracranial gliomas. *Proceedings of the National Academy of Sciences of the United States of America* 97: 12846-12851

Abouantoun TJ, MacDonald TJ (2009) Imatinib blocks migration and invasion of medulloblastoma cells by concurrently inhibiting activation of platelet-derived growth factor receptor and transactivation of epidermal growth factor receptor. *Molecular cancer therapeutics* 8: 1137-1147

Abounader R (2009) Interactions between PTEN and receptor tyrosine kinase pathways and their implications for glioma therapy. *Expert review of anticancer therapy* 9: 235-245

Adler M, Polinkovsky M, Gutierrez E, Groisman A (2009) Generation of oxygen gradients with arbitrary shapes in a microfluidic device. *Lab Chip* 10: 388-391

Ahmed N, Ratnayake M, Savoldo B, Perlaky L, Dotti G, Wels WS, Bhattacharjee MB, Gilbertson RJ, Shine HD, Weiss HL, Rooney CM, Heslop HE, Gottschalk S (2007) Regression of experimental medulloblastoma following transfer of HER2-specific T cells. *Cancer research* 67: 5957-5964

Ahmed T, Shimizu TS, Stocker R (2010) Bacterial Chemotaxis in Linear and Nonlinear Steady Microfluidic Gradients. *Nano Lett* 10: 3379-3385

Akbasak A, Sunar-Akbasak B (1992) Oncogenes: cause or consequence in the development of glial tumors. *Journal of the neurological sciences* 111: 119-133

Albini A, Iwamoto Y, Kleinman HK, Martin GR, Aaronson SA, Kozlowski JM, McEwan RN (1987) A rapid in vitro assay for quantitating the invasive potential of tumor cells. *Cancer research* 47: 3239-3245

Altman DA, Atkinson DS, Jr., Brat DJ (2007) Best cases from the AFIP: glioblastoma multiforme. *Radiographics : a review publication of the Radiological Society of North America, Inc* 27: 883-888

Alves TR, Lima FR, Kahn SA, Lobo D, Dubois LG, Soletti R, Borges H, Neto VM (2011) Glioblastoma cells: a heterogeneous and fatal tumor interacting with the parenchyma. *Life sciences* 89: 532-539

Amberger VR, Avellana-Adalid V, Hensel T, Baron-van Evercooren A, Schwab ME (1997) Oligodendrocyte-type 2 astrocyte progenitors use a metalloendoprotease to spread and migrate on CNS myelin. *The European journal of neuroscience* 9: 151-162

Amberger VR, Hensel T, Ogata N, Schwab ME (1998) Spreading and migration of human glioma and rat C6 cells on central nervous system myelin in vitro is correlated with tumor malignancy and involves a metalloproteolytic activity. *Cancer research* 58: 149-158

Amit I, Citri A, Shay T, Lu Y, Katz M, Zhang F, Tarcic G, Siwak D, Lahad J, Jacob-Hirsch J, Amariglio N, Vaisman N, Segal E, Rechavi G, Alon U, Mills GB, Domany E, Yarden Y (2007) A module of negative feedback regulators defines growth factor signaling. *Nature genetics* 39: 503-512

Annabi B, Rojas-Sutterlin S, Laflamme C, Lachambre MP, Rolland Y, Sartelet H, Beliveau R (2008) Tumor environment dictates medulloblastoma cancer stem cell expression and invasive phenotype. *Molecular cancer research : MCR* 6: 907-916

Arora A, Scholar EM (2005) Role of tyrosine kinase inhibitors in cancer therapy. *The Journal of pharmacology and experimental therapeutics* 315: 971-979

Assanah M, Lochhead R, Ogden A, Bruce J, Goldman J, Canoll P (2006) Glial progenitors in adult white matter are driven to form malignant gliomas by platelet-derived growth factor-expressing retroviruses. *The Journal of neuroscience : the official journal of the Society for Neuroscience* 26: 6781-6790

Assanah MC, Bruce JN, Suzuki SO, Chen A, Goldman JE, Canoll P (2009) PDGF stimulates the massive expansion of glial progenitors in the neonatal forebrain. *Glia* 57: 1835-1847

Atencia J, Beebe DJ (2005) Controlled microfluidic interfaces. *Nature* 437: 648-655

Balagadde FK, You L, Hansen CL, Arnold FH, Quake SR (2005) Long-term monitoring of bacteria undergoing programmed population control in a microchemostat. *Science* 309: 137-140

Bao S, Wu Q, Sathornsumetee S, Hao Y, Li Z, Hjelmeland AB, Shi Q, McLendon RE, Bigner DD, Rich JN (2006) Stem cell-like glioma cells promote tumor angiogenesis through vascular endothelial growth factor. *Cancer research* 66: 7843-7848

Baumann N, Pham-Dinh D (2001) Biology of oligodendrocyte and myelin in the mammalian central nervous system. *Physiological reviews* 81: 871-927

Beadle C, Assanah MC, Monzo P, Vallee R, Rosenfeld SS, Canoll P (2008) The role of myosin II in glioma invasion of the brain. *Molecular biology of the cell* 19: 3357-3368

Beebe DJ, Mensing GA, Walker GM (2002) Physics and applications of microfluidics in biology. *Annu Rev Biomed Eng* 4: 261-286

Belcher SM, Ma X, Le HH (2009) Blockade of estrogen receptor signaling inhibits growth and migration of medulloblastoma. *Endocrinology* 150: 1112-1121

Belien AT, Paganetti PA, Schwab ME (1999) Membrane-type 1 matrix metalloprotease (MT1-MMP) enables invasive migration of glioma cells in central nervous system white matter. *The Journal of cell biology* 144: 373-384

Bellail AC, Hunter SB, Brat DJ, Tan C, Van Meir EG (2004) Microregional extracellular matrix heterogeneity in brain modulates glioma cell invasion. *The international journal of biochemistry & cell biology* 36: 1046-1069

Benedetti S, Pirola B, Pollo B, Magrassi L, Bruzzone MG, Rigamonti D, Galli R, Selleri S, Di Meco F, De Fraja C, Vescovi A, Cattaneo E, Finocchiaro G (2000) Gene therapy of experimental brain tumors using neural progenitor cells. *Nature medicine* 6: 447-450

Bernard A, Renault JP, Michel B, Bosshard HR, Delamarche E (2000) Microcontact Printing of Proteins. *Advanced Materials* 12: 1067–1070

Betsholtz C, Westermark B, Ek B, Heldin CH (1984) Coexpression of a PDGF-like growth factor and PDGF receptors in a human osteosarcoma cell line: implications for autocrine receptor activation. *Cell* 39: 447-457

Bhoopathi P, Chetty C, Gogineni VR, Gujrati M, Dinh DH, Rao JS, Lakka SS (2011) MMP-2 mediates mesenchymal stem cell tropism towards medulloblastoma tumors. *Gene therapy*

Biegel JA, Janss AJ, Raffel C, Sutton L, Rorke LB, Harper JM, Phillips PC (1997) Prognostic significance of chromosome 17p deletions in childhood primitive neuroectodermal tumors (medulloblastomas) of the central nervous system. *Clinical cancer research : an official journal of the American Association for Cancer Research* 3: 473-478

Bigner SH, McLendon RE, Fuchs H, McKeever PE, Friedman HS (1997) Chromosomal characteristics of childhood brain tumors. *Cancer genetics and cytogenetics* 97: 125-134

Bird RB, Stewart WE, Lightfoot EN (2002) Transport Phenomena . 2nd ed. New York: John Wiley & Sons, Inc.: Textbook

Boyden S (1962) The chemotactic effect of mixtures of antibody and antigen on polymorphonuclear leucocytes. *The Journal of experimental medicine* 115: 453-466

Breckenridge MT, Egelhoff TT, Baskaran H (2010) A microfluidic imaging chamber for the direct observation of chemotactic transmigration. *Biomed Microdevices* 12: 543-553

Briancon-Marjollet A, Balenci L, Fernandez M, Esteve F, Honnorat J, Farion R, Beaumont M, Barbier E, Remy C, Baudier J (2010) NG2-expressing glial precursor cells are a new potential oligodendroglioma cell initiating population in N-ethyl-N-nitrosourea-induced gliomagenesis. *Carcinogenesis* 31: 1718-1725

Brockmann MA, Ulbricht U, Gruner K, Fillbrandt R, Westphal M, Lamszus K (2003) Glioblastoma and cerebral microvascular endothelial cell migration in response to tumor-associated growth factors. *Neurosurgery* 52: 1391-1399; discussion 1399

Burger PC, Vogel FS, Green SB, Strike TA (1985) Glioblastoma multiforme and anaplastic astrocytoma. Pathologic criteria and prognostic implications. *Cancer* 56: 1106-1111

Byers SW, Sommers CL, Hoxter B, Mercurio AM, Tozeren A (1995) Role of E-cadherin in the response of tumor cell aggregates to lymphatic, venous and arterial flow: measurement of cell-cell adhesion strength. *Journal of cell science* 108 (Pt 5): 2053-2064

Cadena DL, Chan CL, Gill GN (1994) The intracellular tyrosine kinase domain of the epidermal growth factor receptor undergoes a conformational change upon autophosphorylation. *The Journal of biological chemistry* 269: 260-265

Calabrese C, Frank A, Maclean K, Gilbertson R (2003) Medulloblastoma sensitivity to 17-allylamino-17-demethoxygeldanamycin requires MEK/ERKM. *The Journal of biological chemistry* 278: 24951-24959

Candolfi M, Curtin JF, Nichols WS, Muhammad AG, King GD, Pluhar GE, McNiel EA, Ohlfest JR, Freese AB, Moore PF, Lerner J, Lowenstein PR, Castro MG (2007) Intracranial glioblastoma models in preclinical neuro-oncology: neuropathological characterization and tumor progression. *Journal of neuro-oncology* 85: 133-148

Carlsson J, Nederman T (1983) A method to measure the radio and chemosensitivity of human spheroids. *Advances in experimental medicine and biology* 159: 399-417

Cattaneo MG, Gentilini D, Vicentini LM (2006) Deregulated human glioma cell motility: inhibitory effect of somatostatin. *Molecular and cellular endocrinology* 256: 34-39

Cayre M, Canoll P, Goldman JE (2009) Cell migration in the normal and pathological postnatal mammalian brain. *Progress in neurobiology* 88: 41-63

Chamberlain MC (2006) MRI in patients with high-grade gliomas treated with bevacizumab and chemotherapy. *Neurology* 67: 2089; author reply 2089

Chan AW, Tarbell NJ, Black PM, Louis DN, Frosch MP, Ancukiewicz M, Chapman P, Loeffler JS (2000) Adult medulloblastoma: prognostic factors and patterns of relapse. *Neurosurgery* 47: 623-631; discussion 631-622

Charles NA, Holland EC, Gilbertson R, Glass R, Kettenmann H (2011) The brain tumor microenvironment. *Glia* 59: 1169-1180

Chen B, Gao Y, Jiang T, Ding J, Zeng Y, Xu R, Jiang X (2011) Inhibition of tumor cell migration and invasion through knockdown of rac1 expression in medulloblastoma cells. *Cellular and molecular neurobiology* 31: 251-257

Chicoine MR, Silbergeld DL (1997) Mitogens as motogens. *Journal of neuro-oncology* 35: 249-257

Chung S, Sudo R, Mack PJ, Wan CR, Vickerman V, Kamm RD (2009) Cell migration into scaffolds under co-culture conditions in a microfluidic platform. *Lab Chip* 9: 269-275

Clark MJ, Homer N, O'Connor BD, Chen Z, Eskin A, Lee H, Merriman B, Nelson SF (2010) U87MG decoded: the genomic sequence of a cytogenetically aberrant human cancer cell line. *PLoS genetics* 6: e1000832

Cocucci E, Racchetti G, Meldolesi J (2009) Shedding microvesicles: artefacts no more. *Trends in cell biology* 19: 43-51

Condeelis J, Segall JE (2003) Intravital imaging of cell movement in tumours. *Nature reviews Cancer* 3: 921-930

Corcoran A, Del Maestro RF (2003) Testing the "Go or Grow" hypothesis in human medulloblastoma cell lines in two and three dimensions. *Neurosurgery* 53: 174-184; discussion 184-175

Crowe CT, Elger DF, Roberson JA (2001) Engineering Fluid Mechanics. 7th ed: John Wiley & Sons, Inc.: Textbook

Dai C, Celestino JC, Okada Y, Louis DN, Fuller GN, Holland EC (2001) PDGF autocrine stimulation dedifferentiates cultured astrocytes and induces oligodendrogliomas and oligoastrocytomas from neural progenitors and astrocytes in vivo. *Genes & development* 15: 1913-1925

Dancey J, Sausville EA (2003) Issues and progress with protein kinase inhibitors for cancer treatment. *Nature reviews Drug discovery* 2: 296-313

Davidson LA, Keller RE (1999) Neural tube closure in Xenopus laevis involves medial migration, directed protrusive activity, cell intercalation and convergent extension. *Development* 126: 4547-4556

Delamarche E, Bernard A, Schmid H, Michel B, Biebuyck H (1997) Patterned delivery of immunoglobulins to surfaces using microfluidic networks. *Science* 276: 779-781

Demuth T, Berens ME (2004) Molecular mechanisms of glioma cell migration and invasion. *Journal of neuro-oncology* 70: 217-228

Dertinger S, Chiu DT, Jeon NL, Whitesides GM (2001) Generation of Gradients Having Complex Shapes using microfluidic Networks. *Anal Chem* 73: 1240-1246

Dhall G (2009) Medulloblastoma. *Journal of child neurology* 24: 1418-1430

Ding Q, Stewart J, Jr., Olman MA, Klobe MR, Gladson CL (2003) The pattern of enhancement of Src kinase activity on platelet-derived growth factor stimulation of glioblastoma cells is affected by the integrin engaged. *The Journal of biological chemistry* 278: 39882-39891

Dong Y, Jia L, Wang X, Tan X, Xu J, Deng Z, Jiang T, Rainov NG, Li B, Ren H (2011) Selective inhibition of PDGFR by imatinib elicits the sustained activation of ERK and downstream receptor signaling in malignant glioma cells. *International journal of oncology* 38: 555-569

Doolittle RF, Hunkapiller MW, Hood LE, Devare SG, Robbins KC, Aaronson SA, Antoniades HN (1983) Simian sarcoma virus onc gene, v-sis, is derived from the gene (or genes) encoding a platelet-derived growth factor. *Science* 221: 275-277

Du Y, Shim J, Vidula M, Hancock MJ, Lo E, Chung BG, Borenstein JT, Khabiry M, Cropek DM, Khademhosseini A (2009) Rapid generation of spatially and temporally controllable long-range concentration gradients in a microfluidic device. *Lab Chip* 9: 761-767

Dudu V, Able R, Rotari V, Vazquez V (2011) Role of Epidermal Growth Factor-triggered PI3K/Akt signaling in the Migration of Medulloblastoma-derived Cells. *Cell and Molecular Bioengineering* In Review

Dudu V, Ramcharan M, Gilchrist ML, Holland EC, Vazquez M (2008) Liposome delivery of quantum dots to the cytosol of live cells. *Journal of nanoscience and nanotechnology* 8: 2293-2300

Duffau H, Khalil I, Gatignol P, Denvil D, Capelle L (2004) Surgical removal of corpus callosum infiltrated by low-grade glioma: functional outcome and oncological considerations. *Journal of neurosurgery* 100: 431-437

Duffner PK, Horowitz ME, Krischer JP, Burger PC, Cohen ME, Sanford RA, Friedman HS, Kun LE (1999) The treatment of malignant brain tumors in infants and very young children: an update of the Pediatric Oncology Group experience. *Neuro-oncology* 1: 152-161

Dufour C, Cadusseau J, Varlet P, Surena AL, de Faria GP, Dias-Morais A, Auger N, Leonard N, Daudigeos E, Dantas-Barbosa C, Grill J, Lazar V, Dessen P, Vassal G, Prevot V, Sharif A, Chneiweiss H, Junier MP (2009) Astrocytes reverted to a neural progenitor-like state with transforming growth factor alpha are sensitized to cancerous transformation. *Stem cells* 27: 2373-2382

Duntsch C, Zhou Q, Weimar JD, Frankel B, Robertson JH, Pourmotabbed T (2005) Up-regulation of neuropoiesis generating glial progenitors that infiltrate rat intracranial glioma. *Journal of neuro-oncology* 71: 245-255

Edelstein K, Spiegler BJ, Fung S, Panzarella T, Mabbott DJ, Jewitt N, D'Agostino NM, Mason WP, Bouffet E, Tabori U, Laperriere N, Hodgson DC (2011) Early aging in adult survivors of childhood medulloblastoma: Long-term neurocognitive, functional, and physical outcomes. *Neuro-oncology*

Ekani-Nkodo A, Fygenson DK (2003) Size exclusion and diffusion of fluoresceinated probes within collagen fibrils. *Physical review E, Statistical, nonlinear, and soft matter physics* 67: 021909

Engebraaten O, Bjerkvig R, Pedersen PH, Laerum OD (1993) Effects of EGF, bFGF, NGF and PDGF(bb) on cell proliferative, migratory and invasive capacities of human brain-tumour biopsies in vitro. *International journal of cancer Journal international du cancer* 53: 209-214

Englert DL, Manson MD, Jayaraman A (2010) Investigation of bacterial chemotaxis in flow-based microfluidic devices. *Nat Protoc* 5: 864-872

Farin A, Suzuki SO, Weiker M, Goldman JE, Bruce JN, Canoll P (2006) Transplanted glioma cells migrate and proliferate on host brain vasculature: a dynamic analysis. *Glia* 53: 799-808

Felber JP, Coombs TL, Vallee BL (1962) The mechanism of inhibition of carboxypeptidase A by 1,10-phenanthroline. *Biochemistry* 1: 231-238

Feng JJ, Wang AJ, Fan J, Xu JJ, Chen HY (2010) Hydrophilic biopolymer grafted on poly(dimethylsiloxane) surface for microchip electrophoresis. *Anal Chim Acta* 658: 75-80

Fisher GH, Orsulic S, Holland E, Hively WP, Li Y, Lewis BC, Williams BO, Varmus HE (1999) Development of a flexible and specific gene delivery system for production of murine tumor models. *Oncogene* 18: 5253-5260

Folch A (2007) BioMEMS and cellular biology: perspectives and applications. *J Vis Exp*: 300

Fomchenko EI, Dougherty JD, Helmy KY, Katz AM, Pietras A, Brennan C, Huse JT, Milosevic A, Holland EC (2011) Recruited cells can become transformed and overtake PDGF-induced murine gliomas in vivo during tumor progression. *PloS one* 6: e20605

Fomchenko EI, Holland EC (2005) Stem cells and brain cancer. *Experimental cell research* 306: 323-329

Forsyth PA, Wong H, Laing TD, Rewcastle NB, Morris DG, Muzik H, Leco KJ, Johnston RN, Brasher PM, Sutherland G, Edwards DR (1999) Gelatinase-A (MMP-2), gelatinase-B (MMP-9) and membrane type matrix metalloproteinase-1 (MT1-MMP) are involved in different aspects of the pathophysiology of malignant gliomas. *British journal of cancer* 79: 1828-1835

Fosser K, Nuzzo R (2003) Characterization of a membrane-based gradient generator for use in. *Anal Chem* 75: 5775-5782

Frevert CW, Boggy G, Keenan TM, Folch A (2006) Measurement of cell migration in response to an evolving radial chemokine gradient triggered by a microvalve. *Lab Chip* 6: 849-856

Friedl P, Borgmann S, Brocker EB (2001) Amoeboid leukocyte crawling through extracellular matrix: lessons from the Dictyostelium paradigm of cell movement. *Journal of leukocyte biology* 70: 491-509

Friedl P, Noble PB, Walton PA, Laird DW, Chauvin PJ, Tabah RJ, Black M, Zanker KS (1995) Migration of coordinated cell clusters in mesenchymal and epithelial cancer explants in vitro. *Cancer research* 55: 4557-4560

Friedl P, Wolf K (2003) Tumour-cell invasion and migration: diversity and escape mechanisms. *Nature reviews Cancer* 3: 362-374

Friedlander DR, Zagzag D, Shiff B, Cohen H, Allen JC, Kelly PJ, Grumet M (1996) Migration of brain tumor cells on extracellular matrix proteins in vitro correlates with tumor type and grade and involves alphaV and beta1 integrins. *Cancer research* 56: 1939-1947

Fruhwald MC, Plass C (2002) Metastatic medulloblastoma--therapeutic success through molecular target identification? *The pharmacogenomics journal* 2: 7-10

Fukazawa T, Miyake S, Band V, Band H (1996) Tyrosine phosphorylation of Cbl upon epidermal growth factor (EGF) stimulation and its association with EGF receptor and downstream signaling proteins. *The Journal of biological chemistry* 271: 14554-14559

Furnari FB, Fenton T, Bachoo RM, Mukasa A, Stommel JM, Stegh A, Hahn WC, Ligon KL, Louis DN, Brennan C, Chin L, DePinho RA, Cavenee WK (2007) Malignant astrocytic glioma: genetics, biology, and paths to treatment. *Genes & development* 21: 2683-2710

Gage FH (2000) Mammalian neural stem cells. *Science* 287: 1433-1438

Galli R, Binda E, Orfanelli U, Cipelletti B, Gritti A, De Vitis S, Fiocco R, Foroni C, Dimeco F, Vescovi A (2004) Isolation and characterization of tumorigenic, stem-like neural precursors from human glioblastoma. *Cancer research* 64: 7011-7021

Gallo V, Zhou JM, McBain CJ, Wright P, Knutson PL, Armstrong RC (1996) Oligodendrocyte progenitor cell proliferation and lineage progression are regulated by glutamate receptor-mediated K+ channel block. *The Journal of neuroscience : the official journal of the Society for Neuroscience* 16: 2659-2670

Gennerich A, Schild D (2002) Anisotropic Diffusion in Mitral Cell Dendrites Revealed by Fluorescence Correction Spectroscopy. *Biophysical J* 83: 510-522

Gentile A, Trusolino L, Comoglio PM (2008) The Met tyrosine kinase receptor in development and cancer. *Cancer metastasis reviews* 27: 85-94

Gibson P, Tong Y, Robinson G, Thompson MC, Currle DS, Eden C, Kranenburg TA, Hogg T, Poppleton H, Martin J, Finkelstein D, Pounds S, Weiss A, Patay Z, Scoggins M, Ogg R, Pei Y, Yang ZJ, Brun S, Lee Y, Zindy F, Lindsey JC, Taketo MM, Boop FA, Sanford RA, Gajjar A, Clifford SC, Roussel MF, McKinnon PJ, Gutmann DH, Ellison DW, Wechsler-Reya R, Gilbertson RJ (2010) Subtypes of medulloblastoma have distinct developmental origins. *Nature* 468: 1095-1099

Giese A, Loo MA, Tran N, Haskett D, Coons SW, Berens ME (1996) Dichotomy of astrocytoma migration and proliferation. *International journal of cancer Journal international du cancer* 67: 275-282

Giese A, Rief MD, Loo MA, Berens ME (1994) Determinants of human astrocytoma migration. *Cancer research* 54: 3897-3904

Gilbertson RJ (2004) Medulloblastoma: signalling a change in treatment. *The lancet oncology* 5: 209-218

Glass R, Synowitz M, Kronenberg G, Walzlein JH, Markovic DS, Wang LP, Gast D, Kiwit J, Kempermann G, Kettenmann H (2005) Glioblastoma-induced attraction of endogenous neural precursor cells is associated with improved survival. *The Journal of neuroscience : the official journal of the Society for Neuroscience* 25: 2637-2646

Gonzalez-Perez O, Quinones-Hinojosa A (2010) Dose-dependent effect of EGF on migration and differentiation of adult subventricular zone astrocytes. *Glia* 58: 975-983

Goulpeau J, Lonetti B, Trouchet D, Ajdari A, Tabeling P (2007) Building up longitudinal concentration gradients in shallow microchannels. *Lab Chip* 7: 1154-1161

Grotendorst GR, Soma Y, Takehara K, Charette M (1989) EGF and TGF-alpha are potent chemoattractants for endothelial cells and EGF-like peptides are present at sites of tissue regeneration. *Journal of cellular physiology* 139: 617-623

Guck J, Lautenschlager F, Paschke S, Beil M (2010) Critical review: cellular mechanobiology and amoeboid migration. *Integrative biology : quantitative biosciences from nano to macro* 2: 575-583

Guessous F, Zhang Y, diPierro C, Marcinkiewicz L, Sarkaria J, Schiff D, Buchanan S, Abounader R (2010) An orally bioavailable c-Met kinase inhibitor potently inhibits brain tumor malignancy and growth. *Anti-cancer agents in medicinal chemistry* 10: 28-35

Guo P, Hu B, Gu W, Xu L, Wang D, Huang HJ, Cavenee WK, Cheng SY (2003) Platelet-derived growth factor-B enhances glioma angiogenesis by stimulating vascular endothelial

growth factor expression in tumor endothelia and by promoting pericyte recruitment. *The American journal of pathology* 162: 1083-1093

Hadjipanayis CG, Van Meir EG (2009) Tumor initiating cells in malignant gliomas: biology and implications for therapy. *Journal of molecular medicine* 87: 363-374

Haibo X, Yi Z, Xin F, Huayong Y, Hongyang D (2008) Study on Characteristics of Interface Between Multiple Laminar Streams and Application for Secondary Etching Inside Microchannels. 243 - 248

Haller MF, Saltzman WM (1998) Localized Delivery of Proteins in the Brain: Can Transport Be Customized? *Pharmaceutical Research* 15: 377-385

Hambardzumyan D, Amankulor NM, Helmy KY, Becher OJ, Holland EC (2009) Modeling Adult Gliomas Using RCAS/t-va Technology. *Translational oncology* 2: 89-95

Hamel W, Westphal M (2000) Growth factors in gliomas revisited. *Acta neurochirurgica* 142: 113-137; discussion 137-118

Hanahan D, Weinberg RA (2000) The hallmarks of cancer. *Cell* 100: 57-70

Hashizume R, Koizumi H, Ihara A, Ohta T, Uchikoshi T (1996) Expression of beta-catenin in normal breast tissue and breast carcinoma: a comparative study with epithelial cadherin and alpha-catenin. *Histopathology* 29: 139-146

Hatton BA, Villavicencio EH, Tsuchiya KD, Pritchard JI, Ditzler S, Pullar B, Hansen S, Knoblaugh SE, Lee D, Eberhart CG, Hallahan AR, Olson JM (2008) The Smo/Smo model: hedgehog-induced medulloblastoma with 90% incidence and leptomeningeal spread. *Cancer research* 68: 1768-1776

Heese O, Disko A, Zirkel D, Westphal M, Lamszus K (2005) Neural stem cell migration toward gliomas in vitro. *Neuro-oncology* 7: 476-484

Hegerfeldt Y, Tusch M, Brocker EB, Friedl P (2002) Collective cell movement in primary melanoma explants: plasticity of cell-cell interaction, beta1-integrin function, and migration strategies. *Cancer research* 62: 2125-2130

Hensel T, Amberger VR, Schwab ME (1998) A metalloprotease activity from C6 glioma cells inactivates the myelin-associated neurite growth inhibitors and can be neutralized by antibodies. *British journal of cancer* 78: 1564-1572

Herbst RS (2005) Erlotinib. *Clinical advances in hematology & oncology : H&O* 3: 125, 141

Hermansson M, Nister M, Betsholtz C, Heldin CH, Westermark B, Funa K (1988) Endothelial cell hyperplasia in human glioblastoma: coexpression of mRNA for platelet-derived growth

factor (PDGF) B chain and PDGF receptor suggests autocrine growth stimulation. *Proceedings of the National Academy of Sciences of the United States of America* 85: 7748-7752

Herms J, Neidt I, Luscher B, Sommer A, Schurmann P, Schroder T, Bergmann M, Wilken B, Probst-Cousin S, Hernaiz-Driever P, Behnke J, Hanefeld F, Pietsch T, Kretzschmar HA (2000) C-MYC expression in medulloblastoma and its prognostic value. *International journal of cancer Journal international du cancer* 89: 395-402

Hernan R, Fasheh R, Calabrese C, Frank AJ, Maclean KH, Allard D, Barraclough R, Gilbertson RJ (2003) ERBB2 up-regulates S100A4 and several other prometastatic genes in medulloblastoma. *Cancer research* 63: 140-148

Heyer J, Kwong LN, Lowe SW, Chin L (2010) Non-germline genetically engineered mouse models for translational cancer research. *Nature reviews Cancer* 10: 470-480

Hiemenz PC, R. R (1997) Principles of Colloid and Surface Chemistry 3rd ed. New York: Marcel Dekker.: Textbook

Higginbotham H, Yokota Y, Anton ES (2011) Strategies for analyzing neuronal progenitor development and neuronal migration in the developing cerebral cortex. *Cerebral cortex* 21: 1465-1474

Hirata A, Ogawa S, Kometani T, Kuwano T, Naito S, Kuwano M, Ono M (2002) ZD1839 (Iressa) induces antiangiogenic effects through inhibition of epidermal growth factor receptor tyrosine kinase. *Cancer research* 62: 2554-2560

Hoelzinger DB, Demuth T, Berens ME (2007) Autocrine factors that sustain glioma invasion and paracrine biology in the brain microenvironment. *Journal of the National Cancer Institute* 99: 1583-1593

Holden MA, Kumarb S, Castellanaa ET, Beskokb A, Cremer PS (2003) Generating fixed concentration arrays in a microfluidic device. *Sensors and Actuators B*: 199-207

Holland EC (2004) Mouse models of human cancer as tools in drug development. *Cancer cell* 6: 197-198

Holland EC, Celestino J, Dai C, Schaefer L, Sawaya RE, Fuller GN (2000) Combined activation of Ras and Akt in neural progenitors induces glioblastoma formation in mice. *Nature genetics* 25: 55-57

Holmen SL, Williams BO (2005) Essential role for Ras signaling in glioblastoma maintenance. *Cancer research* 65: 8250-8255

Huang TT, Sarkaria SM, Cloughesy TF, Mischel PS (2009) Targeted therapy for malignant glioma patients: lessons learned and the road ahead. *Neurotherapeutics : the journal of the American Society for Experimental NeuroTherapeutics* 6: 500-512

Huang Y, Agrawal B, Sun D, Kuo JS, Williams JC (2011) Microfluidics-based devices: New tools for studying cancer and cancer stem cell migration. *Biomicrofluidics* 5: 13412

Hujanen ES, Terranova VP (1985) Migration of tumor cells to organ-derived chemoattractants. *Cancer research* 45: 3517-3521

Huse JT, Holland EC (2010) Targeting brain cancer: advances in the molecular pathology of malignant glioma and medulloblastoma. *Nature reviews Cancer* 10: 319-331

Hynes RO (1987) Integrins: a family of cell surface receptors. *Cell* 48: 549-554

Hynes RO (2002) Integrins: bidirectional, allosteric signaling machines. *Cell* 110: 673-687

Irimia D, Geba DA, Toner M (2006) Universal microfluidic gradient generator. *Anal Chem* 78: 3472-3477

Izquierdo S, Valdés JR, Martínez M, Accolti M, Woudberg S, Asinari P, Miana M, Du Plessis JP (2010) Porous-layer model for laminar liquid flow in rough microchannels. *Microfluid Nanofluid*: 1-13

Jeon NL, Baskararn H, Dertinger S, Whitesides GM, Water LV, Toner M (2002) Neutrophil chemotaxis in linear and complex gradients of interleukin-8 formed in a microfabricated device. *Nature Biotechnology* 20: 826-830

Jeon NL, Dertinger S, Chiu DT, Choi IS, Stroock AD, Whitesides GM (2000) Generation of Solution and Surface Gradients Using Microfluidic Systems. *Langmuir, American Chemical Society* 16: 8311-8316

Johnson R, Wright KD, Gilbertson RJ (2009) Molecular profiling of pediatric brain tumors: insight into biology and treatment. *Current oncology reports* 11: 68-72

Johnston AL, Lun X, Rahn JJ, Liacini A, Wang L, Hamilton MG, Parney IF, Hempstead BL, Robbins SM, Forsyth PA, Senger DL (2007) The p75 neurotrophin receptor is a central regulator of glioma invasion. *PLoS biology* 5: e212

Kakita A, Goldman JE (1999) Patterns and dynamics of SVZ cell migration in the postnatal forebrain: monitoring living progenitors in slice preparations. *Neuron* 23: 461-472

Kamholz AE, Weigl BH, Finlayson BA, Yager P (1999) Quantitative analysis of molecular interaction in a microfluidic channel: the T-sensor. *Anal Chem* 71: 5340-5347

Kamholz AE, Yager P (2001) Theoretical analysis of molecular diffusion in pressure-driven laminar flow in microfluidic channels. *Biophys J* 80: 155-160

Kamotani Y, Huh D, Futai N, Takayama S (2007) At the Interface: Advanced Microfluidic Assays for Study of Cell Function. *Biomems and biomedical nanotechnology*: 55-78

Kanamori M, Vanden Berg SR, Bergers G, Berger MS, Pieper RO (2004) Integrin beta3 overexpression suppresses tumor growth in a human model of gliomagenesis: implications for the role of beta3 overexpression in glioblastoma multiforme. *Cancer research* 64: 2751-2758

Kanegasaki S, Nomura Y, Nitta N, Akiyama S, Tamatani T, Goshoh Y, Yoshida T, Sato T, Kikuchi Y (2003) A novel optical assay system for the quantitative measurement of chemotaxis. *J Immunol Methods* 282: 1-11

Kanu OO, Hughes B, Di C, Lin N, Fu J, Bigner DD, Yan H, Adamson C (2009) Glioblastoma Multiforme Oncogenomics and Signaling Pathways. *Clinical medicine Oncology* 3: 39-52

Keenan TM, Folch A (2008) Biomolecular gradients in cell culture systems. *Lab Chip* 8: 34-57

Keunen O, Johansson M, Oudin A, Sanzey M, Rahim SA, Fack F, Thorsen F, Taxt T, Bartos M, Jirik R, Miletic H, Wang J, Stieber D, Stuhr L, Moen I, Rygh CB, Bjerkvig R, Niclou SP (2011) Anti-VEGF treatment reduces blood supply and increases tumor cell invasion in glioblastoma. *Proceedings of the National Academy of Sciences of the United States of America* 108: 3749-3754

Kim D, Lokuta MA, Huttenlocher A, Beebe DJ (2009) Selective and tunable gradient device for cell culture and chemotaxis study. *Lab Chip* 9: 1797-1800

Kim H, Muller WJ (1999) The role of the epidermal growth factor receptor family in mammary tumorigenesis and metastasis. *Experimental cell research* 253: 78-87

Kim MJ, Breuer KS (2004) Enhanced diffusion due to motile bacteria. *Physics of Fluids* 16

Kim S, Kim HJ, Jeon NL (2010) Biological applications of microfluidic gradient devices. *Integrative biology : quantitative biosciences from nano to macro* 2: 584-603

Kim SK, Kim SU, Park IH, Bang JH, Aboody KS, Wang KC, Cho BK, Kim M, Menon LG, Black PM, Carroll RS (2006) Human neural stem cells target experimental intracranial medulloblastoma and deliver a therapeutic gene leading to tumor regression. *Clinical cancer research : an official journal of the American Association for Cancer Research* 12: 5550-5556

Kleihues P, Sobin LH (2000) World Health Organization classification of tumors. *Cancer* 88: 2887

Kobel S, Lutolf M (2010) High-throughput methods to define complex stem cell niches. *Biotechniques* 48: ix-xxii

Kong Q, Able RA, Jr., Dudu V, Vazquez M (2010) A microfluidic device to establish concentration gradients using reagent density differences. *Journal of biomechanical engineering* 132: 121012

Kong Q, Majeska RJ, Vazquez M (2011) Migration of connective tissue-derived cells is mediated by ultra-low concentration gradient fields of EGF. *Experimental cell research* 317: 1491-1502

Konopka G, Bonni A (2003) Signaling pathways regulating gliomagenesis. *Current molecular medicine* 3: 73-84

Koochekpour S, Jeffers M, Rulong S, Taylor G, Klineberg E, Hudson EA, Resau JH, Vande Woude GF (1997) Met and hepatocyte growth factor/scatter factor expression in human gliomas. *Cancer research* 57: 5391-5398

Kranich S, Hattermann K, Specht A, Lucius R, Mentlein R (2009) VEGFR-3/Flt-4 mediates proliferation and chemotaxis in glial precursor cells. *Neurochemistry international* 55: 747-753

Kreutzer DL, O'Flaherty JT, Orr W, Showell HJ, Ward PA, Becker EL (1978) Quantitative comparisons of various biological responses of neutrophils to different active and inactive chemotactic factors. *Immunopharmacology* 1: 39-47

Kruger JS, Reddy KB (2003) Distinct mechanisms mediate the initial and sustained phases of cell migration in epidermal growth factor receptor-overexpressing cells. *Molecular cancer research : MCR* 1: 801-809

Labbe D, Provencal M, Lamy S, Boivin D, Gingras D, Beliveau R (2009) The flavonols quercetin, kaempferol, and myricetin inhibit hepatocyte growth factor-induced medulloblastoma cell migration. *The Journal of nutrition* 139: 646-652

Lang I, Scholz M, Peters R (1986) Molecular mobility and nucleocytoplasmic flux in hepatoma cells. *The Journal of cell biology* 102: 1183-1190

Larjavaara S, Mantyla R, Salminen T, Haapasalo H, Raitanen J, Jaaskelainen J, Auvinen A (2007) Incidence of gliomas by anatomic location. *Neuro-oncology* 9: 319-325

Lassman AB (2004) Molecular biology of gliomas. *Current neurology and neuroscience reports* 4: 228-233

Lassman AB, Dai C, Fuller GN, Vickers AJ, Holland EC (2004) Overexpression of c-MYC promotes an undifferentiated phenotype in cultured astrocytes and allows elevated Ras and Akt signaling to induce gliomas from GFAP-expressing cells in mice. *Neuron glia biology* 1: 157-163

Lauffenburger DA, Horwitz AF (1996) Cell migration: a physically integrated molecular process. *Cell* 84: 359-369

Lee I, Chan K, Phillips DL (1998) Growth of electrodeposited platinum nanocrystals studied by atomic force microscopy *Applied Surface Science* 136: 321-330

Lee J, Hu Y, Li D (2005) Electrokinetic concentration gradient generation using a converging–diverging microchannel. *Analytica Chimica Acta* 543: 99-108

Lenkiewicz M, Li N, Singh SK (2009) Culture and isolation of brain tumor initiating cells. *Current protocols in stem cell biology* Chapter 3: Unit3 3

Levicar N, Nuttall RK, Lah TT (2003) Proteases in brain tumour progression. *Acta neurochirurgica* 145: 825-838

Li CW, Chen R, Yang M (2007) Generation of linear and non-linear concentration gradients along microfluidic channel by microtunnel controlled stepwise addition of sample solution. *Lab Chip* 7: 1371-1373

Li Jeon N, Baskaran H, Dertinger SK, Whitesides GM, Van de Water L, Toner M (2002) Neutrophil chemotaxis in linear and complex gradients of interleukin-8 formed in a microfabricated device. *Nature biotechnology* 20: 826-830

Li Y, Lal B, Kwon S, Fan X, Saldanha U, Reznik TE, Kuchner EB, Eberhart C, Laterra J, Abounader R (2005) The scatter factor/hepatocyte growth factor: c-met pathway in human embryonal central nervous system tumor malignancy. *Cancer research* 65: 9355-9362

Li YH, Zhu C (1999) A modified Boyden chamber assay for tumor cell transendothelial migration in vitro. *Clinical & experimental metastasis* 17: 423-429

Li Z, Song J, Mantini G, Lu MY, Fang H, Falconi C, Chen LJ, Wang ZL (2009) Quantifying the traction force of a single cell by aligned silicon nanowire array. *Nano letters* 9: 3575-3580

Liang Y, Diehn M, Bollen AW, Israel MA, Gupta N (2008) Type I collagen is overexpressed in medulloblastoma as a component of tumor microenvironment. *Journal of neuro-oncology* 86: 133-141

Lim DA, Cha S, Mayo MC, Chen MH, Keles E, VandenBerg S, Berger MS (2007) Relationship of glioblastoma multiforme to neural stem cell regions predicts invasive and multifocal tumor phenotype. *Neuro-oncology* 9: 424-429

Lin F (2004) Generation of dynamic temporal and spatial concentration gradients using microfluidic devices. *Generation of dynamic temporal and spatial concentration gradients using microfluidic devices* 4: 164-167

Lindberg N, Kastemar M, Olofsson T, Smits A, Uhrbom L (2009) Oligodendrocyte progenitor cells can act as cell of origin for experimental glioma. *Oncogene* 28: 2266-2275

Liu TF, Tatter SB, Willingham MC, Yang M, Hu JJ, Frankel AE (2003) Growth factor receptor expression varies among high-grade gliomas and normal brain: epidermal growth factor receptor has excellent properties for interstitial fusion protein therapy. *Molecular cancer therapeutics* 2: 783-787

Lo HW (2010) Targeting Ras-RAF-ERK and its interactive pathways as a novel therapy for malignant gliomas. *Current cancer drug targets* 10: 840-848

Loan CE, Aberle T, Burchard W (2000) Structure Properties of Dextran. 2. Dilute Solution. *Macromolecules* 33: 5730 -5739

Lohof AM, Quillan M, Dan Y, Poo MM (1992) Asymmetric modulation of cytosolic cAMP activity induces growth cone turning. *The Journal of neuroscience : the official journal of the Society for Neuroscience* 12: 1253-1261

Lokker NA, Sullivan CM, Hollenbach SJ, Israel MA, Giese NA (2002) Platelet-derived growth factor (PDGF) autocrine signaling regulates survival and mitogenic pathways in glioblastoma cells: evidence that the novel PDGF-C and PDGF-D ligands may play a role in the development of brain tumors. *Cancer research* 62: 3729-3735

Louis DN (2006) Molecular pathology of malignant gliomas. *Annual review of pathology* 1: 97-117

Louis DN, Ohgaki H, Wiestler OD, Cavenee WK, Burger PC, Jouvet A, Scheithauer BW, Kleihues P (2007) The 2007 WHO classification of tumours of the central nervous system. *Acta neuropathologica* 114: 97-109

Lund-Johansen M, Bjerkvig R, Humphrey PA, Bigner SH, Bigner DD, Laerum OD (1990) Effect of epidermal growth factor on glioma cell growth, migration, and invasion in vitro. *Cancer research* 50: 6039-6044

MacDonald TJ, Tabrizi P, Shimada H, Zlokovic BV, Laug WE (1998) Detection of brain tumor invasion and micrometastasis in vivo by expression of enhanced green fluorescent protein. *Neurosurgery* 43: 1437-1442; discussion 1442-1433

Madhavan M, Srinivas P, Abraham E, Ahmed I, Mathew A, Vijayalekshmi NR, Balaram P (2001) Cadherins as predictive markers of nodal metastasis in breast cancer. *Modern pathology : an official journal of the United States and Canadian Academy of Pathology, Inc* 14: 423-427

Maher EA, Furnari FB, Bachoo RM, Rowitch DH, Louis DN, Cavenee WK, DePinho RA (2001) Malignant glioma: genetics and biology of a grave matter. *Genes & development* 15: 1311-1333

Maiti AK, Ghosh K, Chatterjee U, Chakrobarti S, Chatterjee S, Basu S (2008) Epidermal growth factor receptor and proliferating cell nuclear antigen in astrocytomas. *Neurology India* 56: 456-462

Masui K, Suzuki SO, Torisu R, Goldman JE, Canoll P, Iwaki T (2010) Glial progenitors in the brainstem give rise to malignant gliomas by platelet-derived growth factor stimulation. *Glia* 58: 1050-1065

McDonald J, Duffy D, Anderson J, Chiu DT, Wu H, Schueller O, Whitesides GM (2000) Fabrication of microfluidic systems in poly(dimethylsiloxane) *Electrophoresis* 21: 27-40

McDonald JC, Whitesides GM (2002) Poly(dimethylsiloxane) as a material for fabricating microfluidic devices. *Accounts of chemical research* 35: 491-499

McKnight TE, Melechko AV, Austin DW, Sims T, Guillorn MA, Simpson ML (2004) Microarrays of Vertically-Aligned Carbon Nanofiber Electrodes in an Open Fluidic Channel. *J Phys Chem B* 108: 7115-7125

McLaurin JA, Yong VW (1995) Oligodendrocytes and myelin. *Neurologic clinics* 13: 23-49

Meco D, Servidei T, Riccardi A, Ferlini C, Cusano G, Zannoni GF, Giangaspero F, Riccardi R (2009) Antitumor effect in medulloblastoma cells by gefitinib: Ectopic HER2 overexpression enhances gefitinib effects in vivo. *Neuro-oncology* 11: 250-259

Menon G, Nair S, Muthurethinam T, Krishnakumar K, Bhattacharya R (2006) Medulloblastoma in children: Prognostic factors and predictors of outcome. *Journal of Pediatric Neuroscience* 1: 16-20

Millet LJ, Stewart ME, Nuzzo RG, Gillette MU (2010) Guiding neuron development with planar surface gradients of substrate cues deposited using microfluidic devices. *Lab Chip* 10: 1525-1535

Miyamoto S, Teramoto H, Coso OA, Gutkind JS, Burbelo PD, Akiyama SK, Yamada KM (1995) Integrin function: molecular hierarchies of cytoskeletal and signaling molecules. *The Journal of cell biology* 131: 791-805

Moriyama T, Kataoka H, Seguchi K, Tsubouchi H, Koono M (1996) Effects of hepatocyte growth factor (HGF) on human glioma cells in vitro: HGF acts as a motility factor in glioma cells. *International journal of cancer Journal international du cancer* 66: 678-685

Mosadegh B, Huang C, Park JW, Shin HS, Chung BG, Hwang SK, Lee KH, Kim HJ, Brody J, Jeon NL (2007) Generation of stable complex gradients across two-dimensional surfaces and three-dimensional gels. *Langmuir* 23: 10910-10912

Motoo K, Toda N, Arai F, Fukuda T, Sekiyama K, Nakajima M (2008) Generation of concentration gradient from a wave-like pattern by high frequency vibration of liquid-liquid interface. *Biomed Microdevices* 10: 329-335

Mott JD, Werb Z (2004) Regulation of matrix biology by matrix metalloproteinases. *Current opinion in cell biology* 16: 558-564

Mueller MM, Werbowetski T, Del Maestro RF (2003) Soluble factors involved in glioma invasion. *Acta neurochirurgica* 145: 999-1008

Nabeshima K, Moriyama T, Asada Y, Komada N, Inoue T, Kataoka H, Sumiyoshi A, Koono M (1995) Ultrastructural study of TPA-induced cell motility: human well-differentiated rectal adenocarcinoma cells move as coherent sheets via localized modulation of cell-cell adhesion. *Clinical & experimental metastasis* 13: 499-508

Nakada M, Niska JA, Miyamori H, McDonough WS, Wu J, Sato H, Berens ME (2004) The phosphorylation of EphB2 receptor regulates migration and invasion of human glioma cells. *Cancer research* 64: 3179-3185

Nakamizo A, Marini F, Amano T, Khan A, Studeny M, Gumin J, Chen J, Hentschel S, Vecil G, Dembinski J, Andreeff M, Lang FF (2005) Human bone marrow-derived mesenchymal stem cells in the treatment of gliomas. *Cancer research* 65: 3307-3318

Nalla AK, Asuthkar S, Bhoopathi P, Gujrati M, Dinh DH, Rao JS (2010) Suppression of uPAR retards radiation-induced invasion and migration mediated by integrin beta1/FAK signaling in medulloblastoma. *PloS one* 5: e13006

Narayana A, Kelly P, Golfinos J, Parker E, Johnson G, Knopp E, Zagzag D, Fischer I, Raza S, Medabalmi P, Eagan P, Gruber ML (2009) Antiangiogenic therapy using bevacizumab in recurrent high-grade glioma: impact on local control and patient survival. *Journal of neurosurgery* 110: 173-180

Natarajan M, Stewart JE, Golemis EA, Pugacheva EN, Alexandropoulos K, Cox BD, Wang W, Grammer JR, Gladson CL (2006) HEF1 is a necessary and specific downstream effector of FAK that promotes the migration of glioblastoma cells. *Oncogene* 25: 1721-1732

Nederman T, Acker H, Carlsson J (1983) Penetration of substances into tumor tissue: a methodological study with microelectrodes and cellular spheroids. *In vitro* 19: 479-488

Nicholson C, Tao L (1993) Hindered diffusion of high molecular weight compounds in brain extracellular microenvironment measured with integrative optical imaging. *Biophysical journal* 65: 2277-2290

Nishikawa R (2010) Standard therapy for glioblastoma--a review of where we are. *Neurologia medico-chirurgica* 50: 713-719

Nister M, Hammacher A, Mellstrom K, Siegbahn A, Ronnstrand L, Westermark B, Heldin CH (1988) A glioma-derived PDGF A chain homodimer has different functional activities from a PDGF AB heterodimer purified from human platelets. *Cell* 52: 791-799

Ohashi K, Yokoyama T, Nakajima Y, Kosovsky M (2006) Methods for Implantation of BD MatrigelTM Matrix into Mice and Tissue Fixation. *BD Biosciences Technical Bulletin #455*

Ohnishi T, Arita N, Hiraga S, Taki T, Izumoto S, Fukushima Y, Hayakawa T (1997) Fibronectin-mediated cell migration promotes glioma cell invasion through chemokinetic activity. *Clinical & experimental metastasis* 15: 538-546

Onishi M, Ichikawa T, Kurozumi K, Date I (2011) Angiogenesis and invasion in glioma. *Brain tumor pathology* 28: 13-24

Orsulic S (2002) An RCAS-TVA-based approach to designer mouse models. *Mammalian genome : official journal of the International Mammalian Genome Society* 13: 543-547

Ostman A, Thyberg J, Westermark B, Heldin CH (1992) PDGF-AA and PDGF-BB biosynthesis: proprotein processing in the Golgi complex and lysosomal degradation of PDGF-BB retained intracellularly. *The Journal of cell biology* 118: 509-519

Paez-Ribes M, Allen E, Hudock J, Takeda T, Okuyama H, Vinals F, Inoue M, Bergers G, Hanahan D, Casanovas O (2009) Antiangiogenic therapy elicits malignant progression of tumors to increased local invasion and distant metastasis. *Cancer cell* 15: 220-231

Paguirigan AL, Beebe DJ (2008a) Microfluidics meet cell biology: bridging the gap by validation and application of microscale techniques for cell biological assays. *BioEssays : news and reviews in molecular, cellular and developmental biology* 30: 811-821

Paguirigan AL, Beebe DJ (2008b) Microfluidics meet cell biology: bridging the gap by validation and application of microscale techniques for cell biological assays. *Bioessays* 30: 811-821

Paliwal S, Iglesias PA, Campbell K, Hilioti Z, Groisman A, Levchenko A (2007) MAPK-mediated bimodal gene expression and adaptive gradient sensing in yeast. *Nature* 446: 46-51

Palmer SL, Goloubeva O, Reddick WE, Glass JO, Gajjar A, Kun L, Merchant TE, Mulhern RK (2001) Patterns of intellectual development among survivors of pediatric medulloblastoma: a longitudinal analysis. *Journal of clinical oncology : official journal of the American Society of Clinical Oncology* 19: 2302-2308

Park CM, Park MJ, Kwak HJ, Lee HC, Kim MS, Lee SH, Park IC, Rhee CH, Hong SI (2006) Ionizing radiation enhances matrix metalloproteinase-2 secretion and invasion of glioma cells through Src/epidermal growth factor receptor-mediated p38/Akt and phosphatidylinositol 3-kinase/Akt signaling pathways. *Cancer research* 66: 8511-8519

Park DM, Rich JN (2009) Biology of glioma cancer stem cells. *Molecules and cells* 28: 7-12

Park JY, Kim SK, Woo DH, Lee EJ, Kim JH, Lee SH (2009) Differentiation of neural progenitor cells in a microfluidic chip-generated cytokine gradient. *Stem Cells* 27: 2646-2654

Payet L, Ponton A, Le ger L, Hervet H, Grossiord JL, Agnely F (2008) Self-Diffusion in Chitosan Networks: From a Gel–Gel Method to Fluorescence Recovery after Photobleaching by Fringe Pattern. *Macromolecules* 41: 9376-9381

Pazzaglia S, Mancuso M, Atkinson MJ, Tanori M, Rebessi S, Majo VD, Covelli V, Hahn H, Saran A (2002) High incidence of medulloblastoma following X-ray-irradiation of newborn Ptc1 heterozygous mice. *Oncogene* 21: 7580-7584

Pazzaglia S, Tanori M, Mancuso M, Gessi M, Pasquali E, Leonardi S, Oliva MA, Rebessi S, Di Majo V, Covelli V, Giangaspero F, Saran A (2006) Two-hit model for progression of medulloblastoma preneoplasia in Patched heterozygous mice. *Oncogene* 25: 5575-5580

Pedersen PH, Edvardsen K, Garcia-Cabrera I, Mahesparan R, Thorsen J, Mathisen B, Rosenblum ML, Bjerkvig R (1995) Migratory patterns of lac-z transfected human glioma cells in the rat brain. *International journal of cancer Journal international du cancer* 62: 767-771

Piperi C, Zisakis A, Lea RW, Kalofoutis A (2005) Role of Cytokines in the Regulation of Glioma Tumour Growth and Angiogenesis. *American Journal of Immunology* 1: 106-113

Pollack IF, Randall MS, Kristofik MP, Kelly RH, Selker RG, Vertosick FT, Jr. (1991) Response of low-passage human malignant gliomas in vitro to stimulation and selective inhibition of growth factor-mediated pathways. *Journal of neurosurgery* 75: 284-293

Qazi H, Shi ZD, Tarbell JM (2011) Fluid shear stress regulates the invasive potential of glioma cells via modulation of migratory activity and matrix metalloproteinase expression. *PloS one* 6: e20348

Rajasekhar VK, Viale A, Socci ND, Wiedmann M, Hu X, Holland EC (2003) Oncogenic Ras and Akt signaling contribute to glioblastoma formation by differential recruitment of existing mRNAs to polysomes. *Molecular cell* 12: 889-901

Ranger A, McDonald W, Moore E, Delmaestro R (2010) The invasiveness of five medulloblastoma cell lines in collagen gels. *Journal of neuro-oncology* 96: 181-189

Rao JS (2003) Molecular mechanisms of glioma invasiveness: the role of proteases. *Nature reviews Cancer* 3: 489-501

Reddy AT (2001) Advances in biology and treatment of childhood brain tumors. *Current neurology and neuroscience reports* 1: 137-143

Reed J, Walczak WJ, Petzold ON, Gimzewski JK (2009) In situ mechanical interferometry of matrigel films. *Langmuir : the ACS journal of surfaces and colloids* 25: 36-39

Reigstad LJ, Varhaug JE, Lillehaug JR (2005) Structural and functional specificities of PDGF-C and PDGF-D, the novel members of the platelet-derived growth factors family. *The FEBS journal* 272: 5723-5741

Rickert CH, Paulus W (2001) Epidemiology of central nervous system tumors in childhood and adolescence based on the new WHO classification. *Child's nervous system : ChNS : official journal of the International Society for Pediatric Neurosurgery* 17: 503-511

Riffkin CD, Gray AZ, Hawkins CJ, Chow CW, Ashley DM (2001) Ex vivo pediatric brain tumors express Fas (CD95) and FasL (CD95L) and are resistant to apoptosis induction. *Neuro-oncology* 3: 229-240

Robel S, Berninger B, Gotz M (2011) The stem cell potential of glia: lessons from reactive gliosis. *Nature reviews Neuroscience* 12: 88-104

Romer JT, Curran T (2004) Medulloblastoma and retinoblastoma: oncology recapitulates ontogeny. *Cell cycle* 3: 917-919

Ronellenfitsch MW, Steinbach JP, Wick W (2010) Epidermal growth factor receptor and mammalian target of rapamycin as therapeutic targets in malignant glioma: current clinical status and perspectives. *Targeted oncology* 5: 183-191

Rood BR, Macdonald TJ, Packer RJ (2004) Current treatment of medulloblastoma: recent advances and future challenges. *Seminars in oncology* 31: 666-675

Rooprai HK, McCormick D (1997) Proteases and their inhibitors in human brain tumours: a review. *Anticancer research* 17: 4151-4162

Rutka JT, Apodaca G, Stern R, Rosenblum M (1988) The extracellular matrix of the central and peripheral nervous systems: structure and function. *Journal of neurosurgery* 69: 155-170

Saadi W, Rhee SW, Lin F, Vahidi B, Chung BG, Jeon NL (2007) Generation of stable concentration gradients in 2D and 3D environments using a microfluidic ladder chamber. *Biomed Microdevices* 9: 627-635

Saadi W, Wang SJ, Lin F, Jeon NL (2006) A parallel-gradient microfluidic chamber for quantitative analysis of breast cancer cell chemotaxis. *Biomedical microdevices* 8: 109-118

Sahai E (2005) Mechanisms of cancer cell invasion. *Current opinion in genetics & development* 15: 87-96

Salomon DS, Brandt R, Ciardiello F, Normanno N (1995) Epidermal growth factor-related peptides and their receptors in human malignancies. *Critical reviews in oncology/hematology* 19: 183-232

Saltzman WM, Radomsky ML, Whaley KJ, Cone RA (1994) Antibody diffusion in human cervical mucus. *Biophys J* 66: 508-515

Sampetrean O, Saga I, Nakanishi M, Sugihara E, Fukaya R, Onishi N, Osuka S, Akahata M, Kai K, Sugimoto H, Hirao A, Saya H (2011) Invasion precedes tumor mass formation in a malignant brain tumor model of genetically modified neural stem cells. *Neoplasia* 13: 784-791

Santini MT, Rainaldi G (1999) Three-dimensional spheroid model in tumor biology. *Pathobiology : journal of immunopathology, molecular and cellular biology* 67: 148-157

Sarkar C, Pramanik P, Karak AK, Mukhopadhyay P, Sharma MC, Singh VP, Mehta VS (2002) Are childhood and adult medulloblastomas different? A comparative study of clinicopathological features, proliferation index and apoptotic index. *Journal of neuro-oncology* 59: 49-61

Scheithauer BW (2009) Development of the WHO classification of tumors of the central nervous system: a historical perspective. *Brain pathology* 19: 551-564

Scherer HJ (1940) The forms of growth in gliomas and their practical significance. *Brain* 63: 1-35

Schiffer D, Annovazzi L, Caldera V, Mellai M (2010) On the origin and growth of gliomas. *Anticancer research* 30: 1977-1998

Schoen I, Hu W, Klotzsch E, Vogel V (2010) Probing cellular traction forces by micropillar arrays: contribution of substrate warping to pillar deflection. *Nano letters* 10: 1823-1830

Schwab ME, Caroni P (1988) Oligodendrocytes and CNS myelin are nonpermissive substrates for neurite growth and fibroblast spreading in vitro. *The Journal of neuroscience : the official journal of the Society for Neuroscience* 8: 2381-2393

Schwartz MS, Morris J, Sarid J (1991) Overexpression of oncogene products can cause tumor progression without parenchymal infiltration in the rat brain. *Cancer research* 51: 3595-3601

Seroogy KB, Gall CM, Lee DC, Kornblum HI (1995) Proliferative zones of postnatal rat brain express epidermal growth factor receptor mRNA. *Brain research* 670: 157-164

Shen JY, Chan-Park MB, He B, Zhu AP, Zhu X, Beuerman RW, Yang EB, Chen W, Chan V (2006) Three-dimensional microchannels in biodegradable polymeric films for control orientation and phenotype of vascular smooth muscle cells. *Tissue engineering* 12: 2229-2240

Shih AH, Dai C, Hu X, Rosenblum MK, Koutcher JA, Holland EC (2004) Dose-dependent effects of platelet-derived growth factor-B on glial tumorigenesis. *Cancer research* 64: 4783-4789

Shih AH, Holland EC (2006) Notch signaling enhances nestin expression in gliomas. *Neoplasia* 8: 1072-1082

Shimato S, Natsume A, Takeuchi H, Wakabayashi T, Fujii M, Ito M, Ito S, Park IH, Bang JH, Kim SU, Yoshida J (2007) Human neural stem cells target and deliver therapeutic gene to experimental leptomeningeal medulloblastoma. *Gene therapy* 14: 1132-1142

Singh S, Dirks PB (2007) Brain tumor stem cells: identification and concepts. *Neurosurgery clinics of North America* 18: 31-38, viii

Skog J, Wurdinger T, van Rijn S, Meijer DH, Gainche L, Sena-Esteves M, Curry WT, Jr., Carter BS, Krichevsky AM, Breakefield XO (2008) Glioblastoma microvesicles transport RNA and proteins that promote tumour growth and provide diagnostic biomarkers. *Nature cell biology* 10: 1470-1476

Sontheimer H (2004) Ion channels and amino acid transporters support the growth and invasion of primary brain tumors. *Molecular neurobiology* 29: 61-71

Spillmann AA, Bandtlow CE, Lottspeich F, Keller F, Schwab ME (1998) Identification and characterization of a bovine neurite growth inhibitor (bNI-220). *The Journal of biological chemistry* 273: 19283-19293

Staflin K, Zuchner T, Honeth G, Darabi A, Lundberg C (2009) Identification of proteins involved in neural progenitor cell targeting of gliomas. *BMC cancer* 9: 206

Stieber VW, Ellis TL (2005) The role of radiosurgery in the management of malignant brain tumors. *Current treatment options in oncology* 6: 501-508

Strommer K, Hamou MF, Diggelmann H, de Tribolet N (1990) Cellular and tumoural heterogeneity of EGFR gene amplification in human malignant gliomas. *Acta neurochirurgica* 107: 82-87

Stupp R, Weber DC (2005) The role of radio- and chemotherapy in glioblastoma. *Onkologie* 28: 315-317

Sung KE, Su G, Pehlke C, Trier SM, Eliceiri KW, Keely PJ, Friedl A, Beebe DJ (2009) Control of 3-dimensional collagen matrix polymerization for reproducible human mammary fibroblast cell culture in microfluidic devices. *Biomaterials* 30: 4833-4841

Tabatabai G, Wick W, Weller M (2011) Stem cell-mediated gene therapies for malignant gliomas: a promising targeted therapeutic approach? *Discovery medicine* 11: 529-536

Tan DC, Yung LY, Roy P (2010) Controlled microscale diffusion gradients in quiescent extracellular fluid. *Biomed Microdevices* 12: 523-532

Tanaka Y, Morishima K, Shimizu T, Kikuchi A, Yamato M, Okano T, Kitamori T (2006) Demonstration of a PDMS-based bio-microactuator using cultured cardiomyocytes to drive polymer micropillars. *Lab Chip* 6: 230-235

Tchougounova E, Kastemar M, Brasater D, Holland EC, Westermark B, Uhrbom L (2007) Loss of Arf causes tumor progression of PDGFB-induced oligodendroglioma. *Oncogene* 26: 6289-6296

Teodorczyk M, Martin-Villalba A (2010) Sensing invasion: cell surface receptors driving spreading of glioblastoma. *Journal of cellular physiology* 222: 1-10

Thorns V, Walter GF, Thorns C (2003) Expression of MMP-2, MMP-7, MMP-9, MMP-10 and MMP-11 in human astrocytic and oligodendroglial gliomas. *Anticancer research* 23: 3937-3944

Torp SH, Gulati S, Johannessen E, Dalen A (2007) Coexpression of c-erbB 1-4 receptor proteins in human glioblastomas. An immunohistochemical study. *Journal of experimental & clinical cancer research : CR* 26: 353-359

Tourovskaia A, Figueroa-Masot X, Folch A (2005) Differentiation-on-a-chip: a microfluidic platform for long-term cell culture studies. *Lab Chip* 5: 14-19

Towner RA, Smith N, Doblas S, Tesiram Y, Garteiser P, Saunders D, Cranford R, Silasi-Mansat R, Herlea O, Ivanciu L, Wu D, Lupu F (2008) In vivo detection of c-Met expression in a rat C6 glioma model. *Journal of cellular and molecular medicine* 12: 174-186

Trembath D, Miller CR, Perry A (2008) Gray zones in brain tumor classification: evolving concepts. *Advances in anatomic pathology* 15: 287-297

Tucker GC (2006) Integrins: molecular targets in cancer therapy. *Current oncology reports* 8: 96-103

Tysnes BB, Larsen LF, Ness GO, Mahesparan R, Edvardsen K, Garcia-Cabrera I, Bjerkvig R (1996) Stimulation of glioma-cell migration by laminin and inhibition by anti-alpha3 and anti-beta1 integrin antibodies. *International journal of cancer Journal international du cancer* 67: 777-784

Valadi H, Ekstrom K, Bossios A, Sjostrand M, Lee JJ, Lotvall JO (2007) Exosome-mediated transfer of mRNAs and microRNAs is a novel mechanism of genetic exchange between cells. *Nature cell biology* 9: 654-659

Van Meir EG, Hadjipanayis CG, Norden AD, Shu HK, Wen PY, Olson JJ (2010) Exciting new advances in neuro-oncology: the avenue to a cure for malignant glioma. *CA: a cancer journal for clinicians* 60: 166-193

Vazquez M, McKinley G, Mitnik L, Desmarais S, Matsudaira P, Ehrlich D (2002) Electrophoretic Injection within Microdevices. *Anal Chem* 74: 1952-1961

Vazquez M, Schmalzing D, Matsudaira P, Ehrlich D, McKinley G (2001) Shear-induced degradation of linear polyacrylamide solutions during pre-electrophoretic loading. *Anal Chem* 73: 3035-3044

Velve-Casquillas G, Berrea ML, Piela M, Tran PT (2010) Microfluidic tools for cell biological research. *Nano Today* 5: 28-47

Verkhratsky A (2007) Glial neurobiology: a textbook. *John Wiley and Sons* 1: 215

Visted T, Enger PO, Lund-Johansen M, Bjerkvig R (2003) Mechanisms of tumor cell invasion and angiogenesis in the central nervous system. *Frontiers in bioscience : a journal and virtual library* 8: e289-304

Wang F (2009) The signaling mechanisms underlying cell polarity and chemotaxis. *Cold Spring Harbor perspectives in biology* 1: a002980

Wang SJ, Saadi W, Lin F, Minh-Canh Nguyen C, Li Jeon N (2004) Differential effects of EGF gradient profiles on MDA-MB-231 breast cancer cell chemotaxis. *Experimental cell research* 300: 180-189

Wang X, Cui M, Wang L, Chen X, Xin P (2010) Inhibition of neurotrophin receptor p75 intramembran proteolysis by gamma-secretase inhibitor reduces medulloblastoma spinal metastasis. *Biochemical and biophysical research communications* 403: 264-269

Waterfield MD, Scrace GT, Whittle N, Stroobant P, Johnsson A, Wasteson A, Westermark B, Heldin CH, Huang JS, Deuel TF (1983) Platelet-derived growth factor is structurally related to the putative transforming protein p28sis of simian sarcoma virus. *Nature* 304: 35-39

Wear MA, Schafer DA, Cooper JA (2000) Actin dynamics: assembly and disassembly of actin networks. *Current biology : CB* 10: R891-895

Wechsler-Reya R, Scott MP (2001) The developmental biology of brain tumors. *Annual review of neuroscience* 24: 385-428

Weibel DB, Whitesides GM (2006) Applications of microfluidics in chemical biology. *Curr Opin Chem Biol* 10: 584-591

Weidner KM, Behrens J, Vandekerckhove J, Birchmeier W (1990) Scatter factor: molecular characteristics and effect on the invasiveness of epithelial cells. *The Journal of cell biology* 111: 2097-2108

Wells JA (1996) Binding in the growth hormone receptor complex. *Proceedings of the National Academy of Sciences of the United States of America* 93: 1-6

Wen PY, Kesari S (2008) Malignant gliomas in adults. *The New England journal of medicine* 359: 492-507

Werbowetski T, Bjerkvig R, Del Maestro RF (2004) Evidence for a secreted chemorepellent that directs glioma cell invasion. *Journal of neurobiology* 60: 71-88

Westermark B, Heldin CH (1989) Platelet-derived growth factor: structural and functional aspects. *Journal of internal medicine* 225: 55-58

Westermark B, Heldin CH (1991) Platelet-derived growth factor in autocrine transformation. *Cancer research* 51: 5087-5092

Whitesides GM (2006) The origins and the future of microfluidics. *Nature* 442: 368-373

Wild-Bode C, Weller M, Rimner A, Dichgans J, Wick W (2001) Sublethal irradiation promotes migration and invasiveness of glioma cells: implications for radiotherapy of human glioblastoma. *Cancer research* 61: 2744-2750

Wolf K, Mazo I, Leung H, Engelke K, von Andrian UH, Deryugina EI, Strongin AY, Brocker EB, Friedl P (2003) Compensation mechanism in tumor cell migration: mesenchymal-amoeboid transition after blocking of pericellular proteolysis. *The Journal of cell biology* 160: 267-277

Wong ST, Winchell LF, McCune BK, Earp HS, Teixido J, Massague J, Herman B, Lee DC (1989) The TGF-alpha precursor expressed on the cell surface binds to the EGF receptor on adjacent cells, leading to signal transduction. *Cell* 56: 495-506

Wu A, Wei J, Kong LY, Wang Y, Priebe W, Qiao W, Sawaya R, Heimberger AB (2010) Glioma cancer stem cells induce immunosuppressive macrophages/microglia. *Neuro-oncology* 12: 1113-1125

Wu H, Huang B, Zare RN (2006) Generation of complex, static solution gradients in microfluidic channels. *J Am Chem Soc* 128: 4194-4195

Wyckoff JB, Segall JE, Condeelis JS (2000) The collection of the motile population of cells from a living tumor. *Cancer research* 60: 5401-5404

Xia P, Bungay PM, Gibson CC, Kovbasnjuk ON, Spring KR (1998) Diffusion coefficients in the lateral intercellular spaces of Madin-Darby canine kidney cell epithelium determined with caged compounds. *Biophysical journal* 74: 3302-3312

Xu CP, Zhang HR, Chen FL, Yao XH, Liang ZQ, Zhang R, Cui Y, Qian C, Bian XW (2010) Human malignant glioma cells expressing functional formylpeptide receptor recruit endothelial progenitor cells for neovascularization. *International immunopharmacology* 10: 1602-1607

Yamada KM, Cukierman E (2007) Modeling tissue morphogenesis and cancer in 3D. *Cell* 130: 601-610

Yamada M, Seki M (2006) Microfluidic particle sorter employing flow splitting and recombining. *Anal Chem* 78: 1357-1362

Yamaguchi Y, Takagic F, Wataric T, Yamashitaa K, Nakamuraa H, Himizua S, Maeda H (2004) Interface configuration of the two layered laminar flow in a curved microchannel. *Chemical Engineering Journal* 101: 367–372

Yamahara T, Numa Y, Oishi T, Kawaguchi T, Seno T, Asai A, Kawamoto K (2010) Morphological and flow cytometric analysis of cell infiltration in glioblastoma: a comparison of autopsy brain and neuroimaging. *Brain tumor pathology* 27: 81-87

Yandava BD, Billinghurst LL, Snyder EY (1999) "Global" cell replacement is feasible via neural stem cell transplantation: evidence from the dysmyelinated shiverer mouse brain. *Proceedings of the National Academy of Sciences of the United States of America* 96: 7029-7034

Yang J, Yang J, Yin ZQ, Svir I, Xu J, Luo HY, Wang M, Cao Y, Hu N, Liao YJ, Zheng XL (2009) Microfluidic pool structure for cell docking and rapid mixing. *Anal Chim Acta* 634: 61-67

Yarden Y (2001) The EGFR family and its ligands in human cancer. signalling mechanisms and therapeutic opportunities. *European journal of cancer* 37 Suppl 4: S3-8

Ye F, Gao Q, Cai MJ (2010) Therapeutic targeting of EGFR in malignant gliomas. *Expert opinion on therapeutic targets* 14: 303-316

Yin XL, Pang JC, Ng HK (2002) Identification of a region of homozygous deletion on 8p22-23.1 in medulloblastoma. *Oncogene* 21: 1461-1468

Yuan K, Singh RK, Rezonzew G, Siegal GP (2006) In Vitro Matrices for Studying Tumor Cell Invasion. 8: 25-54

Yuan L, Santi M, Rushing EJ, Cornelison R, MacDonald TJ (2010) ERK activation of p21 activated kinase-1 (Pak1) is critical for medulloblastoma cell migration. *Clinical & experimental metastasis* 27: 481-491

Zaman MH, Trapani LM, Sieminski AL, Mackellar D, Gong H, Kamm RD, Wells A, Lauffenburger DA, Matsudaira P (2006) Migration of tumor cells in 3D matrices is governed by matrix stiffness along with cell-matrix adhesion and proteolysis. *Proc Natl Acad Sci U S A* 103: 10889-10894

Zhang J, Yang PL, Gray NS (2009) Targeting cancer with small molecule kinase inhibitors. *Nature reviews Cancer* 9: 28-39

Zhang X, Wang W, Yu W, Xie Y, Zhang Y, Ma X (2005) Development of an in vitro multicellular tumor spheroid model using microencapsulation and its application in anticancer drug screening and testing. *Biotechnology progress* 21: 1289-1296

Zhao B, Moore JS, Beebe DJ (2001) Surface-directed liquid flow inside microchannels. *Science* 291: 1023-1026

Zhong J, Paul A, Kellie SJ, O'Neill GM (2010) Mesenchymal migration as a therapeutic target in glioblastoma. *Journal of oncology* 2010: 430142

Zhou YH, Hess KR, Liu L, Linskey ME, Yung WK (2005) Modeling prognosis for patients with malignant astrocytic gliomas: quantifying the expression of multiple genetic markers and clinical variables. *Neuro-oncology* 7: 485-494

Zhou YH, Hess KR, Raj VR, Yu L, Liu L, Yung AW, Linskey ME (2010) Establishment of prognostic models for astrocytic and oligodendroglial brain tumors with standardized quantification of marker gene expression and clinical variables. *Biomarker insights* 5: 153-168

Zigmond SH, Hirsch JG (1973) Leukocyte locomotion and chemotaxis. New methods for evaluation, and demonstration of a cell-derived chemotactic factor. *The Journal of experimental medicine* 137: 387-410

Ziu M, Schmidt NO, Cargioli TG, Aboody KS, Black PM, Carroll RS (2006) Glioma-produced extracellular matrix influences brain tumor tropism of human neural stem cells. *Journal of neuro-oncology* 79: 125-133

Zohrabian VM, Forzani B, Chau Z, Murali R, Jhanwar-Uniyal M (2009) Rho/ROCK and MAPK signaling pathways are involved in glioblastoma cell migration and proliferation. *Anticancer research* 29: 119-123

Zucker S, Cao J, Chen WT (2000) Critical appraisal of the use of matrix metalloproteinase inhibitors in cancer treatment. *Oncogene* 19: 6642-6650

Zwick E, Bange J, Ullrich A (2001) Receptor tyrosine kinase signalling as a target for cancer intervention strategies. *Endocrine-related cancer* 8: 161-173